CRANFIELD UNIVERSITY

IAN BUTTERWORTH

NANOPARTICLE REINFORCED POLYAMIDE 66 GLASS FIBRE COMPOSITES FOR AUTOMOTIVE UNDER-THE-BONNET-APPLICATIONS

SCHOOL OF AEROSPACE, TRANSPORT AND MANUFACTURING

PhD THESIS
Academic Year: 2012- 2016

Supervisor: Dr Hrushikesh Abhyankar
Co-supervisor: Dr James Brighton
October 2016

CRANFIELD UNIVERSITY

SCHOOL OF AEROSPACE, TRANSPORT AND MANUFACTURING

PhD Thesis

Academic Year 2012 - 2016

IAN BUTTERWORTH

NANOPARTICLE REINFORCED POLYAMIDE 66 GLASS FIBRE COMPOSITES FOR AUTOMOTIVE UNDER-THE-BONNET-APPLICATIONS

Supervisor: Dr Hrushikesh Abhyankar
Co-supervisor: Dr James Brighton
October 2016

This thesis is submitted in fulfilment of the requirements for the degree of Doctor of Philosophy in Transport Systems

Abstract

This work focus on an engine oil pan application which expects component materials operate at elevated temperatures due to returning oil heating up during operation. Mechanical properties of thermoplastic composites are known to be temperature dependent with performance losses elevated temperatures. A pilot study was conducted to benchmark the current state-of-the-art glass reinforced polyamide materials at elevated temperatures to address a gap in this knowledge. Experiments included tensile, 3-point flexural, and gas gun impact where conducted at elevated temperatures 23°C, 65°C, 90°C and 120°C. Experimental results demonstrated the trade-off in the mechanical properties of the two materials especially when one of the materials had been impact modified with an elastomer (PA66-GF-E). PA66-GF-E mechanical and impact performance can be considered fit of purpose as a suitable material for an oil pan application but is more expensive. As an extra compounding step is required to graft the elastomer to the PA66 matrix.

Literature studies into replacements for the elastomer suggested nanoparticles as they can be compounded at the same time as the GF and in turn eliminate secondary compounding costs. Six 3-phase nanocomposite where then compounded using a twin screw extruder. Additions of OMMT and SiO_2 where done in 2, 3 and 4wt.% for each nanocomposite.

Testing of the 3-phase nanocomposites indicated the GF reduction has reduced mechanical strength in all results, but still demonstrates each nanomaterial and volume has been successful. Thermomechanical testing and aging suggests an optimised SiO_2 in wt.% of 2 or 3 could replace an elastomer as an impact modifier. OMMT grades did not have a significant improvement to over the SiO_2 grades to consider suitable for the oil pan application. However this work does builds a strong case for further work to continue developing 3-phase nanocomposites by improving the compounding setup.

Keywords: Nanocomposites, oil pan, melt compounding, twin screw extruder, injection moulding, thermo-mechanical testing, impact testing and thermal aging

Acknowledgements

I am grateful to Zakaria Mouti and Keith Westwood from EATON Corporation UK and Engineering and Physical Sciences Research Council (EPSRC) Grant Ref No: EP/P504147/1 and Grant Ref No: EP/J500203/1 for financial support on current research program at Cranfield University.

I would especially like to thank my first supervisor, Dr Hrushikesh Abhyankar for his advice and comments. Dr Hrushikesh Abhyankar put me back on track when I had a change of first supervisor half way through my project. Dr Hrushikesh Abhyankar took over from Dr James Njuguna who I would like to thank for originally accepting on to this research project and his guidance at the beginning of my project.

I am also grateful to Zakaria Mouti from EATON Corporation UK, Nick Brown from VANTAGE Polymers Ltd UK and Dean Fosbury from RTP Corporation UK for providing me materials and material samples for testing.

I would like to express my gratitude to all others who gave me the possibility to complete the study. I want to thank to Dr David Ayre, Dr James Brighton, Dr Lawrence Cook, Mrs Christine Kimpton, Mr Jim Hurley, Mr Ben Hopper, Mr Simon Stranks and my colleagues – Laura and Jinchun for their help in my material preparation, characterisation, and analysis.

I would especially like to thank my current line manager David Williams at the University of Warwick for not only employing me for my first research job but allowing me 20% of my time in work to finish my PhD. I'm also grateful to Vannessa Goodship at the University of Warwick for reading and giving advice on my draft thesis.

List of abbreviations

ABS	Acrylonitrile Butadiene Styrene
ASTM	American Society for Testing and Materials
BASF	Badische Anilin- und Soda-Fabrik
CAD	Computer Aided Design
CNT	Carbon Nanotubes
CO_2	Carbon Dioxide
EPDM	Ethylene–Propylene Diene Monomer rubber
EPR	Ethylene Propylene Rubber
FEA	Finite Element Analysis
GF	Glass Fibre
IC	Internal Combustion
IR	infrared
IMA	In Mould Assembly
ISBM	Injection Stretch-Blow Moulding
ISO	International Organization for Standardization
MIM	Manufacture In Mould
MWCNT	Multiwall Carbon Nanotubes
NO_x	mono-nitrogen oxides
PA	Polyamide
PA6	Polyamide 6
PA66	Polyamide 66
PET	Poly (ethylene terephthalate)
PP	Polypropylene
PFV	Photron Fastcam Viewer
rpm	revolutions per minute
SEM	Scanning Electron Microscopy
Tg	glass transition temperature
XRD	X-Ray Diffraction

Units

g	gram
N	Nowton
kN	kilonewton
m	meter
kg	kilogram
MPa	megapascal
GPa	gigapascal

Table of contents

List of figures

Chapter 1. Introduction

1.1 Background

The history of materials used in the automotive industry is becoming more diverse and has seen wood been phased out and replaced with steel. Steel is an ideal material when considering it has excellent all round mechanical performance with relatively low cost and ease of manufacture. However using high percentages of steel in vehicles has resulted in the total weight of a vehicle to increase. Figure 1-1 illustrates typical materials used historically in domestic vehicles since 1906 to 2007.

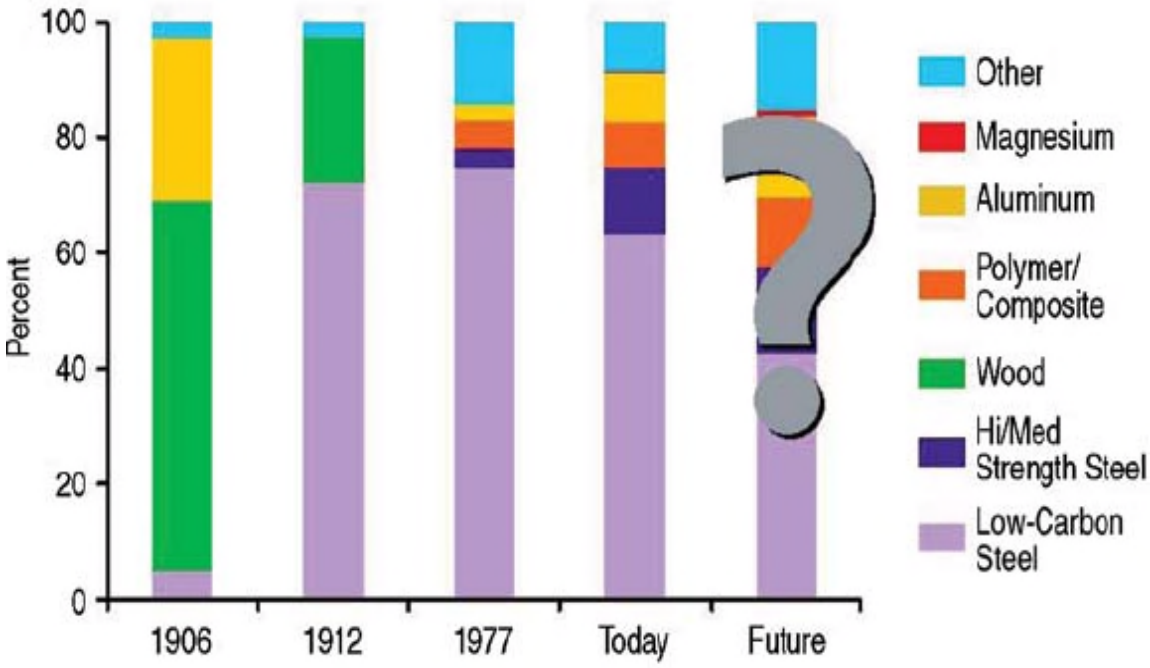

Figure 1-1: The materials in a typical automobile—historical perspective (2007) [1]

Vehicle efficiency and emissions are two areas of concern for both the automotive manufacture and the end customer. Where automotive manufactures in Europe have to comply with Euro standards to sell vehicles in Europe. The latest standard is Euro 6 standard which is currently in force since January 2014. One of the Euro 6 new directives is to see a reduction NO_x emissions from diesel cars, from 180 mg/km to 80 mg/km [2]. CO_2 is another concern for transportation which contributes around 20 percent of world CO_2

emissions [3]. To address this the European Parliament in 2009 passed new car CO_2 legislation which set an emissions cap of 130 g/km averaged over all new vehicles produced by each manufacturer by 2015. With a subsequent limit has been agreed of 95 g/km for 2021. However the end customers are not regulated by emissions as such, but pay duties and tax related to their vehicles. In the UK each vehicles tax rate is based on engine size, or fuel type and carbon dioxide (CO_2) emissions, depending on when the vehicle was registered [4]. Rising fuel prices and fuel economy is often a consideration made by most vehicle owners due to day to day running may not be cost effective. Figure 1-2 illustrates the rising diesel and unleaded petroleum fuel prices in the United Kingdom between years 1978 to 2016.

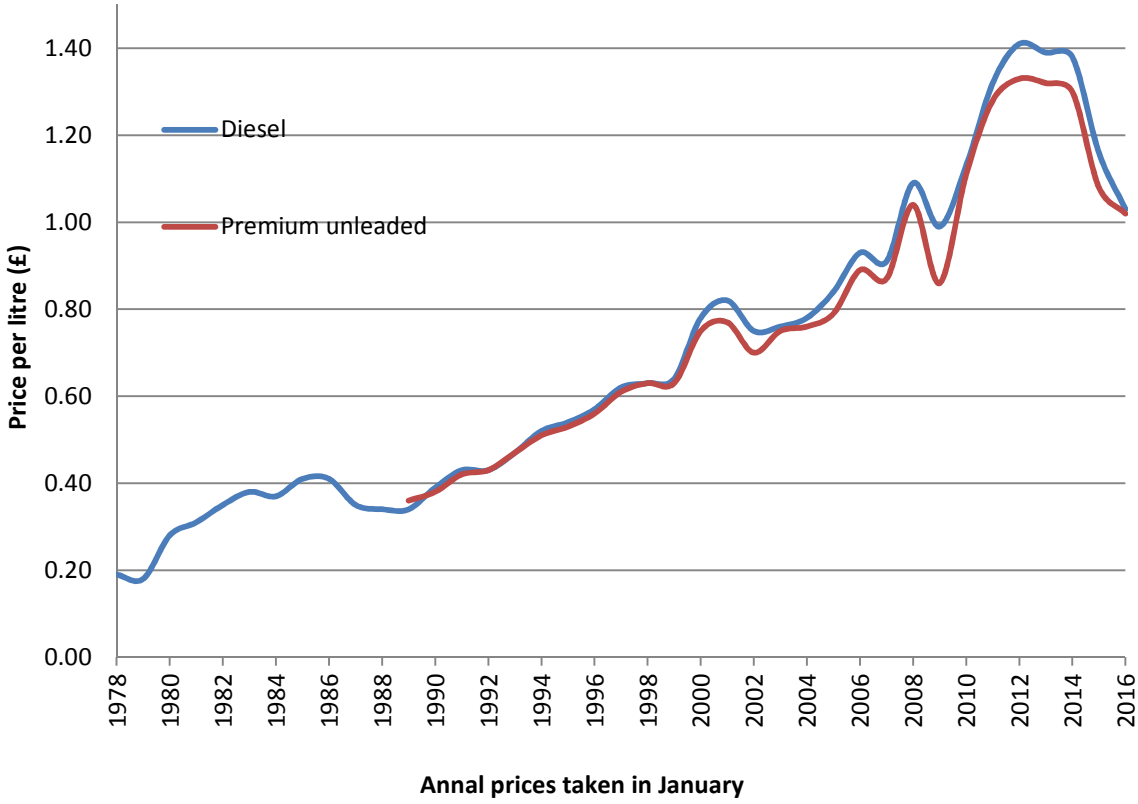

Figure 1-2: typical retail prices of fuel in the United Kingdom 1978 to 2016 (Reinterpreted from GOV.UK data) [5]

A key area to achieve better fuel economy and reduce emissions is to reduce the total vehicle weigh. This is to say a lighter weight vehicle will need less energy to move and accelerate while generating fewer total emissions to make each journey. In the last few decades the uses of composites and alloy materials have evolved to replace steel components as way to save on component weight. Weight saving under-the-bonnet requires structural components to operate in harsh operation conditions such as high temperature, an environment originally suited to metals. High performance thermoplastics such as PA6 and PA66 have a high melting points around 220°C and 260°C respectfully with good mechanical and chemical resistance properties. High performance polymer matrix composites also offered sound and vibration damping properties a key advantage over metals. This unique selling point has quickly been adopted by all manufacturers in the last decade for an expanding range of under-the-bonnet components such as air ducting, module housing, connectors, engine covers and radiator covers.

More recently the commercialisation of PA-GF oil pans using BASF Ultramid A3HG7 PA66 35%GF has been successful, however a concern for localised impact response has highlighted a reduced service life of such a component. There are many studies into glass reinforced polyamine oil pans highlighting stone and debris impact from a typical road surfaces and these are considered a real issue to component failure [6]–[12]. Mouti [13] studied the BASF Ultramid A3HG7 PA66 35%GF and second BASF grade Ultramid A3WG7-OSI PA66 35%GF which included an elastomer modifier for improved impact performance. Mouti's findings showed an elastomer modifier improves impact performance through improved material toughness at room temperatures. Other studies into elastomers used as a third phase are also in agreement with Mouti's findings [14]–[16]. However this has left thermomechanical performance (quasi static and impact at elevated temperatures) unstudied and does not fully represent the running conditions found under-the-bonnet. This work picks up from Mouti's work by bench marking the BASF Ultramid A3HG7 and A3WG7-OSI with thermo-mechanical

and impact testing and explores the thermomechanical performance of these materials.

Material grade optimisation can then be taken further to find an alternative to the elastomer to further improve thermo-mechanical performance. This is to say A3WG7-OSI offers stone impact protection, but not all components under-the-bonnet are exposed (at risk of stone impact). Components such as the cylinder block and gearbox housing are more structural requiring improved mechanical strength at elevated temperatures. Micro reinforcing partials and fibres within an existing PA matrix are commercially successful due to decades of use and optimisation. PA matrix property tailoring using nano reinforcement is the current state-of-the-art in additions as small as 3wt.% offering significant reinforcing effects which include improved mechanical stress, strain or modulus. Current 2-phase nanocomposites when compared to pure matrix, exhibit enhanced mechanical and thermal properties, with improved barrier performance in PA6 and PA66 grades [17]–[23]. Indeed, it is known that an addition of up to 5wt.% of inorganic nano-particles in polymers is enough for a considerable improvement in the material's mechanical properties compared to micro fillers, which require about >30wt.% [24]–[28]. It is currently not known what effect nano fillers would offer as a third phase to GF reinforced PA66 matrix as the interaction between matrix, GF and nano reinforcements could be minor or significant. It is also unknown what effect temperature and aging will have on mechanical performance.

1.2 Aim and objectives

Thermoplastic oil pans using BASF Ultramid material grades A3HG7 and A3WG7-OSI have been proven in service. However, lab testing conditions of the two materials have only been conducted at room temperature which does not represent an accurate service condition for the application. Stone impact protection gained from an elastomer modifier has drawback of trading mechanical strength for strain resulting in a material only suited for stone impact protection. A reinforcement that can improve mechanical strength while improving or stabilising strain can open up new applications such as a gearbox

housing. Therefore this thesis starts off by benchmarking the BASF A3HG7 and A3WG7-OSI grades to address lack of thermo-mechanical and thermo-impact data. Studies into suitable replacements to the elastomer phase that can be introduced at the same time as the glass fibres was essential to make the new materials cost effective.

Aim:

Development of a suitable material grade manufacturing mythology that can be scaled up from the lab to industry. Followed by thermo-mechanical and thermo-impact performance of 3-phase nanocomposite can then be compared back to the BASF grades.

Objectives included:

- Benchmarking of BASF Ultramid material grades A3HG7 and A3WG7-OSI by investigating and benchmarking the effects of temperature increase from 23°C to 120°C for quasi static and dynamic impact
- Determine an alternative reinforcement phase to the elastomer which can be melt compounded into a PA66 matrix with glass fibre reinforcement, including processing methods
- Conduct melt compounding and determine if dispersion of the nanoparticles can be achieved
- Using benchmarked materials results to evaluate formulations utilising the addition of nanofillers
- To experimentally determine the thermal and quasi static performance of the selected materials to suit an automotive oil pan application
- To experimentally study accelerated aging of the selected materials to identify any possible lose in performance over time
- Analyse physical performance and morphology to evaluate and understand the mechanisms and interactions of composite phases
- Identify an optimum formulation to take forward

1.3 Methodology

This study is focused on experiment work to develop a new PA-GF material system with the intention to replace an existing PA-GF-E grade currently used in the automotive industry. Figure 1-3 illustrates the gaps in current knowledge related to testing and compounding which has been covered in this work.

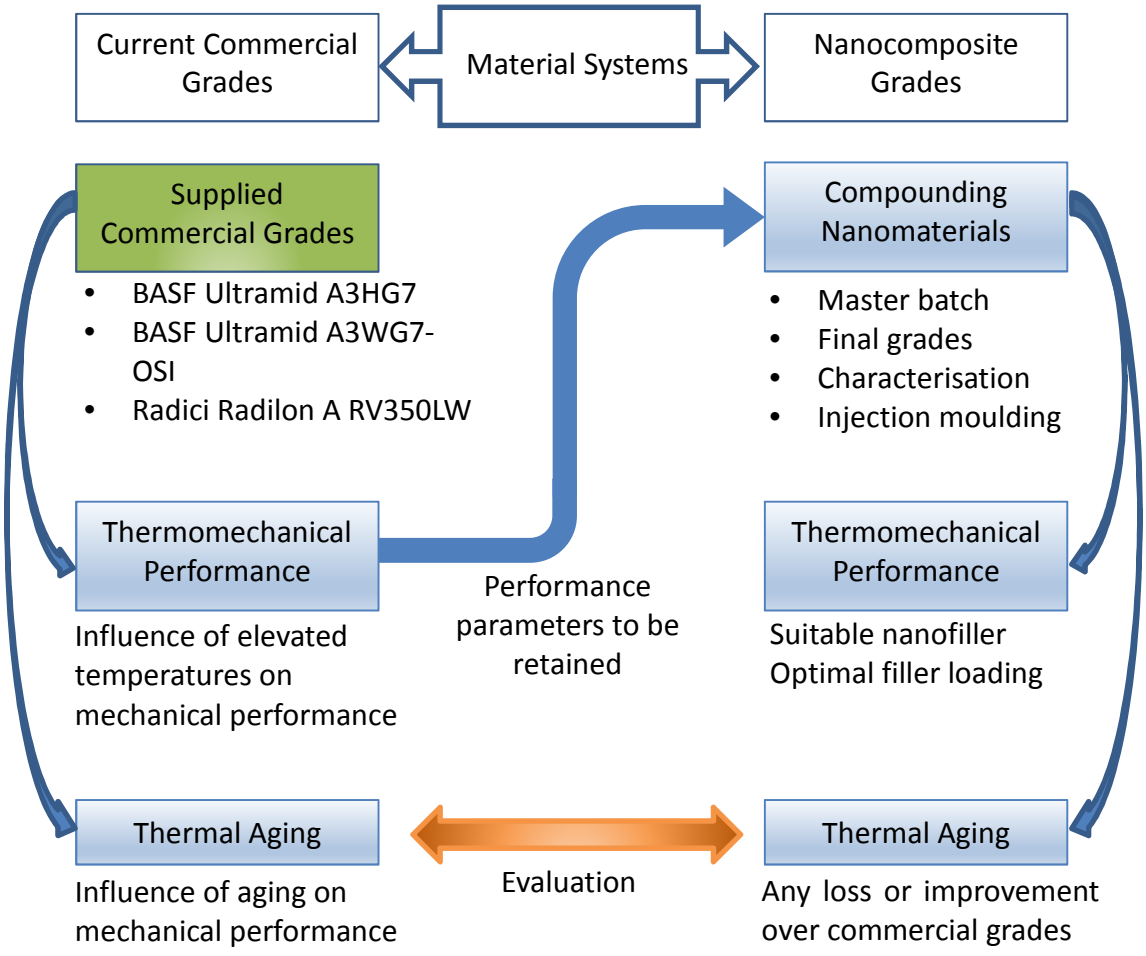

Figure 1-3: Gap in current knowledge in relation to experimental work

A benchmarking study on existing commercial grades, considering thermomechanical and localised impact testing at elevated temperatures was important to represent a realistic service life condition of oil pan component. Benchmarking of commercial grades at elevated temperatures not only address a gap in knowledge but give a bassline on what mechanical properties will be important when replacing the elastomer phase in the current PA-GF-E material grade used in industry.

Studies into replacement fillers highlighted nanocomposites to be state-of-the-art and offer reinforcing effects for mechanical stress, strain and modulus in additions of 1 to 5wt.% when used in a pure matrix material.

Compounding nanocomposite grades adopted a master batch compounding process followed by final grades was deemed necessary to disperse nanofillers effectively. XRD and SEM characterisation studies where done to determine the level of dispersion. Final compounded material grades where injection moulded in to test samples.

Thermomechanical and localised impact testing at elevated temperatures was repeated on the nanocomposite grades to compare the performance from the commercial grades. Thermal aging of material grades has also been considered to determine if performance degradation will affect service lift for the end application. This not only address a gap in knowledge but builds confidence in the materials performance if adopted in to industry.

This study concludes then offers suggestions for further work by optimising the compounding process and hi-rate testing to develop suitable material cards FEA simulation.

1.4 Outline of the thesis

Chapter 1 introduces the thesis background, aims, objectives and methodology. With key interests of this work is to understand the thermal performance of such PA-GF composites by taking testing further and to investigate new reinforcing materials to further improve the PA-GF's performance with the intention to open up new under-the-bonnet applications.

Chapter 2 reviews state-of-the-art literature on glass fibre reinforced polyamide composites. Glass fibre reinforced thermoplastics are also identified for under-the-bonnet automotive applications that require thermal and mechanical performance. Nanomaterials are then identified as a new state-of-the-art reinforcing phase used in a thermoplastic matrices to give similar or improved mechanical performance over typical micro reinforcements. Key findings of the literature review and gaps in the subject knowledge are summarised.

Chapter 3 takes existing work further by benchmarking effects of temperature on the current PA66-GF and PA66-GF-elastomer grades used for oil pans. The study is intended to simulate the elevated temperature an oil pan component is expected to operate at, using thermal conditioning to determine the influence of temperature on quasi-static and dynamic properties response.

Chapter 4, in this study several 3-phase nanocomposites of interest are melt compounded. Nano grades included two types of nanoparticles, OMMT and SiO_2 which were compounded in to an existing PA66-GF composite grade. SEM and XRD characterisation was conducted to evaluate each grade after compounding to determine nano partial dispersion and exfoliation. Analytical studies also looked at glass fibre breakage to determine what effect a two-step compounding process would have on fibre length. Chapter also describes test sample injection moulding of test bars and plaques.

Chapter 5 assesses the mechanical and impact properties of the compounded 3-phase nanocomposites to benchmark each grade at a room temperature in an unaged condition. Room temperature in an unaged condition

was necessary to detach them as possible influencing factors when benchmarking each nano grade. Therefore study intention is to demonstrate if OMMT or SiO_2 has any effect on an existing PA-GF composite, as well as finding out if loading content in wt.% for each nano particle also has any influence on performance.

Chapter 6 investigates the influence of temperature on each of the nano grades mechanical properties and impact performance during testing. The study is intended to simulate the elevated temperature an oil pan component is expected to operate at as conducted in chapter 3. Thermal conditioning of the nano grades will also highlight if there is any improvement or degradation of quasi-static and dynamic properties response when introducing nano as a third phase.

Chapter 7 investigates the influence of thermal aging of the PA-GF reference grade with the six nano grades compounded in Chapter 4 and characterised mechanical performance over a six week (1008 hour) thermal aging study. Sampling was taken out on a weekly basis to help map any effect on mechanical performance as a cross sections of material performance over time.

Chapter 8 concludes and summarises each chapter of this thesis work. This research project does not directly contribute to the oil pan or other under-the-bonnet components when considering the nano grades in their current state of development, but does show the Radici PA-GF grade has comparable impact response to the BASF PA-GF-elastomer grade without needing the elastomer phase. However work does build on knowledge of nano composites when a micro and nano reinforcement are compounded in to a PA matrix. Further work and process optimisations for testing are also suggested. Suggested compounding process optimisations is where a three phase nano composite is going to have greatest impact for mechanical properties tailoring.

Chapter 2. Literature review

2.1 Introduction and background

Eaton Limited works with other industries to develop, fabricate and supply a broad range of highly engineered components. Eaton is a global innovator of plastic moulded parts with a wide assortment of parts offering reduced weight, component integration and durability. A need to improve Noise Vibration Harshness (NVH) and temperature management of these highly engineered parts has facilitated a shift from metal to plastic components. Through this project, Eaton is attempting to further develop a polymer matrix material system for automotive engine oil pans.

The engine's oil pan provides one of the greatest challenges in under the bonnet applications as it is mounted low on the undercarriage, where it is subject to impact from stones and gravel kicked up by tires. In winter climates, oil pans are also exposed to road salt which is potentially damaging to both plastics and metals. The structural requirement of most oil pans can lead to complex internal and external geometries. In metals, this can translate to heavy, multi-piece assemblies requiring numerous manufacturing steps.

2.2 Oil pan

The oil pan is located directly below the engine, meaning that it is the most exposed part of the engine to the road (see Figure 2-1a Cummins ISF engine [29]). The oil used to lubricate the engine's moving parts pools in the oil pan, which plays the role of reservoir [30]. During normal engine operation, an oil pump will draw oil from the pan and circulate it through the engine. After the oil has passed through the engine, it is allowed to return to the oil pan due to gravity [31]. In a wet sump system as shown in Figure 2-1b, the amount of oil that an engine can hold is directly related to the size of the oil pan [13], [32]. In service, Cummins found out that stone impact could cause their new plastic oil pans to fail. In order to enhance impact properties of the Cummins oil pan shown in Figure 2-1b, studies were conducted on two material variations of PA66: Ultramid A3HG7 and elastomer modified PA66 (Ultramid A3WG7-OSI). Both have 35 wt.% of discontinuous glass fibre reinforcement.

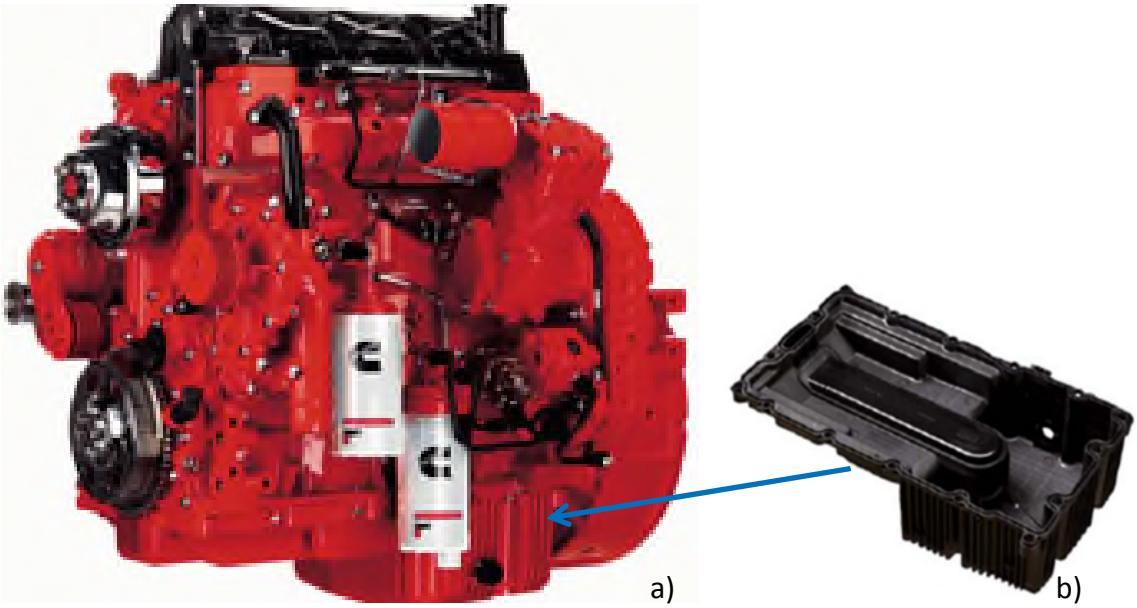

Figure 2-1 a) Cummins light commercial ISF engine[29] b) Oil pan Ultramid A3ZG7 [33].

2.2.1 Temperature from IC engine to oil pan

Figure 2-2 illustrates the oil circulation cycle in an IC engine, showing temperatures found during normal operation.

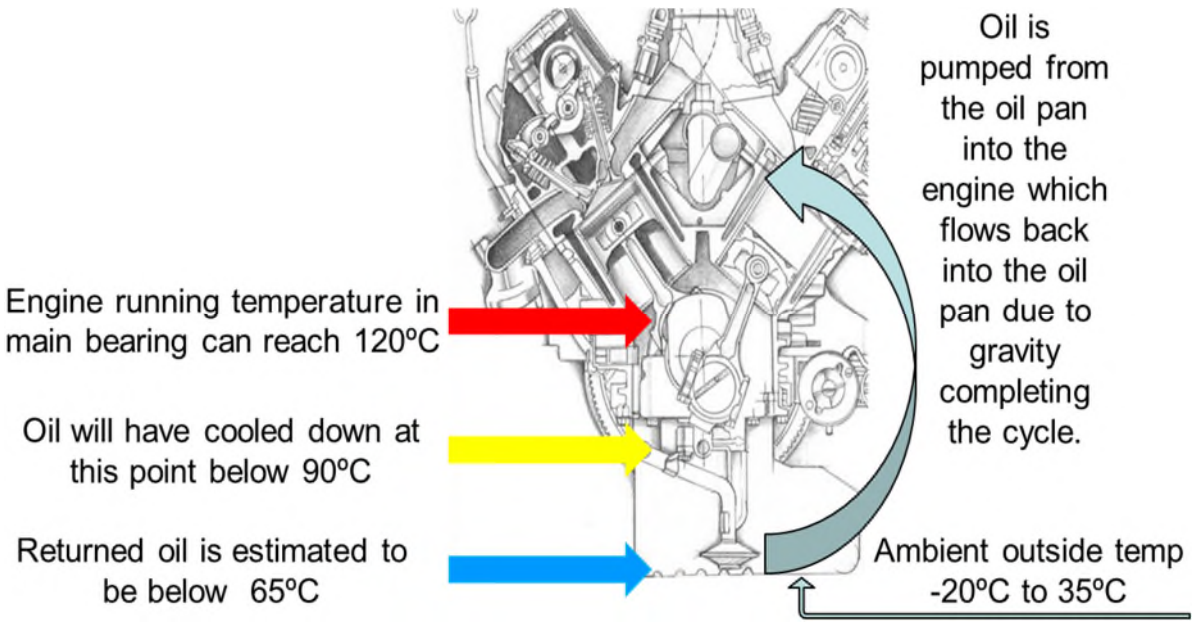

Figure 2-2: Oil circulation cycle and links to temperatures regens

The standard air temperature of 23°C in ISO 291 [34] is the most common test temperature conducted in labs. This allows fair comparison with other work and represents the temperature of an engine before it has started on a normal day.

Testing at 90°C was selected based on a typical oil operating temperature for IC engines of around 90°C to 100°C. This was also close to the SAE J300 standard [35], in which the Kinematic Viscosity of engine oil is tested at a standard temperature of 100°C representing the temperature of the oil in a typical IC engine.

Testing at 65°C was selected as a returning oil temperature and middle-ground temperature between 23°C and 90°C and also to prevent a large gap between 23°C and 90°C.

120°C was selected to represent a case of engine overheating. It is unlikely that this temperature will ever be transferred to the oil pan due to engine cooling and the pan itself losing heat to the environment.

2.3 Polyamide

Polyamide (PA) is a semi-crystalline thermoplastic material used in a wide range of applications such as electronic, household appliances and automotive components. Polyamide is gaining much recognition due to grades such as PA6, PA11, PA12, PA46 and PA66. All are produced using addition polymerisation. Addition polymerisation is a reaction process using ring compounds to form PA6, PA11, PA12 PA46 and PA66 variations [36].

A polyamide contains amide functional groups resulting from the reaction of an acid group and an amine group (see Figure 2-3 for the monomer of PA6 and PA66 [37], [38]). These materials have particular utility in performing mechanical duties that traditionally relied on metal parts, thanks to their outstanding properties including high tensile strength, chemical and heat resistance and low coefficient of friction [38]. Table 2-1 gives an overview of some polyamides including PA6 and PA66. Other polyamides were selected based on their high melting temperatures with comparison to typical metals that can be found under the bonnet.

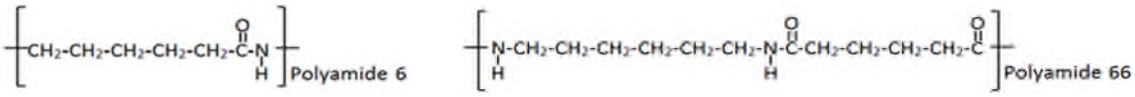

Figure 2-3 Monomer of PA6 and PA66 [37]

Table 2-1 An Overview of PAs and metal properties [39][40]

		Polyamide					Metals				Reinforced Polyamides	
Properties	Units	PA6	PA11	PA12	PA46	PA66	Low Carbon Steel	Stainless Steel 301	Aluminium 1000	Magnesium AZ91C-T6	PA66 35% Glass Fibre Ultramid A3HG7	PA66 30% Carbon Fibre Radilon A CF300K NER
Density	g/cm³	1.12	1.03	1.01	1.2	1.14	7.83	8.03	2.7	1.8	1.41	1.27
Water Absorption	%	4.74	1.29	1.30	10.4	4.32	N/A	N/A	N/A	N/A	4.70 - 5.30	6
Mechanical Properties												
Ultimate Tensile Strength (UTS)	MPa	66.1	52	79.6	107	72.6	779	515	111	275	150 - 200	255
Modulus of Elasticity	Gpa	2.17	1.07	5.34	2.51	2.46	202	212	68.4	44.8	8.5 – 11.2	23
Poisson Ratio	No unit	0.35	-	-	-	0.41	0.29	-	0.33	0.35	0.35	0.35
Hardness	Rockwell	115 R	107 R	103 R	N/A	116 R	89.4 B	N/A	N/A	77 E	N/A	N/A
Elongation at Break	%	86.9	122	53.5	48.9	67.2	20.4	40	13.5	6	3 - 5	2.1
Compressive Yield Strength	MPa	31	-	69.6	-	49.4	1480	-	-	145	N/A	N/A
Thermal Properties												
Melting Point	°C	219	183	177	295	258	1430	1400	652	421	260	260

2.4 Polyamide 66 Reinforced Composites

A typical two-phase, polymer reinforced composite material system consists of a matrix, in this case polyamide, and a second reinforcing material which can be fibres or particles. Figure 2-4 illustrates the basic concept of a fibre reinforced polymer composite. The matrix holds the reinforcement, while the reinforcing material improves the mechanical properties of the matrix. The benefits to the mechanical performance can be seen in Table 2-1 by comparing PA66 against PA66 with 35% glass fibre (GF) or PA66 with 30% carbon fibre (CF). Benefits come from improved mechanical strength and modulus and a trade-off with elongation at break which is also considered a benefit to most structural applications, especially automotive.

A short glass fibre reinforcement allows conventional methods such as injection moulding, to be used as a large volume fabrication route. This offers improvements in stiffness and strength properties over unreinforced PA66 while also reducing the ultimate strain [13], [41], [42]. Injection moulding also allows complex geometers to be produced in one cycle. This is a huge advantage over metal stamping and casting, which require secondary operations to form the final component.

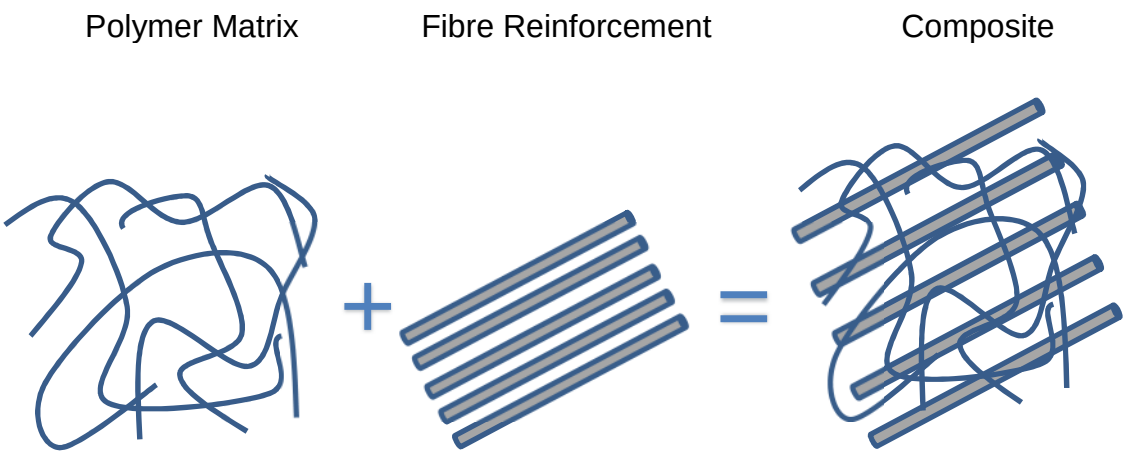

Figure 2-4: Typical composite illustration showing fibres reinforcing a polymer matrix

2.5 Commercially available polymer composite components

The use of high performance thermoplastics with short glass fibre reinforcement is now commonplace for under-the-bonnet structural components such as engine covers, oil pans, intake manifolds, inlet gas compressor exits, oil filter modules, air ducting, heating and cooling systems [11], [13], [33], [43]–[47]. High performance thermoplastics are typically grades that have good mechanical properties at elevated temperatures as well as good chemical resistance properties. Table 2-2 gives an overview of thermoplastics that can be found under-the-bonnet ranging from a basic function to more structural application, each using glass fibres to improve material properties. The good thermal strength for moderate cost provided by a heat-stabilized polyamide's matrices is seen as a way to reduce fuel consumption and reduce CO_2 emissions, as they can weigh up to 40% less then steel counterparts [48]–[51]. Thermoplastic oil pans are also known to reduce transmitting noise from engine or gearbox [52]. The reduction of engine noise has been a unique selling point of thermoplastic engine covers in the automotive industry since1997 [53].

All the listed components in Table 2-2 are manufactured using injection moulding, which requires complex tooling to form each part. This means that all of the polymer components require much higher capital investment to begin with. The advantages of injection moulding, such as complex geometries and fast cycle times in high volumes, negates the high tooling cost and results in a reduced individual component cost. This work will have to consider injection moulding as the primary manufacturing process for not only the oil pan application, but for the majority of all polymer components found under-the-bonnet.

Table 2-2 Examples of thermoplastic with fibre reinforcement used to make under-the-bonnet components [11], [45], [52]

Automotive Under the Bonnet Products	Polymers & Grades	Glass Fibre content GF (%)	Model example	Characteristics over counterparts
Engine Covers	PA6	30-35%	 DuPont PLS 95G35DH Cadillac CTS GM	- good surface finish -Temperature range 210°C continuous to 230°C Peak - durability - low deformation - Mould cycles under a minute
Air Duct	PPS PPS	Fortron 1115LO 15% Fortron FX430T7 30%	 Fortron 1115LO and FX4330T7	- Very good flow properties - Toughness - High strength - High stiffness - Temperature up to 240°C - Low moisture absorption - Under Bonnet chemical resistant
Oil Filter Modules	PA6/6	35%	 BASF A3WG7 HRX BK Chrysler 2011MY	- weight reduction 43% - 60% cost saving - Greater part reliability - Temperature range 120-130°C - Extended heat aging - Reduce swelling
Heating and Cooling Systems	PA6/10	65%	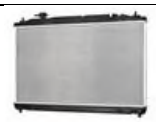 DuPont Zytel PA6/10 Toyota Camry 2010MY	- 40% bio-plastic derived by castor bean oil - Heat resistance - Chemical resistance - Carbon footprint is less than other polymers
Oil Sump Reservoir	PA6 PA66	35% 35%	 BASF A3HG7 PA6/6 Actros BR 500 class 8	- Increased capacity 30% - Acoustic damping - 50% weight reduction over aluminium - Corrosion resistance - 50% reduction in tooling cost

2.6 Fibre Reinforcement of Polyamide Composites

Many variables of fibres have been studied, such as material, diameter, length, volume loading weight percentage (wt.%) and dispersion. Each have their own influence on the mechanical properties of the resulting composite.

2.6.1 Effect of Fibre Diameter

The effect of fibre diameter is a consideration for synthetic fibres as they can be fabricated to desired sizes. As glass fibre is the most common synthetic fibre used to reinforce a polymer matrix, studies can be found linked to the effect of fibre diameter.

Thomason studied the effect of fibre diameter on injection moulded long glass fibre-reinforced PA66 and found that strength and elongation to failure were shown to be significantly dependent on the residual fibre length, fibre diameter and fibre concentration [54]. Thomason's fibre diameter conclusions found that composite strength decreases linearly with increasing fibre diameter. The apparent level of interfacial shear strength was found to decrease to a lesser extent with increasing fibre diameter whereas, with decreasing fibre diameter, elongation appeared to become more prominent [54].

Thomason also found that fibre diameter and content did have a significant effect on composite unnotched impact. From results, long fibres at 40 wt.% loading show that fibres with a diameter of 17µm have an impact response of approximately 60kJ/m^2, fibres with a diameter of 14µm have an impact response of approximately 69kJ/m^2 and fibres with a diameter of 10µm have an impact response of approximately 84kJ/m^2. This demonstrates that fibre diameter does influence the unnotched impact performance [55]. Another study by Thomason into the effect of an average fibre diameter between 9-18µm found that tensile modulus exhibited no dependence on fibre diameter. A significant effect on unnotched impact and tensile strength was seen where performance was reduced with increase of fibre diameter between the 9-18µm, range similar to his other work [56].

Ramstein et al also studied glass fibre reinforced polyamide using fibre diameters between 10-24µm and found unnotched Charpy impact response is affected by fibre diameter, with 10µm offering the best performance and subsequent increases in diameter up to 24µm reducing impact performance. This agrees with Thomason's results [56], [57].

Ramstein et al [57] also found that tensile strength had a significant response on fibre diameter with a diameter of 10µm offering the best performance and the strength reducing up to a diameter of 24µm. Tensile modulus and notched Charpy impact show less effect and, at elevated temperatures, notched Charpy impact shows better performance to be offered by larger diameter fibres.

2.6.2 Effect of Fibre Length

Fibre length is often a variable in a fibre reinforced thermoplastic matrix. Lengths are often referred to as short, long and continuous. Short fibres suited to injection moulding are around 20µm to 3mm, whereas long fibres start from 3mm. Continuous fibres are typically the length of the component and can be woven in different orientations. The effect of fibre length is a subject area that has been widely studied in fibre reinforced composites [54], [58], [59]. Preference is to use long and continuous fibre lengths, as long fibre lengths are known to offer improved mechanical, impact and wear performance over short fibres [55], [58], [60]–[62]. Figure 2-5 shows tensile strength and modulus are improved with longer GF in a PA66 matrix at 3 different fibre volumes.

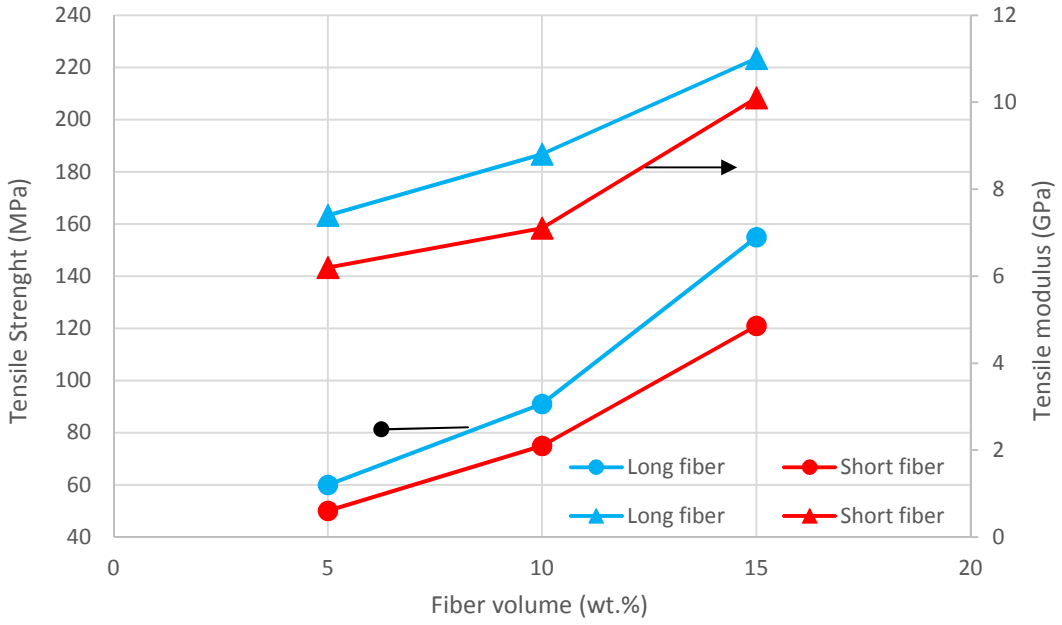

Figure 2-5: Illustrates tensile strength and modulus is improved with both increased fibre length and volume (replotted from Hassan et al [60]).

The availability of very long and continuous fibres is limited due to a limitation in the injection moulding process, where fibres below 3mm in length are preferred in order to prevent entanglement issues with the screw feeds and mould runners and gating flow issues.

The mechanical properties of a fibre reinforced thermoplastic can be affected by fibre length, where short fibre reinforced composite may not have sufficient surface area to bond to the matrix, thus reducing mechanical strength. There is a critical fibre length necessary for effective strengthening and stiffening of a fibre reinforced polymer composite. The critical length is dependent upon the effect of fibre diameter and tensile strength on the fibre matrix bond strength [63], [64]. At critical length, fibres pulled out in tension will offer the best strength performance. Any increase beyond this length will not offer any further benefit. The fibre matrix surface area bond is linked to the ratio between length and diameter (known as the fibre aspect ratio). An aspect ratio of 1:1 (length 10μm, diameter 10μm) would offer much as a reinforcement due

to having the same length as the diameter, whereas 20:1 fibre in a matrix would offer load reinforcement in tension.

Thomason [55] studied the effect of fibre length in glass fibre reinforced PA66 using Izod and Charpy impact testing and found that fibre length did have an effect on notched impact tests. Notched Charpy results showed that, at 40wt% fibre loading, long fibres withstood 21.2kJ/m^2 impact and short fibres 14.6 kJ/m^2. A 31% reduction in impact performance. Whereas in unnotched Charpy impact tests, fibre length did not have any significant effect between short and long fibre at 30wt% fibre loading. However, at 40wt% fibre loading, long fibres withstood 84kJ/m^2 impact and short fibres 94kJ/m^2. A 10.6% improvement in impact performance. Drop tower testing was also conducted and it was found that longer fibres allowed samples to absorb a significantly higher level of total energy compared to a short fibre reference sample.

Silverman [65] studied the effect of glass fibre length on creep and impact resistance on 3 different thermoplastic matrix materials: PC, ABS and PP. All showed improved impact properties when reinforced with long fibres when compared to short (see Table 2-3 for comparisons [65]). Table 2-3 clearly shows that fibre length affects impact strength for all matrix materials, with long fibres offering more than four times the total energy to break than short fibres. The effect of fibre length on creep (conducted at 121°C) demonstrated that long fibre reinforcement leads to excellent creep resistance whereas short fibres had a decreased loadbearing ability due to the matrix having to taking up more load. The uses of long fibres in PC, ABS and PP matrices has resulted in improved mechanical strength. This improved benefit can be linked to long fibres having a larger surface area (aspect ratio) for the matrix to bond to. Another benefit to this is that fracture and creep resistance are also improved, as longer fibres require more impact energy or load to pull out, resulting in the fibre breaking instead of excessive pull out when compared to short fibres. In terms of creep, longer fibres will help prevent the matrix from deforming.

Table 2-3 showing results from drop impact tests [65]

Matrix Material	Fibre length	Energy to initial damage (j)	Total energy to break (j)
Polypropylene	Short Glass	0.5	6.8
Polypropylene	Long Glass	5.1	26.1
ABS	Short Glass	<0.1	4.5
ABS	Long Glass	2.8	37.4
Polycarbonate	Short Glass	<0.1	9.1
Polycarbonate	Long Glass	7.9	46.5

Srinivasan et al. [61] studied the wear behaviour of long and short glass fibre reinforced plastics and found that long glass fibres offered better frictional and wear resistance compared to short glass fibres. They concluded that long fibres are more difficult to pull out from the matrix. This conclusion would be expected, as a large fibred matrix would have a much larger bound surface area than a short fibred matrix.

2.6.3 Effect of Fibre Loading wt%

In polymer matrix composites, it is often observed that an increase in fibre content leads to an increase in the strength and modulus of fibre reinforced polymer matrix composites [66]–[71].

Güllü et al. [72] investigated the effect of glass fibre addition on the mechanical properties of PA6 at fibre loadings of 15 and 30wt.%. Results show 15 and 30 wt.% fibre reinforcements improved the tensile strength of PA6 by 74% and 111% respectively, whilst reducing tensile strain of PA6 by 83% and 84% respectively. As a conclusion, the mechanical properties of the plastic matrix composite are heavily dependent on fibre weight/volume fraction.

Increasing the fibre content can lead to an increase in the strength and modulus. Beyond the optimal loading point, however, further loading can result a drop off in performance and significant weakening of the composite to the extent that performance will fall below the performance of the polymer matrix with no fibre loading. Many studies have also commented that an increase in

fibre content offers improvement on mechanical performance to a certain limit, which then decreases with further loading of fibre content [66], [73]–[76].

Fibre loading can be split into three loading levels: low, intermediate and high. At low levels of fibre content, the composites show poor mechanical properties due to poor fibre population and low load transfer capacity of one another. As a result, stress accumulates at certain points of the composites and highly localized strains occur in the matrix [66]. At intermediate levels of fibre loading, fibres actively participate in stress transfer. Decrease in strength of fibre/polypropylene composite at higher fibre content is a direct consequence of poor fibre/matrix adhesion. This leads to microcrack formation at the interface under loading and non-uniform stress transfer due to fibre agglomeration in the matrix [66]. Higher wt% of fibre content also leads to an increase in fibre–fibre interaction which results in dispersion difficulties in the fibres within the matrix [66]. The three levels of fibre loading can easily be seen in work undertaken by Thomason, reinforcing polypropylene with different percentage weights of glass fibre which can be seen in Figure 2-6. Optimum mechanical performance can be found in the 30–50 wt% fibre content range.

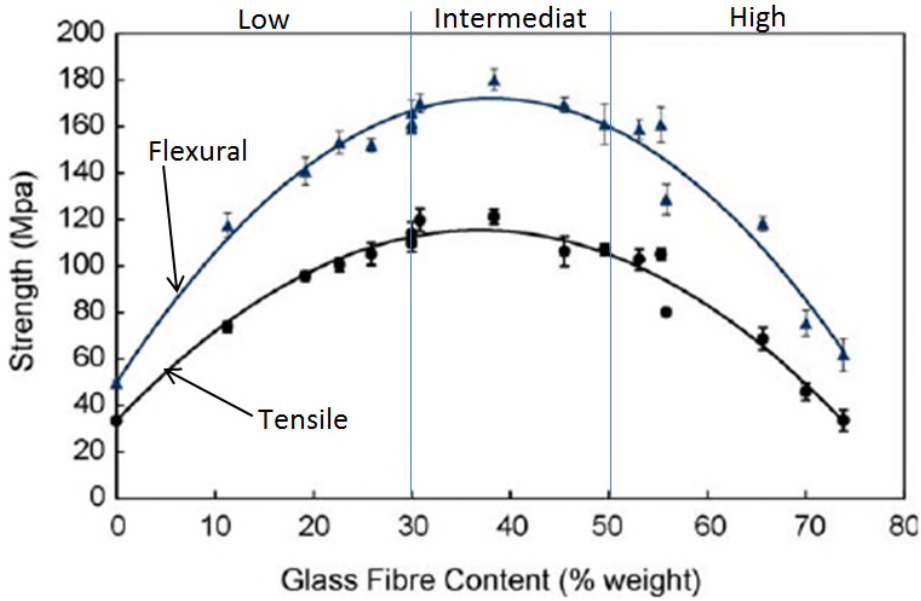

Figure 2-6: Strength versus fibre content. Taken from results by Thomason [76].

2.6.4 Effect of Fibre Dispersion/Orientation

Different configurations related to fibre orientation can play an important role in determining the mechanical properties in a composite material system. Configurations lie between two extremes - parallel alignment of one or two directions for all fibres and inconstant random alignment across all possible axes for each fibre. The difference between the common configurations of the two extremes can have a significant effect on resulting mechanical properties [63]. Random fibre reinforcement relies on orientation inconsistency of each fibre for optimal performance in an X, Y, Z coordinate system offering multi axial mechanical performance. Notta-Cuvier et al. stated that a typical assumption linked to reinforced composite materials is that short fibres are assumed to be uniformly dispersed in a matrix. A fundamental assumption is that the fibres carry loads only in their direction of orientation. Their linear elastic behaviour is therefore assumed unidimensional. Each fibre is characterised by an orientation vector expressed in the global system of coordinates (i.e. linked to the composite or equivalently to the matrix) [77]. The result of a random fibre reinforced composite is a significant improvement in the overall multi axial mechanical properties over that of the pure polymer resin.

2.6.5 Fibre Reinforcement of Polyamide Composites summary

The effect of fibre length, diameter, dispersion and orientation have been well studied for the last few decades and are known to have a significant influence within a polymer matrix. However, further studies into this will not address any significant gaps in knowledge. An established commercial PA-GF grade used for automotive applications would incorporate all of the above variables for an optimised glass fibre reinforcement. Further development will have to come from a third additional phase to tailor mechanical properties.

2.7 Three Phase Material/Fillers

2.7.1 Fibre Hybrids

A hybrid reinforced polymer matrix consists of at least two different reinforcing materials [78]. A variety of reinforcing fibres could offer balanced reinforcement, for instance carbon fibres (CF) provide strong, stiff and low density reinforcement but are relatively expensive, while glass fibres are relatively cheap and have better fracture strain and fracture stress but lack stiffness [79].

Phua and Ishak [78] found that a polycarbonate reinforced with glass and carbon short fibres did not perform to expectation. The expectation was that, with the addition of carbon fibre, the strength will go up. This was not the case. SEM micrograph studies were conducted and it was found that glass fibre had good matrix interaction whereas carbon fibre had poor interaction. Charpy impact testing on PC with 40wt% CF had the lowest performance and a large amount of scatter for notched and unnotched coupons. When introducing more glass fibre as a replacement to carbon fibre, the performance starts to improve until 40wt% GF is reached. At this point, impact performance noticeably goes up with reduced scatter compared to 40wt% CF.

Anuar et al. [80] studied carbon and kenaf fibres in a thermoplastic natural rubber and polyolefin matrix. Total fibre content was fixed at 15% wt loading whilst ratios of carbon fibre to kenaf fibre were 100:0, 70:30, 50:50, 30:70, and 0:100. Mechanical testing showed composite grades with a single type of reinforcement were better compared to those of a hybrid composite.

Kasama and Nitinat [81] studied glass and sisal fibre in PP matrix, loading in wt.% of sisal and glass fibres were 20/10, 15/15 and 10/20wt.%. Results in Table 2-6 show no real significant improvement for fibre hybrids at different loadings which is also commented on in the conclusions of the paper.

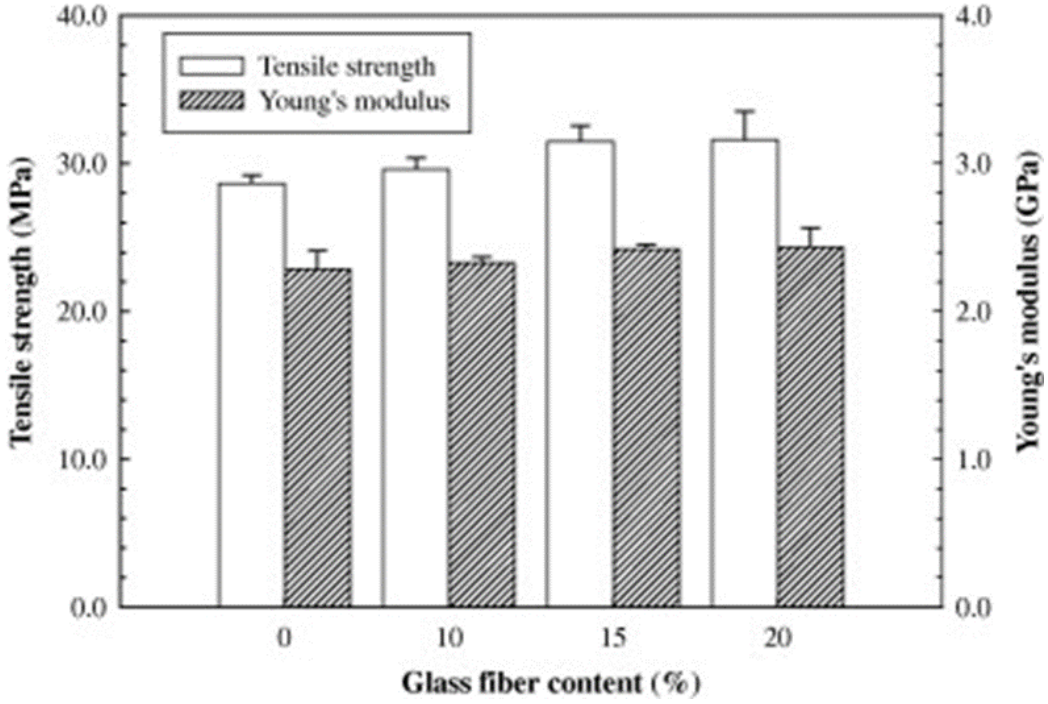

Figure 2-7: Effect of glass fibre content on tensile properties for a GF and sisal fibre hybrid in a PP matrix [81].

2.7.2 Elastomers Co-Polymers with Fibre Reinforcement

Three-phase composites that include glass fibre and a elastomer phase are well proven reinforcements in thermoplastic matrices, resulting in improved toughness and impact response [42], [82]–[87].

Mouti investigated two commercial grades of reinforced PA66, both with 35wt% of discontinuous glass fibre. One of the grades was rubber toughened to improve impact performance. Mechanical test results showed the addition of an elastomer modifier to reduce tensile and flexural strength by 35% and 36% respectively but to increase tensile and flexural strain by 37% and 43%, resulting in an improvement in toughness for the elastomer modified grade. Unnotched Charpy impact testing showed no significant difference in impact strength but, in drop tower testing, the glass reinforced PA66 started to fail at 3J whereas rubber toughened PA66 fails at 3.5J due to improved energy displacement [13].

Alsewailem and Gupta studied the effect of two types of rubber on the properties of glass fibre filled PA66. Styrene-Ethylene-Butylene-Styrene and Ethylene-Propylene elastomers grafted with maleic anhydride (SEBS-g-MA and EP-g-MA, respectively) were used to toughen the matrix composites. Mechanical testing found tensile and flexural strength decreased, whereas impact strength and elongation at break were found to increase with increasing rubber content in both cases. From results at 23.62wt% glass fibre loading without rubber filler, tensile strength is 134MPa, strain 6.8% and notched Izod impact 62J/m^2. For SEBS-g-MA, tensile strength reduced by 58.2%, whereas strain and notched Izod impact increased by 38.2% and 257% respectively. EP-g-MA tensile strength reduced by 52.2%, whereas strain and notched Izod impact increased by 13.2% and 286% respectively [88].

Glass fibre reinforced PA66 optimised for stone impact is a low flow velocity PA66 to suit an injection moulding process. It is reinforced using 35% short glass fibres to improve mechanical properties. “Optimised for stone impact” means that this is a development on the PA66 35% short glass fibres, as there is an elastomer modifier added to the matrix material to improve the matrix impact properties. The material stabilization gained is high resistance to heat aging but this is less suitable if high demands are required from the material’s electrical properties [43]. Figure 2-1b shows a current Cummins light commercial vehicle oil pan, injection moulded using PA66 optimised for stone impact. To gain an understanding of the unknown elastomer and volume loading in percentage, a study was conducted (the result of this study is not known as this was a BASF trade secret). Three promising types of elastomers used as toughening agents for polyamides were found when added as copolymers in addition of about 20-25wt.% in the form of small particles. These were Ethylene Propylene Rubber (EPR), Ethylene Propylene Diene Monomer rubber (EPDM) and Acrylonitrile Butadiene Styrene (ABS). The polyamides were copolymerised with the EPR and EPDM chains on the terminal amine groups of the polyamide. The graft copolymers produced aided dispersion, creating separate phases in the solid and enhancing interfacial adhesion

[5,18,19]. Some work has shown that PA6/ABS blends with imidised acrylic compatibiliser are extremely tough but show a discrete ABS phase dispersion in polyamides [83]. Another factor worth considering is water absorption of polyamide materials [91]–[93], which was found to have an influence on tensile properties of 35% glass reinforced PA66. It was found that, when completely saturated, strain increased by 36% to failure and tensile stress reduced by 48% [13]. However, flexure properties also showed an increase in strain of 14% and an increase in stress of 17%. Moisture barrier properties should be considered if the component requires high strength and stiffness to be retained for its application.

As polymers are being used to replace metal counterparts for weight reduction, it is worth discovering whether the current polymer composites still offer good weight saving versus metal counterparts for up to 120°C temperature applications. Glass fibre reinforced PA66 composites offer over an 80% weight reduction over steels, about a 50% weight reduction over aluminium and a 20% weight reduction over magnesium.

2.7.3 Nano Fillers

Nanocomposites are new materials produced in the last few decades made with fillers which have nanosize reinforcement. Nanosized inclusions are defined as those that have at least one dimension in the range 1 to 100 nm [94]. Therefore, a nanocomposite is a multiphase solid material where one of the phases has one, two or three dimensions of less than 100 nanometres (nm), or structures having nanoscale repeat distances between the different phases that make up the material [95]. An alternative three phase composite route could use nanofillers instead. This is becoming more established for structural enhancement as nanoparticles can be added during fibre addition as part of a melt compounding stage, at the same time as fibre addition, or as a separate master batch before fibre addition [96]–[98]. The major issue with nanoparticle addition is in scaling up for mass production, as nanoparticles have a tendency to amalgamate in any fabrication process that has material flow. Chemical

treatments are necessary for certain nanoparticles. For instance, different amino acids affect the interlayer distance of MMT. Figure 2-8 helps describe the effect of 12-aminolauric acid on layered clay to disperse layers which then allows the nylon matrix to flow between the clay layers [99].

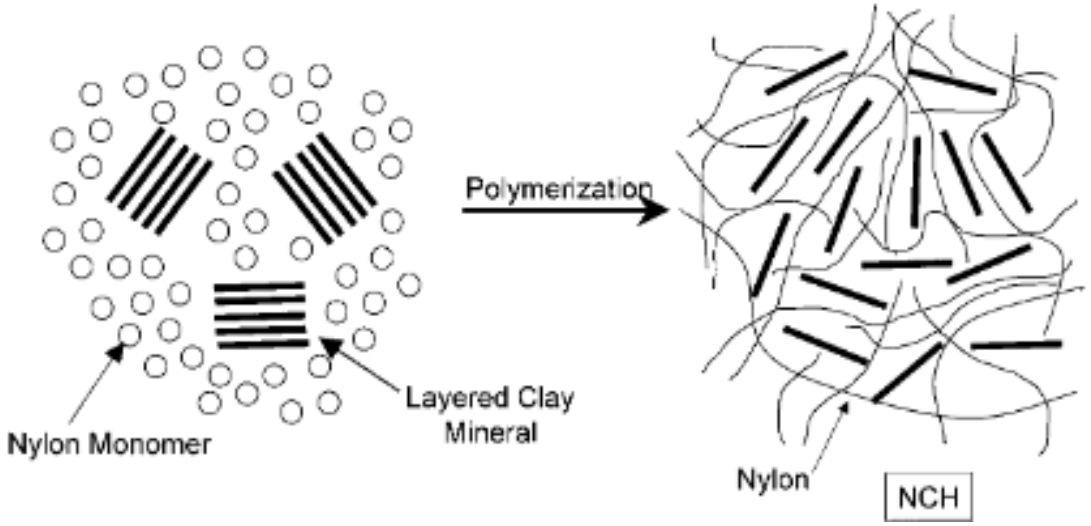

Figure 2-8 Before and after 12-aminolauric acid treatment producing a Nano Clay Hybrid (NCH) [99].

2.7.4 Three Phase Material/Fillers summary

Hybrid fibre reinforced matrices using two different materials have a high chance of being novel, but literature has shown that results can be the sum total of the negative qualities for each fibre material rather than the desired positive. Using an elastomer as an alternative third phase offers the improved toughness for the automotive application, though further development would have limited possibilities to be novel for this work. The current PA66/GF/Elastomer grade (BASF Ultramid A3WG7-OSI) used for oil pans does, however, set the minimum mechanical performance requirement for under the bonnet applications. There is currently no knowledge of a three-phase composite in which one of the fillers is in the nanoscale in an existing PA66/GF. The addition of nanofillers can be carried out in the same compounding stage as glass fibres which would also give a cost saving advantage over PA66/GF/Elastomer grade.

2.8 Polyamide Nanocomposites

Material system development will be one of the main objectives of this project. Routes that could be taken to improve the current material system could be nanoreinforcement of the matrix material or exploiting nano, in addition to fibre reinforcement, in order to address the current material deficiencies in a similar way to the addition of elastomer. The poor dispersion within a matrix material due to tendency of nanoparticle agglomeration will cause an issue with the use of nanomaterials [100].

2.8.1 Polyamide/Nano MMT nanocomposites

PA6 using nanoclays has been found to increase mechanical properties in key areas useful for automotive under bonnet applications. Developments of nylon clay hybrids (NCH) at Toyota Japan have found increased strength, modulus and heat distortion temperature over PA6. Toyota also considers impact strength to be comparable with a 2.4% reduction to PA6 on a Charpy impact test [21]. PA/MMT nanocomposites were typically reinforced with MMT in a range of 1-5wt.% additions [101]–[106]. Table 2-4 gives an overview of PA6 with different percentages MMT, which indicates an optimal MMT loading for strength and modulus improvement is around 4 to 5wt.% however Izod impact strength reduces with every increase of MMT so a trade-off for mechanical performance is likely to occur with a polyamide matrix that will also have glass fibres as a reinforcing filler.

Table 2-4: gives an overview of PA6 with different percentages MMT

	Properties										
	Tensile strength		Tensile modulus		Flexural strength		Flexural modulus		Izod impact strength	Charpy impact strength	Heat Distortion Temperature
	23°C	120°C	23°C	120°C	23°C	120°C	23°C	120°C	23°C	23°C	23°C
Units	MPa		GPa		MPa		GPa		J/m	KJ/m²	°C
Montmorillonite Filler PA6 Comparing temperatures 23°C and 120°C											
Pure PA6	68.6	26.6	1.11	0.19	89.3	12.5	1.94	0.29	20.6	6.21	65
Nylon 6-clay montmorillonite 4.7 wt. %	97.2	32.3	1.87	0.61	143	32.7	4.36	1.16	18.1	6.06	152
PA6-1/ODA-MMT molecular weight 18,000 room temperature test condition											
0 wt.% MMT	71.1 (±0.5)		-		84.2 (±0.5)		1.85 (±0.05)		31 (±1)	-	66.3 (±1)
2.8wt.% MMT	84.3 (±0.5)		-		121.6 (±0.6)		3.09 (±0.07)		28 (±1)	-	118 (±1.5)
4.3wt.% MMT	91.5 (±0.6)		-		130.1 (±0.7)		3.51 (±0.07)		25 (±1)	-	136 (±1.5)
6.6wt.% MMT	87.2 (±0.5)		-		134.6 (±0.7)		3.97 (±0.07)		23 (±1)	-	142 (±1.5)
PA6-2/ODA-MMT molecular weight 21,000 room temperature test condition											
0 wt.% MMT	71.6 (±0.5)		-		85.1 (±0.5)		1.89 (±0.05)		33 (±1)	-	66.7 (±1)
2.8wt.% MMT	86.7 (±0.5)		-		131.3 (±0.7)		3.25 (±0.07)		31 (±1)	-	122 (±1.5)
4.2wt.% MMT	95.3 (±0.6)		-		139.2 (±0.7)		3.83 (±0.07)		28 (±1)	-	141 (±1.5)
6.7wt.% MMT	91.5 (±0.6)		-		144.5 (±0.7)		4.26 (±0.08)		25 (±1)	-	148 (±1.5)

Okada and Usuki reviewed twenty years of polymer-clay nanocomposites and found that the mechanical property's saturation point was approximately 3.9wt.% addition of clay in a PA6 matrix. The 3.9wt.% addition of clay offered a 41% tensile strength and a 60% flexural strength improvement over pure PA6 [104]. Liu et. al. also produced a PA6/MMT nanocomposite compound using a twin-screw extruder to mix each grade and found that composites containing 3wt% of MMT in the PA6 matrix offered a 19% tensile strength and a 29% flexural strength improvement over pure PA6. A 5wt.% addition of MMT reduced tensile strength by 5% with a slight flexural strength improvement of 3% compared to pure PA6. When explained by TEM characterisation, it was found that the 3wt.% of MMT loading showed good dispersion capability in the PA6 matrix, based on the TEM observation. A 5wt.% of MMT loading also showed good dispersion capability in the PA6 matrix. Some domains of the TEM micrograph also found that it combined MMT clusters [107]. A reason why Liu

et. al. found clusters in their 5wt.% MMT could be that the twin-screw compounding process cannot effectively disperse MMT above 5wt.%. Further processing will be required to further disperse MMT in a polyamide matrix.

Chung et. al. worked on PA66/MMT nanocomposites produced using a twin-screw extruder. Results found that PA66 with 3wt.% MMT offered the highest tensile stress improvement of 15% compared to pure PA66 with a matrix saturation point somewhere between 3wt.% and 5wt.% with no significant difference in this range [105]. Chung et. al. also worked on PA66/3wt.% MMT with the addition of a 2wt.% and 4wt.% compatibilizer polypropylene-grafted-maleic anhydride (PP-g-MAH). The results showed a reduction in mechanical properties with high scatter at a 2wt.% addition due to the high hydrophilicity of PA66. The most interesting result was that Izod impact strength was reduced from 83J/m at 0wt.% loading by, with additions 2wt.% and 4wt.% compatibilizer, 65% and 64% respectively [105]. This may be explained by the fact that MMT is known to improve mechanical strength with little to no improvement in strain, resulting in a brittle material response to impact testing. Meszaros et. al. worked on pure PA6, PA6/MMT, PA6/basalt fibre (BF) and PA6/MMT/BF grades which were melt mixed using a twin-screw extruder. Grades that included MMT were in additions of 1wt.% and BF was in 30wt.% [106]. Both reinforcements (basalt fibres and MMT) offered tensile/flexural strength improvements which can be seen below in Figure 2-9.

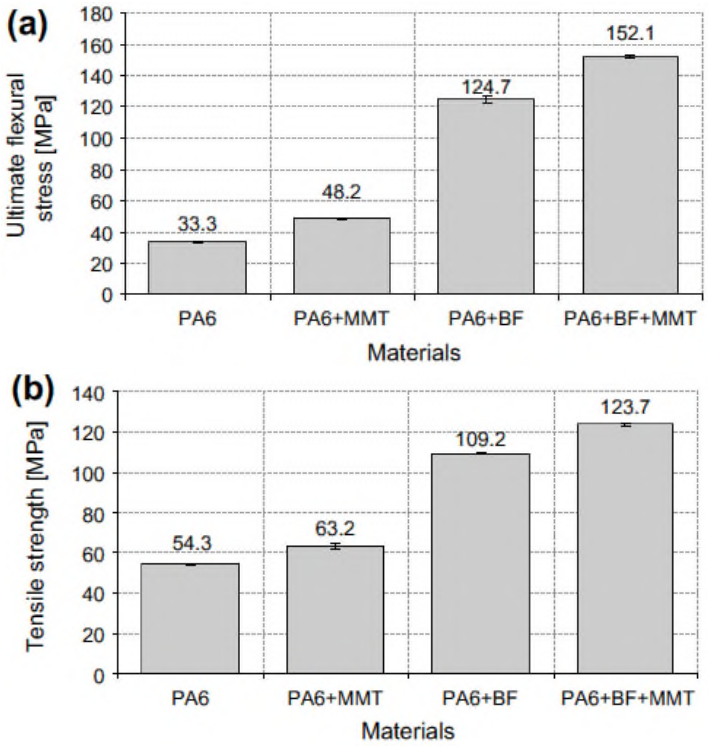

Figure 2-9 Results for each material grade: (a) flexural stress; (b) Tensile strength [106].

2.8.2 Polyamide/Nano SiO_2 nanocomposites

PA/SiO_2 nanocomposites are typically reinforced PA with SiO_2 in a range of 1-5wt.% additions [17], [108]–[110]. SiO_2 fillers were considered more challenging to fully and uniformly disperse within a polymer matrix. So the best surface treatment would have to be considered along with the optimum weight percent. PA6 using nano SiO_2 has been found to increase mechanical properties but is more effective when they have been functionalized using organosilanes to modify the surface of the silica [111]. An observation that can be made from the results in the stress/strain plot in the work undertaken by Mahfuz at al. [111] is that the strain is a third lower for functionalized nano SiO_2 PA6. This implies that it is likely to give poor impact resistance as toughness is more than halved. PA12 containing nano SiO_2 using two different fabrication processes can affect mechanical properties over pure PA12. Table 2-5 shows the effect of nano SiO_2 using two different preparation processes compared to pure PA12. D-nano SiO_2/PA12 is prepared by a dissolution precipitation whilst

M-nano SiO_2/PA12 is prepared by a mechanical mixing process. Both use 3% nano SiO_2. D-nano SiO_2/PA12 shows the best mechanical properties [100].

Table 2-5 shows the improvements nano SiO_2 offers over neat PA6.

	Properties					
	Tensile strength		Tensile modulus		Charpy impact strength	Elongation at break (%)
	23°C	120°C	23°C	120°C	23°C	23°C
Units	MPa		GPa		KJ/m²	%
Nanosilica Filler PA6 and PA12 room temperature test condition						
Pure PA6	210 ± 10		1.10 ± 0.10		-	-
1% SiO_2-PA6	285 ± 8		1.41 ± 0.15		-	-
1% SiO_2-silane PA6	370 ± 25		1.70 ± 0.17		-	-
Pure PA12	38.3		1.42		36.7	36.7
D-nanosilica/ PA12	46.3		1.98		40.2	40.2
M-nanosilica/ PA12	38.6		1.74		30.4	30.4

Xu et. al. studied the effect of two surface modifications; 3-aminopropyltriethoxy-silane (APS) and Hexamethyldisilazane (HMS) with an unmodified SiO_2 (UMS) on the mechanical properties of a PA66 matrix in additions of 1, 2, 3, 4 and 5wt.%. All test samples were produced by melt compounding using a twin-screw extruder. Results for UMS showed no significant improvement for tensile strength but reduced notched Charpy impact strength in increments for each increase in addition. Addition of APS offered the best tensile strength of 78MPa at 3wt.% addition, a 7% improvement over pure PA66, with no improvement for impact strength across all additions. Whereas addition of HMS produced a reduced tensile strength in increments for each additional increase. The best impact strength of 9kJ/m^2 was found at 3wt.%, a 45% improvement over pure PA66. The three different interfacial structures formed between nanofillers and matrix resulted in different mechanical properties of nanocomposites. Owing to the presence of flexible interfacial

layers, the addition of HMS and AMS, to some extent, could improve the material toughness. However, it was found that enhancement of final material toughness was also related to the density of PA66 chains grafted to nanoparticles surfaces [17].

Lu et. al. studied the effect of SiO_2 surface modified with hexamethyldisilazane in additions of 1wt.% and 3wt.%. It was seen that the tensile strength of PA66 increased by 7% with the addition of 3wt.% SiO_2. It was also noted that the tensile modulus increased significantly by 39% for both 1wt.% and 3wt.% additions. The nanocomposites also exhibited an increase in the elongation at break. For 1wt.% addition it increased by 58% and for 3wt% addition it increased by 72%. An observation for this was explained in terms of load transfer with higher nanosilica concentration, which facilitates plastic deformation [108].

Gendre et. al. studied the effect of unsurfaced modified SiO_2 in a 30wt.% glass fibre reinforced PA6 matrix (PA6/GF). SiO_2 was added at 0.5, 1, 1.5 and 3wt.%. 1wt.% SiO_2 was the only addition which showed an improvement in both tensile strength and modulus compared to PA6/GF composite [112].

2.8.3 Polyamide Nanocomposites summary

Both MMT and SiO_2 offer distinctive advantages in polyamide matrices in additions of 1 to 5 wt.%. It is currently unknown if MMT or SiO_2 would offer any improvement to polyamide matrices with a glass fibre reinforcement phase. It also not known if the same quantity of addition would give the best mechanical property performance. However, the study by Meszaros et. al. [106] on PA6/basalt fibre compared to PA6/MMT/basalt fibre illustrates that mechanical strength can be improved, even when a microfibre is also used.

2.9 Properties

2.9.1 Impact performance - stone impact

The stone impact phenomenon was the main focus of previous work which still holds relevance to this project when developing a new material system. A study was conducted in order to quantify the size of stone likely to cause damage to an oil pan, a search and a selection of random granite stones were collected from regular roads [1,5,69]. Although this project's main focus is structural development of the material system it is still very important to understand and test for impact. A new material system could detract from impact performance if the matrix material is developed. Impact damage is also a primary consideration for design and maintainability of aircraft composite structures. Low velocity impact damage to aircraft is due to both operational and maintenance activities. In the operational environment, there are typically few incidents of low velocity impact damage and most can be attributed to hailstone strikes and foreign object damage such as runway debris [113].

2.9.2 Thermo and Electrical conductivity

Commonly used plastics, such as polypropylene (PP) or polyamide (PA) are intrinsically electrical insulators with a low thermal conductivity. New applications, like heat sinks in electronic packaging, require new composites with higher thermal conductivity. By the addition of fillers to plastics such as metal particles or carbon nanotubes, the thermal behaviour of polymers can be increased significantly [114].

Thermal conductivity could be an important material property to understand as it will affect the oil temperature for both the oil pan and gearbox. Developing the matrix material system with filler can affect thermal behaviour [114] but, based on the low percentages of fillers that could be used, may not have that much effect [25,30]. Developing the matrix material system with layered, thin films could have a bigger effect as the layers could insulate and not allow heat to dissipate.

Typical gear failures like wear, scuffing, micro pitting and pitting are influenced by the oil temperature in the lubrication system. High temperatures lead to high viscosities and thus, thin lubricant films in the gear mesh with generally detrimental influence on performance leading to potential failure [116]. Low temperatures lead to low viscosities. This reduces oil flow, causing moving parts not to be sufficiently coated and protected by the oil. Table 2-6 demonstrates PA66 and PA66 composites having very low thermal conductivity compared to metals which would lead to high oil temperatures.

Electrical conductivity is a very important material property to understand when designing components in the electronics industry, as electrical conductivity can be desirable or non-desirable depending on the intended application. Polymers are generally poor conductors of electricity which is an advantage if insulating properties are required [117]. Electrical conductivity is considered of low importance for an oil pan application.

Table 2-6 an overview of materials thermal and electrical conductivity

	Stainless Steel	Low Carbon Steel	Aluminium Casting Alloy	Magnesium Alloy	PA66 Pure USX200	PA66 35%GF A3HG7	PA66 35%GF A3ZG7	PA66 30%CF CF300K
Thermal Conductivity (W/m-K)	16.5 [39]	49.0 [39]	135 [39]	91.5 [39]	0.274 [40] [118]	0.35 [43] [40]	0.35 [43] [40]	N/A
Volume Resistivity (ohm-cm)	0.0000738 [39]	0.0000223 [39]	0.00000559 [39]	0.0000106 [39]	1e+15 [40] [118]	1e+15 [43] [40]	1e+15 [43] [40]	1e+4 [40] [119]

2.9.3 Compounding of the three phase composite

In recent years, research on the effect of certain nanoparticle materials and shapes on an existing material system has grown. When compared with their near counterparts, the nanocomposites exhibit superior properties such as enhanced mechanical and thermal characteristics, improved barrier performance and wear resistance [17], [120]–[126]. A nanoparticle introduced as a third phase in a composite has a high chance of being novel due to the vast combinations of materials available. The existing PA66 reinforced with 35wt.%

glass fibre and elastomer improves impact performance as the elastomer increases toughness.

2.10 Key finding of the literature review

From this literature review, composite materials are still being used for under-the-bonnet applications as a replacement for metals. Composite materials such as short glass fibre reinforced PA6 and PA66 offer benefits such as weight reduction, excellent formability, noise reduction, corrosion and chemical resistance.

The use of short glass fibre reinforced PA6 and PA66 for engine covers, ducting and modules is ideal for their application, but the oil pan requires impact protection due to its location. The current grade PA66 with 35wt.% glass fibre used in the automotive industry now has a third elastomer modifier phase. The elastomer improves the strain performance of the PA-GF, thus improving impact performance. However, the addition of the elastomer adds more cost to the new grade, due to a second grafting process for the polyamide and elastomer. The elastomer also trades some of the mechanical strength of the existing PA-GF grade, so a possible alternative third phase that can retain mechanical strength and improve strain response to impact would have further automotive applications.

The effect of fibre in a PA66 matrix has great significance when considering material, diameter, length, volume, loading wt.% and dispersion but can be considered optimised in commercial grades such as BASF A3HG7 (PA66 with 35wt.%GF). Fibre hybrids are unlikely to be a valid alternative to an elastomer, as a best of both has not been proven for different combinations of fibre materials in a polyamide matrix. It is plausible to replace the elastomer third phase with an alternative reinforcing material in the nano scale.

To progress this work, benchmarking tests on the original BASF material grades need to be taken further by including elevated temperatures. This addresses the first gap in knowledge in this study.

The next question: Can the elastomer be replaced with a nanoparticle reinforcement and still have a similar or better performance? There are gaps in knowledge with relation to addition of nanofillers into a PA66-GF grade. There are several unknowns such as: What is the optimal addition in wt.% to offer any improvements when an existing microfibre is used as a primary reinforcing phase? What compounding routes and techniques can be successfully used to disperse and exfoliate the nanofillers in the PA matrix? What types of nanoparticles and material will offer any effect or improvement to an existing PA-GF composite?

Chapter 3. Benchmarking commercial PA-GF and PA-GF-elastomer grades

3.1 Introduction

The oil pan application is to collect and hold engine oil, this means constant elevated temperatures generated from the engine and returned oil. There were concerns about PA66-GF materials used for oil pans as the pans can be damaged by stone and other types of debris found on a typical road surface. Recent studies have proven PA66-GF with an elastomer third phase, increases impact performance when tested at a typical lab temperature of 23°C [6]–[8], [14], [127], [128]. Room temperature testing PA66-GF and PA66-GF-elastomer are well known however elevated temperatures are less established epically gas gun impact testing. This chapter goes on to take existing work further by benchmarking effects of temperature on the current PA66-GF and PA66-GF-elastomer grades used for oil pans. Temperature testing conditions of 23°C, 65°C, 90°C and 120°C where selected based on temperatures illustrated in section 2.2.1 in the literature review.

Benchmarking and understanding the effects of temperature on short glass fibre reinforced PA66 materials are important to understand as changes in mechanical properties will affect material suitability for application that involves heat. Therefore this chapter studies the effect of an elastomer modifier on tensile, flexural and impact properties of short glass fibre reinforced PA66 under thermal conditioning to determine the influence of temperature on quasi-static and dynamic properties.

3.2 Mechanical testing

3.2.1 Materials and tests sample preparation

Two commercial grades of polyamide 66 with 35 wt.% of discontinuous glass fibre, Ultramid A3HG7 and Ultramid A3WG7-OSI, (henceforth denoted as Material A and B respectively) were produced by BASF. BASF materials where supplied and injection moulded into test samples (tensile ISO 527 [129], flexural

ISO 178 [130] impact plaque ISO 6603 [131]) by Eaton ltd. Material B included rubber toughened and has been intimately melt-blended into the base PA66 material [13]. Details on samples can be found in Table 3-1 for material, shape and size.

Table 3-1 material data and sample type used

Material	Manufacturer	Product Code	Tensile shape/size	Flexural shape/size	Impact shape/size	Thickness
A	BASF	A3HG7	Type 1A	80x10mm	70x70mm	4mm
B	BASF	A3WG7 -OSI	Type 1A	80x10mm	70x70mm	4mm

3.2.2 Tensile tests

The testing followed ISO standard 527 shape type 1A [129], [132]. Test and material conditioning was done using different temperatures 23°C, 65°C, 90°C and 120°C. Each temperature was checked using a K-type thermocouple on the sample surface with a soaking time given to 65°C, 90°C and 120°C of 2, 4 and 6 minutes respectfully, before starting each test (this was to allow the core of the samples to reach the right temperature). To gain accurate strain data retro-reflectors where attached to the samples 50mm apart ±2mm to suit the sample type 1A gauge length in ISO 527-2[132]. Testing was conducted on an Instron 5500R screw driven universal test machine using a 30kN load cell and a laser extensometer. A data acquisition system was used to capture cross head movement, load cell and laser extensometer readings. Figure 3-1 shows the typical setup for a tensile test using grips, thermocouple and positioning of the retro reflective tape. The grips where nipped up as not much gripping force was required hold each sample preventing surface damage. A second set of grips were used for testing at high temperatures due to sample slipping requiring a finer gripping surface. The testing speed for all sample was 1 mm/min.

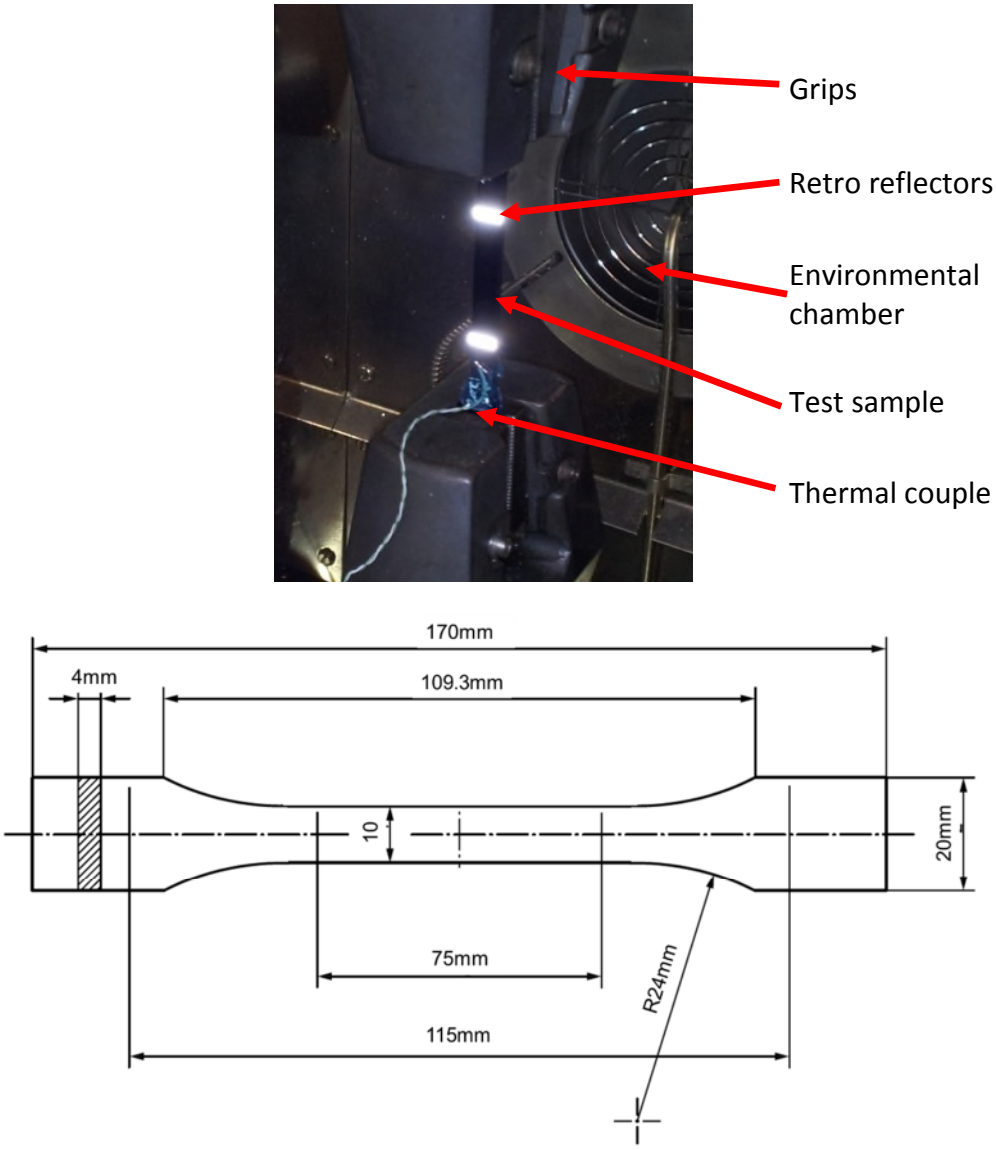

Figure 3-1 Above: Typical tensile setup using a laser extensometer with retro reflective tape to measure gauge length to the mid-point of the sample; Below: Schematic of type 1A tensile sample used in this work (taken from ISO 527-1 [129]).

3.2.3 Flexure tests

The testing was conducted following ISO standard 178 and all samples were tested at 2 mm/min [130]. Tests were done using different temperatures 23°C, 65°C, 90°C and 120°C. Each temperature was checked using a K-type thermocouple on the sample surface with a soaking time given to 65°C, 90°C and 120°C of 2, 4 and 6 minutes respectfully, before starting each test (this was to allow the core of the samples to reach the right temperature). Testing was

conducted on an Instron 5500R screw driven universal test machine using a 30kN load cell. Figure 3-2 shows the typical setup for a 3-point bending test. Samples (non-lubricated) were centralised on the two points and squared using a steel ruler.

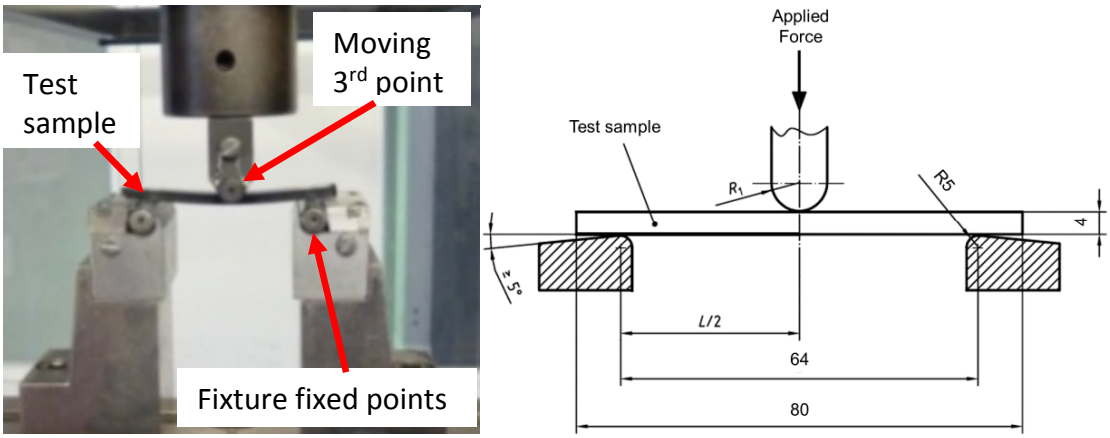

Figure 3-2: Left: Typical setup of a 3-point bending test; Right: Schematic of 3-point bending bar with dimensions (taken from ISO 178 [130]).

3.2.4 Low velocity impact tests

As there is no set standard related to gas gun testing previous work conducted on oil pans was used as a guide to setup, which included projectile selection and impact velocity which was linked to stone impact [6], [8], [13]. The gas gun testing equipment included an optical velocity measurement system mounted to the muzzle of the gas gun. Due to limited instrumentation for the gas gun setup displacement information could not be captured for each test. For repeatable targeting a class 2 laser held in a mounting block was used to sit in the barrel of the gun between shots to ensure accurate alignment to barrel centre. Gas gun setup and projectile can be seen in Figure 3-3a and b. Plaque fixture can be seen in Figure 3-3c and was designed to suit the plaque sample's leaving a 50x50mm window as the impact area. Answer recorded

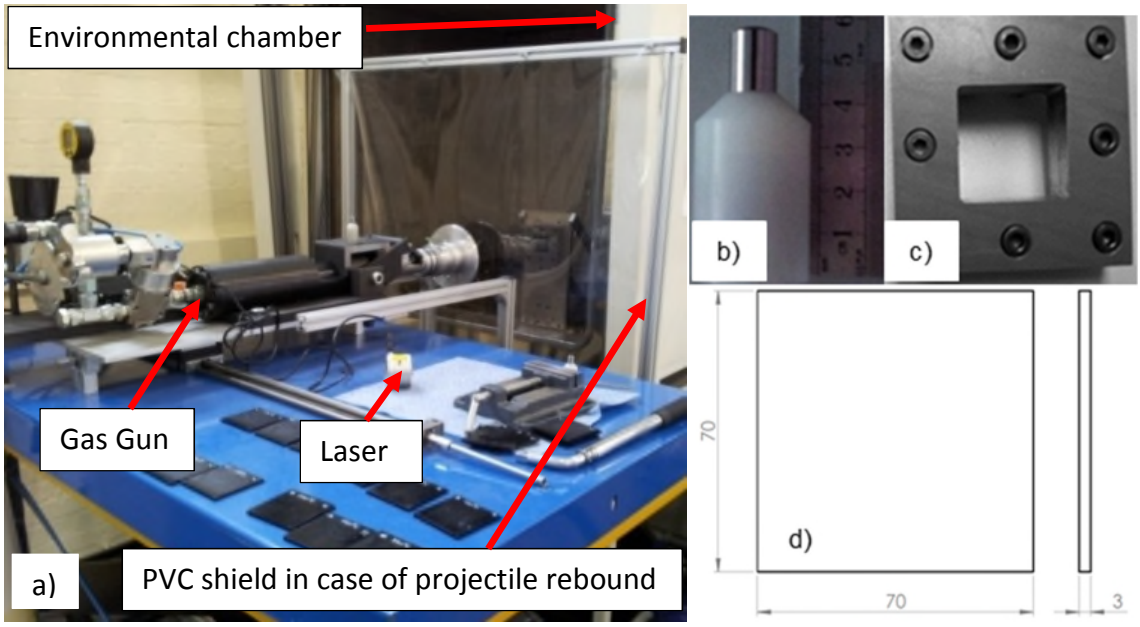

Figure 3-3 a) showing gas gun setup in front of environmental chamber b) shows projectile type selected for the testing c) window plaque fixture d) plaque schematic

The gas gun impact test was conducted using 10mm hemi-spherical projectile weighting 22g (Figure 3-3b). Testing was done using 7.5 J as an input impact energy which remained constant for all samples tested. The selection for 7.5 J was based on previous work conducted by Mouti *et.*al. [13] and the need for fracture damage on the samples, without destroying them, but to allow enough fracture to be assessed on the surfaces. As the gas gun could only detect velocity as a quantifiable output data the energy was worked out as a velocity of 26.11m/s for the projectile being used in the test, see equation (1). The impacts were reproduced at least three times per test for each material and temperature to be tested using a new plaque for each shoot. Testing was done over a range of different temperatures ranging from -20°C, 23°C, 65°C, 90°C up to 120°C. Temperature measurement was done for each impact test to ensure accurate testing using a K-type thermo couple on the plaque fixture which was monitored throughout testing and an infra-red thermometer was used to check the sample surface just before the shot. There are two reasons why the K-type thermo couple was used on the plaque fixture, one is to keep the probe away from the impact area and two is to provide a backup reading for the infra-red

thermometer. A soaking time given to -20°C, 65°C, 90°C and 120°C of 2, 4 and 6 minutes respectfully, before starting each test (this was to allow the core of the samples to reach the right temperature). Sample setup was done using an angle plate to hold the plaque fixture 90° to the gas gun barrel at a 400mm distance.

v = Velocity E = Energy M = Mass of projectile

$$v = \sqrt{\frac{E}{\frac{1}{2} \cdot m}} \quad (1)$$

3.2.5 Thermal conditioning

Environmental chambers where used for temperature conditioning for all tests. Tensile and flexure testing used the same chamber (operating range 23 to 150°C) which was designed to work with the Instron 5550R. Environmental chamber used with gas gun had operating range of -40 to 150°C. Before running each test a preheat time of 1 hour given to equipment and the fixtures to ensure test setup was repeatable. Materials were also given time to preheat this was to ensure the core of each sample was at temperature not just the surface.

3.2.6 SEM characterisation

Tensile fracture surfaces were analysed on a SFEG Philips XL30 field emission SEM. Fracture samples where parted off hand saw then carbon taped to sample stages before being sputter coated with gold-palladium.

3.3 Results and discussion

3.3.1 Effect of temperature on tensile strength

Tensile test data was taken from each material tested. Data from the laser extensometer was plotted in Figure 3-4 showing the relationship between stress and strain. Plots showed a clear difference between the two materials tested across the range of temperatures. Table 3-2 represents the tensile strength and

strain with extra information on tensile modulus for the two materials at the different temperatures tested. The stress-strain curves in Figure 3-4 can be linked to curve D in ISO 527 [129] which shows the typical stress-strain curves that are often plotted. The ISO 527 standard curve D represents tough materials without a yield point [129].

Table 3-2 results of tensile strength, modulus a strain worked as mean

Temperature (°C)	Material	Strength (MPa)	Strain (%)	Modulus (GPa)
23°C	A	149.1 ±0.4	3.3 ±0.2	5.5 ±0.1
65°C	A	107.2 ±1.9	5.2 ±0.3	6 ±0.3
90°C	A	94.5 ±0.8	5.3 ±0.1	5.2 ±0.5
120°C	A	80.8 ±2.1	4.9 ±0.2	4.7 ±0.4
23°C	B	114.4 ±0.3	4.1 ±0.2	4.5 ±0.2
65°C	B	87.8 ±0.4	9.6 ±0.2	4.5 ±0.2
90°C	B	81.2 ±44.5	10.1 ±5.5	4.4 ±2.4
120°C	B	73.7 ±40.4	11.4 ±6.2	3.7 ±2

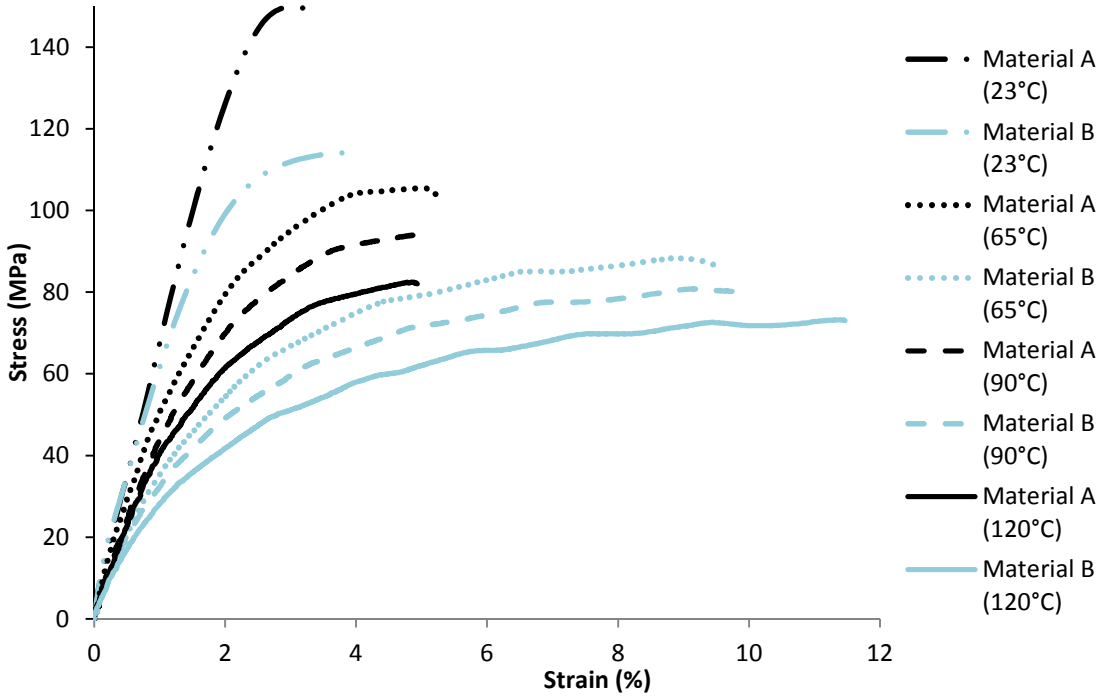

Figure 3-4 tensile stress-strain plot for materials A and B including temperatures tested

Testing results at 23°C, Material A performs better for tensile strength 149.1 MPa which is 23.3% better then material B 114.4MPa. Material A also performs

better for Young's modulus 5.5 GPa which works out 18.2% better then material B 4.5 GPa. Material B's maximum strain is 4.1% which is 25% over material A's 3.3%. There is a clear difference in how the elastomer modifier in material B can affects toughness by allowing the material to achieve higher strain before failing but loses maximum stress when compared to material A. As the gain in strain was much higher than a loss in stress for material B the elastomer used for toughening proved to offer an improvement to its toughness at 23°C. Results for material A at 23°C were in agreement with results by Mouhmid et al [41] projecting what 35% glass fibre tested at 20°C was likely to be. There was disagreement in the values when comparing both A and B to work done by Mouti [13] under similar conditions. Sample storage could account for some of the discrepancies found in the testing samples. Where mechanical performance could have degraded from a two year shelf life and moisture pickup, due to improper package sealing. This reasoning can be backed up from the effect of water uptake results by Mouti [13] having similar results to testing done 23°C in this work. Under tensile testing conducted by Mouti [13] testing speed was 2mm/min which may also effect the test results when compared to testing speed in this work that was done at 1mm/min following ISO 527.

At 65°C testing, material A now reads 107.2 MPa of stress with a strain of 5.2% with almost no tailing off before failing. 65°C test results show a clear reduction to maximum stress 28% sustained and a 58% increase to the strain compared to Material A at 23°C. The curve has a slight kink at 80 MPa and second kink just before reaching 107.2 MPa before failing. Material B's stress strain curve steadily increments to about 87.8 MPa of stress with a strain of 9.6%. There is some tailing off before failing but this could be related to kinks (waviness) across the curve. 65°C test results showed a clear reduction to maximum stress 23% sustained and a 134% increase to the strain compared to Material B at 23°C. The curve has kinks at 40 MPa, 65 MPa, 76 MPa and 84 MPa before failing at 87.8 MPa. Testing results at 65°C, Material A performs better for tensile strength 107.2 MPa which is 18.1% better than material B 87.8 MPa. Material A also performs better for Young's modulus 6 GPa which works

out 25% better than material B's 4.5%. Material B's maximum strain is 9.6% which is 44.8% over material A's 5.2%.

90°C testing, Material A's stress strain curve steadily increments to about 94.5 MPa of stress with a strain of 5.3%, there's almost no tailing off before failing. 90°C test results show a reduction to maximum stress 36.6% sustained and a 61% increase to the strain compared to Material A at 23°C. The curve has slight kinks, 42 MPa and 90 MPa, producing slightly noticeable waviness to the plot before failing at 94.5 MPa. This curve is more similar to Material A at 65°C than Material A at 23°C. Material B's stress strain curve steadily increments to about 81.2 MPa of stress with a strain of 10.1%, there's almost no tailing off before failing. 90°C test results show a clear reduction to maximum stress 29% sustained and a 206% increase to the strain compared to Material B at 23°C. The curve has kinks at 54 MPa, 64 MPa, 72 MPa, 78 MPa and had 80 MPa before failing at 81.2 MPa. This curve was similar to Material B at 23°C but has a notable waviness to curve shape which is almost exactly the same as Material B at 65°C. Testing results at 90°C, Material A performs better for tensile strength 94.5 MPa, which was 14.1% better than material B's 81.2 MPa. Material A also performs better for Young's modulus 5.2 GPa which works out 15.4% better than material B's 4.4 GPa. Material B's maximum strain was 10.1% which is 50.5% over material A's 5%.

120°C testing, Material A's stress strain curve steadily increments to about 80.8 MPa of stress with a strain of 4.9%, there's almost no tailing off before failing. 120°C test results showed a clear reduction to maximum stress, 45.8% sustained, and a 48% increase to the strain compared to Material A's at 23°C. The curve has slight kinks at 60 MPa and 74 MPa producing waviness to the plot before failing at 80.8 MPa. This curve was similar to Material A's at 65°C and 90°C. Material B's stress strain curve steadily increments to about 73.7 MPa of stress with a strain of 11.4%, there's almost no tailing off before failing. 120°C test results show a clear reduction to maximum stress 35.6% sustained and a 245% increase to the strain compared to Material B's at 23°C. The curve has kinks at 32 MPa, 50 MPa, 60 MPa, 64 MPa, 76 MPa and 73 MPa before

failing at 73.7 MPa. This curve is similar to Material B's at 23°C but has a notable waviness to curve shape which was almost exactly the same as Material B's at 65°C and 90°C. Testing results at 120°C, Material A performs better for tensile strength, 80.8 MPa, which is 8.8% better than material B's 73.7 MPa. Material A also performs better for Young's modulus, 4.7 GPa, which works out 21.3% better than material B's 3.7 GPa. Material B's maximum strain is 11.4% which is 57% over material A's 4.9%.

Material A's Temperatures 65°C, 90°C and 120°C show consistency with each other for their curve characteristic with a 10% stress step between each temperature increase when comparing to 23°C. Strain results for all tests done on material A fail within a 3.3 to 5.3mm range of 23° to 120°C suggesting material A has good stiffness across a range of different temperatures. Material B's curves share similar shape characteristics with each other with decreases in stress and strain in expansion related to increases in heat. Temperatures 65°C, 90°C and 120°C show waviness in the plotted results. This could relate to the thermal chamber turning on and off to regulate the temperature for the experiment and which could introduce an oscillation effect in the results. With increases of temperature Material B becomes more ductile and less stiff with a decrease in tensile strength. Temperature clearly affects properties of the Material A. This can be seen in Figure 3-4 stress versus strain. 23°C results perform the best out of all the temperatures tested demonstrating better toughness. Temperatures 65°C, 90°C and 120°C show a 28% to 46% in tensile strength reduction to 23°C which means a loss in toughness is affected by the increase of temperature. The results from material A testing do go in line with expectations where an increase in temperature is likely to reduce tensile strength. Load and stress were likely to decrease with an increase in temperature and extension and strain will react less as the material is stiffer without being impact modified.

Temperatures also clearly affect the properties of material B as well when looking at Figure 3-4 stress versus strain. 23°C results perform the best out of all the temperatures tested for strength but not for extension as this increased

the most at 120°C offering about the same level of toughness for each temperature tested. Temperatures 65°C, 90°C and 120°C show a 23% to 36% in tensile strength reduction to 23°C which means a loss in toughness is affected by the increase of temperature. The results from material B testing do go in line with expectations where an increase in temperature is likely to reduce tensile strength. Tensile stress was also likely to decrease with an increase in temperature and extension and strain will increase from the material becoming more ductile. This information also demonstrates the trade-off's in the mechanical properties of the two materials when one of the materials has been modified with an elastomer. Linking the tensile results for each temperature tested to an application subjected to elevated temperatures does raise some concern for material A as loss in strength which could translate into a reduce impact performance. Whereas as material B is more fit for purpose due to increased toughness for all temperatures tested.

Testing at high temperatures 90°C had some issues that can be related to failure where material B samples would slip in the grips. To compensate for this, the grips were done up tighter but the issue still occurred and became more of an issue at 120°C. This issue was fixed by replacing the grip wedges with wedges with a finer gripping surface. A reason why this may have happened is the elastomer in material B makes the matrix softer at high temperature allowing the samples to slip out of the grips which could translate as a wear issue depending on the material application. The effects of temperature on the wear of PA6 has been studied by Watanabe and Yamaguchi [133] observed maximum friction is temperature dependent for nylon and was found that samples slide continuously at some fixed velocities, 0.1 mm/s at 100°C, which is similar to the test speed in this work of at 0.017 mm/s (1mm/min) at temperatures 90°C and 120°C. The shear strength of nylon becomes larger as the sliding velocity increases because nylon is a viscoelastic material as observed by Watanabe and Yamaguchi [133]. As the matrix material in this work is PA66 rather than PA6 studied by Watanabe and Yamaguchi material A with the addition of glass fibre was less affected than martial B with the extra

addition of an elastomer which has similar results as PA6 under similar conditions. The tensile failure mechanism was a single break with no necking or strain marks at the fracture point for all samples tested. The failure itself can be defined as a brittle fracture in agreement with Mouhnid et al [41] and can be explained by the contribution of the glass fibre as a brittle tough material.

3.3.2 Effect of temperature on flexural strength

Flexural test data was then plotted in Table 3-3 and represents the flexural strength and strain with extra information on modulus for the two materials at the different temperatures tested. The stress-strain plots in Figure 3-5 show the results for the materials and temperatures tested. The stress-strain curves in Figure 3-5 can be linked to curve B stated in ISO 178 [130] which shows the typical stress-strain curves that are often plotted. Curve B represents samples that gives a maximum and then breaks before the conventional deflection.

Table 3-3 results of flexural strength, strain and modulus worked out as mean

Temperature (°C)	Material	Strength (MPa)	Strain (%)	Modulus (GPa)
23°C	A	255.3 ±1.6	5.8 ±0.1	5.2 ±0.1
65°C	A	162.8 ±1.4	6.4 ±0.2	5 ±0.2
90°C	A	141.6 ±2.4	6.2 ±0.1	4.5 ±0.3
120°C	A	122.3 ±1.4	6 ±0.1	4.6 ±0.1
23°C	B	190.9 ±1.8	8 ±0.1	4.3 ±0.1
65°C	B	120.8 ±1.1	9.5 ±0.4	3.7 ±0.1
90°C	B	106.9 ±1	10 ±0.4	3.2 ±0.1
120°C	B	87.8 ±1.9	11.3 ±0.5	3.3 ±0.1

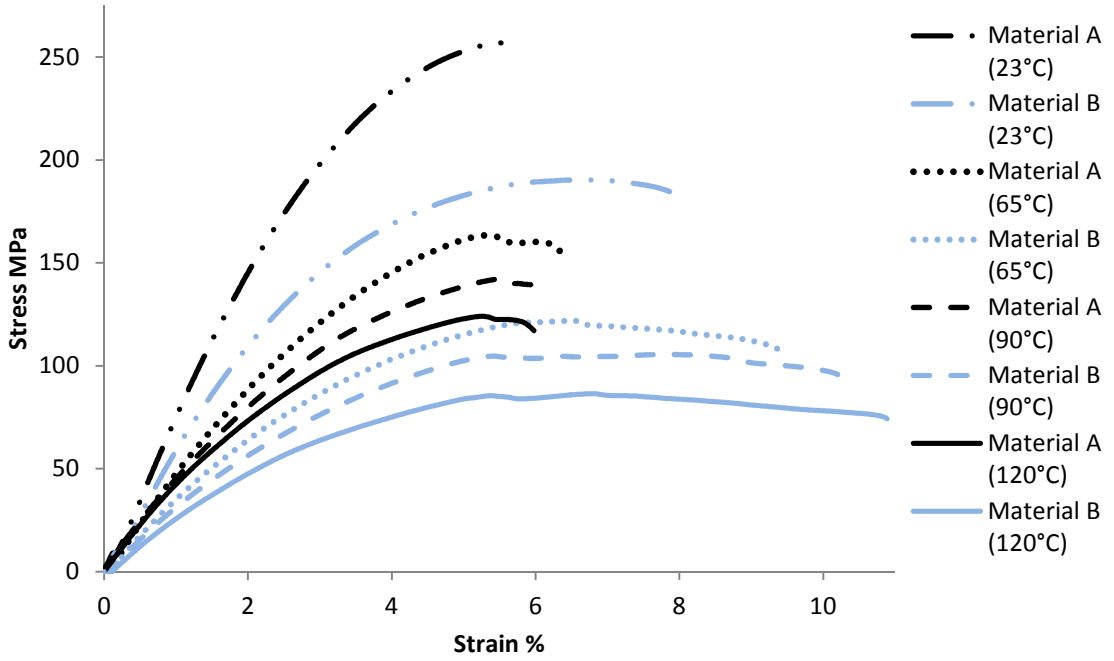

Figure 3-5 flexure stress-strain plot for materials A and B including temperatures tested

Testing results at 23°C using results in Table 3-3, Material A performs better for flexural strength, 255.3 MPa, which is 25.2% better than material B's 190.9 MPa. Material A also performs better for Young's modulus, 5.2 GPa, which works out 17.3% better than material B's 4.3 GPa. Material B's maximum strain is 8% which is 27.5% over material A's 5.8%.

Testing results at 65°C using results in Table 3-3, Material A performs better for flexural strength, 162.8 MPa, which is 25.8% better than material B's 120.8 MPa. Material A also performs better for Young's modulus 5 GPa which works out 26% better than material B's 3.7 GPa. Material B's maximum strain is 9.5% which is 32.6% over material A's 6.4%.

Testing results at 90°C using results in Table 3-3, Material A performs better for flexural strength, 141.6 MPa, which is 24.5% better than material B's 106.9 MPa. Material A also performs better for Young's modulus 4.5 GPa which works out 28.9% better than material B's 3.2 GPa. Material B's maximum strain is 10% which is 38% over material A's 6.2%.

Testing results at 120°C using results in Table 3-3, Material A performs better for flexural strength, 122.3 MPa, which is 28.2% better than material B's 87.8 MPa. Material A also performs better for Young's modulus 4.6 GPa which works out 28.3% better than material B's 3.3 GPa. Material B's maximum strain is 11.3% which is 46.9% over material A's 6%.

There is also an obvious stress difference for material A and B tests done between 23°C and 65°C which could be put down to the temperature increase of 42°C between the 23°C and 65°C set of tests. The maximum stress difference of Material A at 23°C to 65°C is 35.3%, for 65°C to 90°C is 12.7%, for 90°C to 120°C is 14.6%. The maximum stress difference of Material B at 23°C to 65°C is 37.5%, for 65°C to 90°C is 12.5%, for 90°C to 120°C is 17.1%. Material A showed little variation to strain from each temperature tested compared to each temperature tested on material B. This can be put down to the elastomer filler which allows material B to strain further when temperature is increased, whereas material A has some stability most likely gained from the addition of glass fibre in a PA66 matrix.

Temperature clearly affects properties of the material A. This can be seen in Figure 3-5 stress versus strain. 23°C results perform the best out of all the temperatures tested demonstrating better stiffness. Temperatures 65°C, 90°C and 120°C shows a 36% to 52% in flexural strength reduction to 23°C which means a loss in toughness and is effected by the increase of temperature. Material stiffness can be considered good as the average strain works out at 6.1% with a deviation of ±0.3%. The results from material A testing were in line with expectations where an increase in temperature is likely to reduce tensile strength, load and stress were likely to decrease with an increase in temperature and extension and strain will react less as the material is more stiff without being impact modified.

Temperatures also clearly affect the properties of material B as well when looking at Figure 3-5 stress versus strain. 23°C results perform the best out of all the temperatures tested demonstrating better toughness and stiffness.

Temperatures 65°C, 90°C and 120°C show a 37% to 46% in flexural strength reduction to 23°C which means a loss in toughness is affected by the increase of temperature. The results from material B testing do go in line with expectations. The expectation was increases of temperature were going to make the material more ductile reducing flexural strength load and stress but increasing extension and strain before failure. Material A shows better strength to material B but has much lower strain values making material A less tough then material B. This can be seen in Figure 3-5. The test results also demonstrate the trade-off's in the mechanical properties of the two materials when one of the materials has been impact modified with an elastomer. Material B demonstrates the best flexure toughness which is likely to translate into the best impact performance for the oil pan application.

There were two types of sample failures that occurred during testing. One type of failure was a full snap where the sample brakes in two halves. This only happened to three samples when testing material A at 23°C. The other type of failure was a partial snap (see Figure 3-6) which was how all other samples failed in the testing. Figure 3-6 illustrates the partial snap failure mechanism where sample experiences a compression and tensile functions at the same time. The sample fails as a tensile rupture on the bottom surface when maximum deflection is reached. Whereas top surface does not fail as part of the rupture but does buckle and blister allowing the sample to deflect and remain intact even though it has failed.

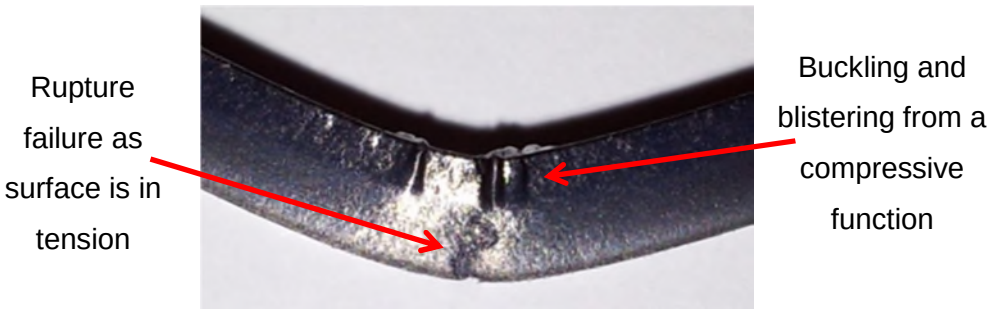

Figure 3-6 showing one of the failed material B specimens from 120°C testing

3.3.3 Morphology studies

SEM micrographs were taken of the fracture surface of the samples used in tensile tests. See Figure 3-7a-h for material A and Figure 3-8a-h for material B from SEM test results. The results are of the two materials at the different temperatures tested to gain some insight of the failure mechanism. The predominant failure mechanisms are fibre deboning (pull out) and matrix plastic deforming (ductile pulling/tearing). Fibre pull out, matrix plastic deforming and matrix brittle fracture is evident across all micrographs taken of material A. Matrix pull away, fraying and plastic deforming is evident across all micrographs taken of material B. SEM micrographs for material A illustrate fibre pull out, matrix brittle fracture, matrix plastic deforming are types of failures that can be found on material A's tensile testing samples. Fibre failure is a less common failure; see Figure 3-7a which shows fibre debris which has a different characteristic to a shear cutting function from the fibre shredding stage when the material was first compounded.

Figure 3-7a-b material A at 23°C shows fibre pull out and brittle matrix fracture in which can be found across most of the fracture surface. Fibres being pulled out have a very thin layer of matrix on them. This could have allowed stress to reach 149.1 MPa due to the matrix having some fibre adhesion. Small areas of matrix plastic deforming could be found but would account for a fourth of the cross sectional area of the sample. A brittle matrix fracture could have contributed to the high tensile strength sustained by the sample at 23°C compared to other temperatures tested for material A.

Figure 3-7c-d material A at 65°C shows fibre pull out with some traces of matrix brittle fracture across different areas of the surface. The fibres that have been pulled out have a very thin layer of matrix on them in the matrix brittle fracture areas. Areas of matrix plastic deforming could be found but would account for a half of the cross sectional area of the sample. The matrix plastic deforming of these areas appear to be larger than what can be seen in Figure 3-7a-f with clean fibre pull out.

Figure 3-7 e-f material A at 90°C and Figure 3-7g-h material A at 120°C show very similar micrographs to each other with fibre pull out, plastic deforming and textured matrix surfaces. This could be seen across the sample's cross section. The fibres being pulled out can be seen to have deposits of matrix material this has likely reduced excessive fibre pull out length compared to test done at 65°C. The matrix appears to be more texture and pitted compared to the sample tested at 65°C. This could have propagated the lower stress and strain results seen in Table 3-2 and Figure 3-4. There were also no signs of brittle fracture which could be seen in 23°C and 65°C, this would suggest that material A has a higher brittle transition point than glass fibre reinforced PA6 tested by Kroll [87]. This also possibly explains why there is a more textured matrix surface seen for temperatures 90°C and 120°C.

SEM micrographs for material B illustrate matrix coated fibre pull out, plastic deforming, matrix voids and matrix fraying are types of failures that can be found on material B's tensile samples. All micrographs taken of material B shows matrix has strong bonding to the glass fibres for each test temperature.

Figure 3-8a-b shows almost no fibre pull out with matrix plastic deforming and fraying which make up the majority of the fracture cross sectional area of the sample. The frayed plastic deformation of the matrix can be put down to the elastomer modifier used in material B.

Figure 3-8c-d for temperatures 65°C shows similar results to testing done at 23°C. However this where the elastomer modified PA66 in material B shows a far greater bond to the GF. This is to say GF no longer pull out from the matrix but the matrix itself is pulling away with GF see Figure 3-8d.

Figure 3-8e-f at 90°C and Figure 3-8g-h at 120°C show very similar micrographs to each other with low fibre pull out as most of the matrix is fully bonded to the fibre surface causing the matrix to fail instead of the GF Some matrix plastic deforming can be found but is not so common.

The effect of elastomer in PA66 short glass fibre matrix results in different failure functions for tensile testing with better surface adhesion to glass fibres which may have contributed for the longer extensions gained for material B. Not forgetting the nature of elastomers having the ability to stretch better then thermosets and thermoplastics and having less strength which has most likely allowed the tensile samples to extend further (higher strains) before failing at lower loads. Voids in the matrix are easily found in material B temperatures 90°C and 120°C. Assuming voids are present in tests conducted at 23°C and 65°C where the fraying does look fibrous which maybe causing its own elastomer fibrous pull out leaving voids from a fibrous ripping function. The fibrous ripping function producing voids is a similar argument made by Bascom et al [91] which can be summed up as dispersion of soft inclusions in a rigid matrix and as a result of dilatation and elongation processes the post-failure fracture surfaces exhibit holes or cavities where the deformed and ruptured particles have relaxed back into holes larger than the original particle size.

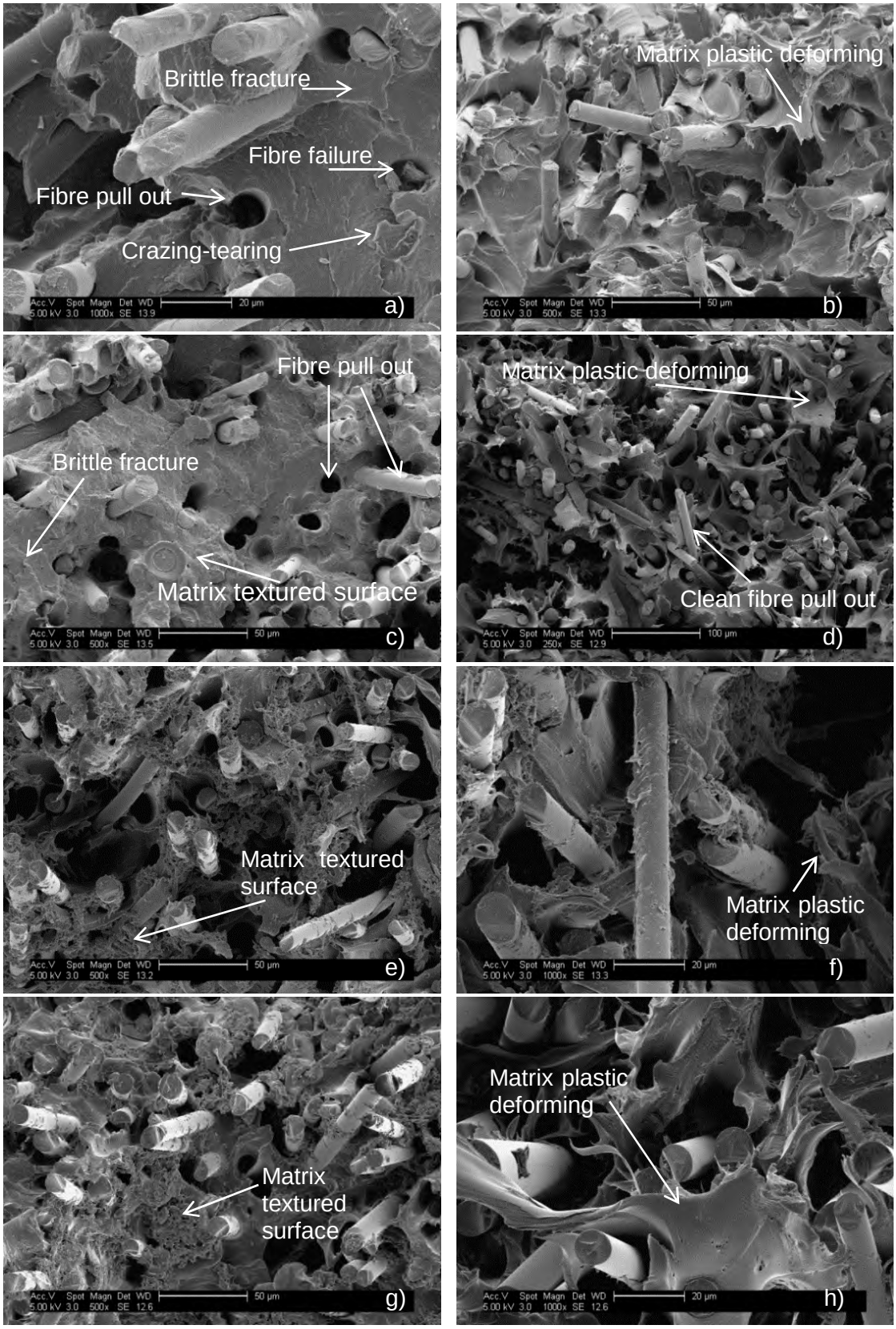

Figure 3-7 SEM micrographs of the fracture surface of material A tensile testing. Temperatures are split up into groups: a-b 23°C; c-d 65°C; e-f 90°C; g-h 120°C

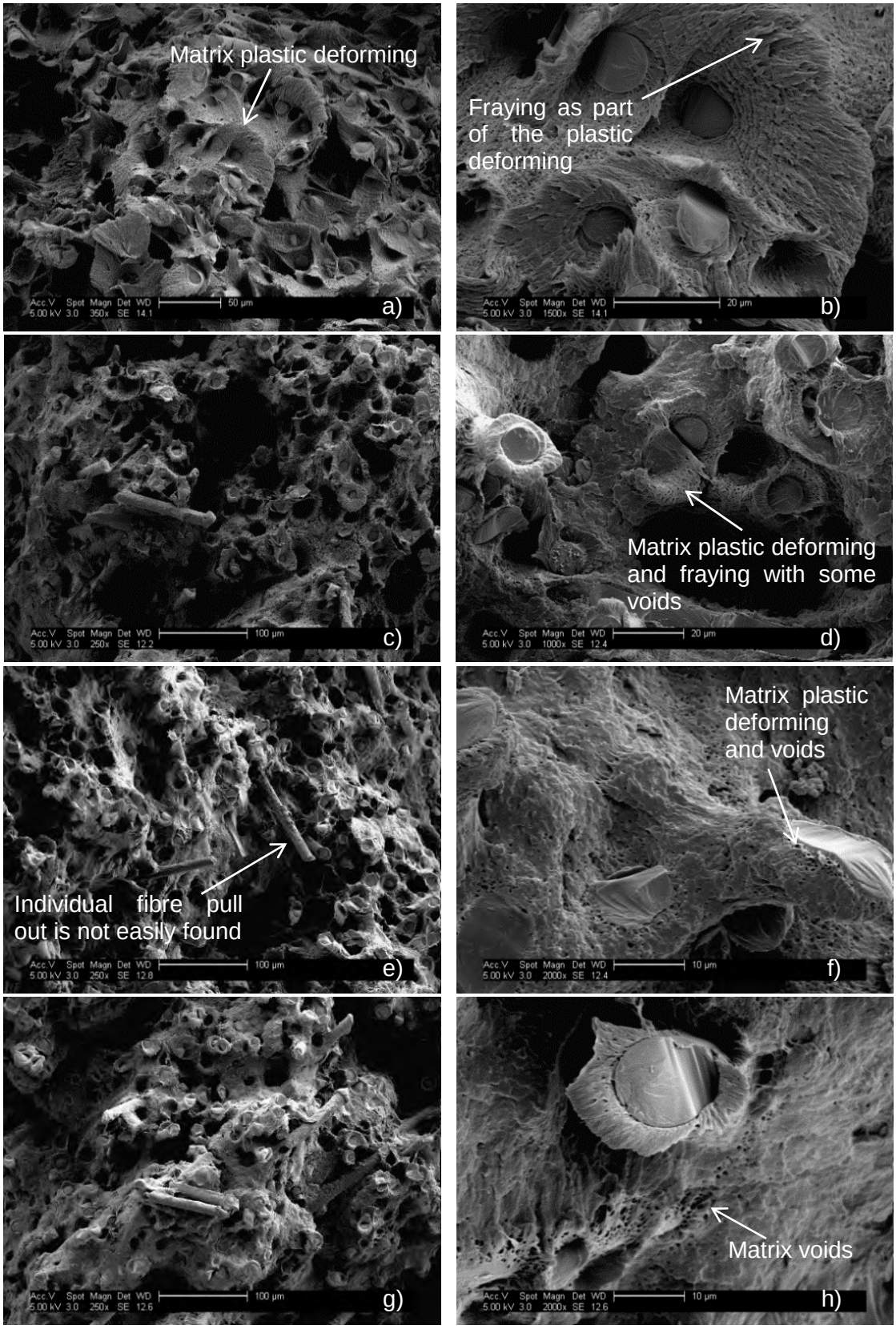

Figure 3-8 SEM micrographs of the fracture surface of material B tensile testing. Temperatures are split up into groups: a-b 23°C; c-d 65°C; e-f 90°C; g-h 120°C

3.3.4 Effect of temperature on low velocity impact testing

The effect of elevated temperature on low velocity impact testing is an important variable that has proven to reduce tensile and flexure stress for both materials outlined in this chapter. Due to the gas gun setup having an environmental chamber with a refrigeration unit (cooling function) -20°C was added to the testing. Testing at -20°C will give some inside on if the impact performance as the oil pan application will have a requirement to be used in countries that have sub-zero climates. An early expectation based on stress-strain results in Figure 3-4 and Figure 3-5 would be that material A would show increased fracture damage for each increase in temperature. Whereas materials B fracture damage would only slightly drift as elevated temperatures increased stain which may compensate for the reduction in stress.

Damage assessment was conducted visually across the non-impacted face of each sample. Size was measured by a steel ruler along crack length and the characterising shapes are represented as characters from the alphabet (X, T, Y and I). Table 3-4 provides assessment for all samples that have cracked from the impact testing with results and image links to pictures taken of the damage to the sample surface. Figure 3-9 images (a-o) capture the range of impact damage for material A. Figure 3-10 images (a-o) capture the range of impact damage for material B. On all samples that showed surface damage from cracking identified in Table 3-4 results section had initiated crack propagation inline of the impact surfaces point to the initial contact of the projectile. This is likely to be a result from the projectile having a 10mm hemi-spherical point which focuses impact energy as a point through the material which fails as a tensile strain rupture when the material cannot dissipate the energy. This is a similar discussion to testing conducted by Bartus and Vaidya, where the same impact response was observed on samples that had been impacted using conical projectile compared to a flat point [134].

Table 3-4, Figure 3-9, Figure 3-10 and images (a-o) which show a trend that crack propagation reduces when testing temperature is increased from

23°C to 120°C for both materials. Material A testing temperatures -20°C and 23°C showed only a small effect when comparing impact damage which manly failed as a X shape with 30 to 40mm rupture length. -20°C to 23°C could be a brittle phase for the matrix material where a decrease in temperature has little effect to crack propagation. Pettarin et al. investigated low temperature impact fracture data of thermoplastic elastomer modified polymers and determined a brittle to ductile transition point when impact testing results show little change below -30°C [135]. Material B at -20°C has no significant increase in performance over material A and would suggest the elastomer modifier in material B has a negative effect which could be caused by embrittlement of the elastomer modifier which has been observed in elastomers at low temperatures [135], [136]. This is likely to be causing some embrittlement making material B less effective at low temperatures where is starts to perform similar to material A. However when comparing material B at 23°C to material A there is a reduction in fracture propagation by 40% based on combined fracture surface length. At 65°C both material A and B now fail as a single rupture both with a reduction in total fracture length by 64% and 71% respectively when compared to 23°C. Testing at 90°C material A now has 80% reduction in total fracture length compared to the 23°C results. However material B now effectively dissipates impact energy though increased strain as see in Figure 3-4 and Figure 3-5 stress-strain plots. As a result material B at 90°C has no visible surface damage except for one result B3 seen in Figure 3-10(image i) which can be dismissed due to impact energy was 7.9% over the required 7.5j. Impact conducted on material A at 120°C can still fracture the sample surface and fracture length has reduced by 88% when compared to impact at 23°C. Once again material B dissipated the impact resulting in no surface damage.

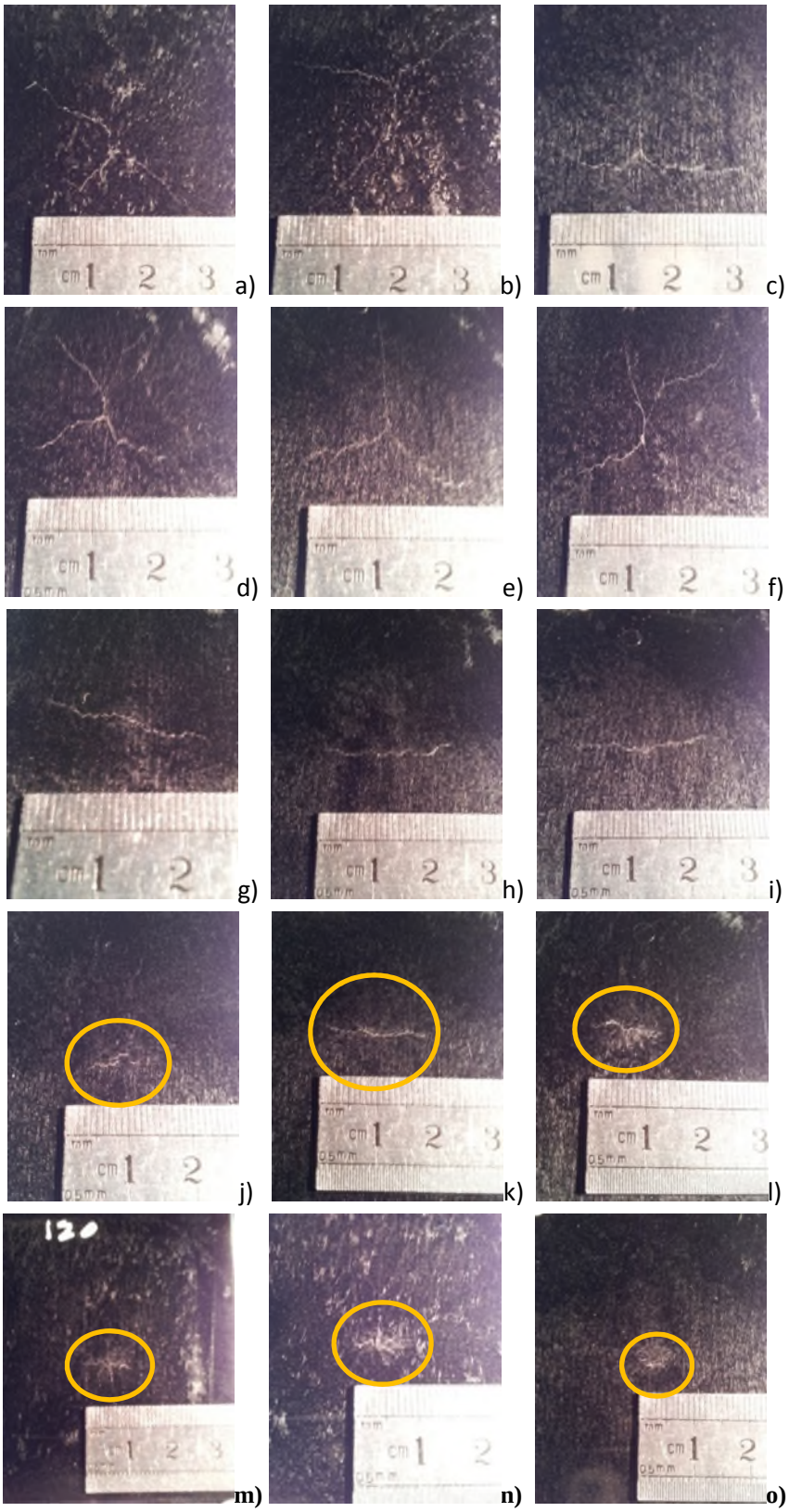

Figure 3-9 shows images of material A results from gas gun testing. Temperatures are slit up into groups: a-c -23°C; d-f 23°C; g-i 65°C; j-l 90°C; m-o 120°C

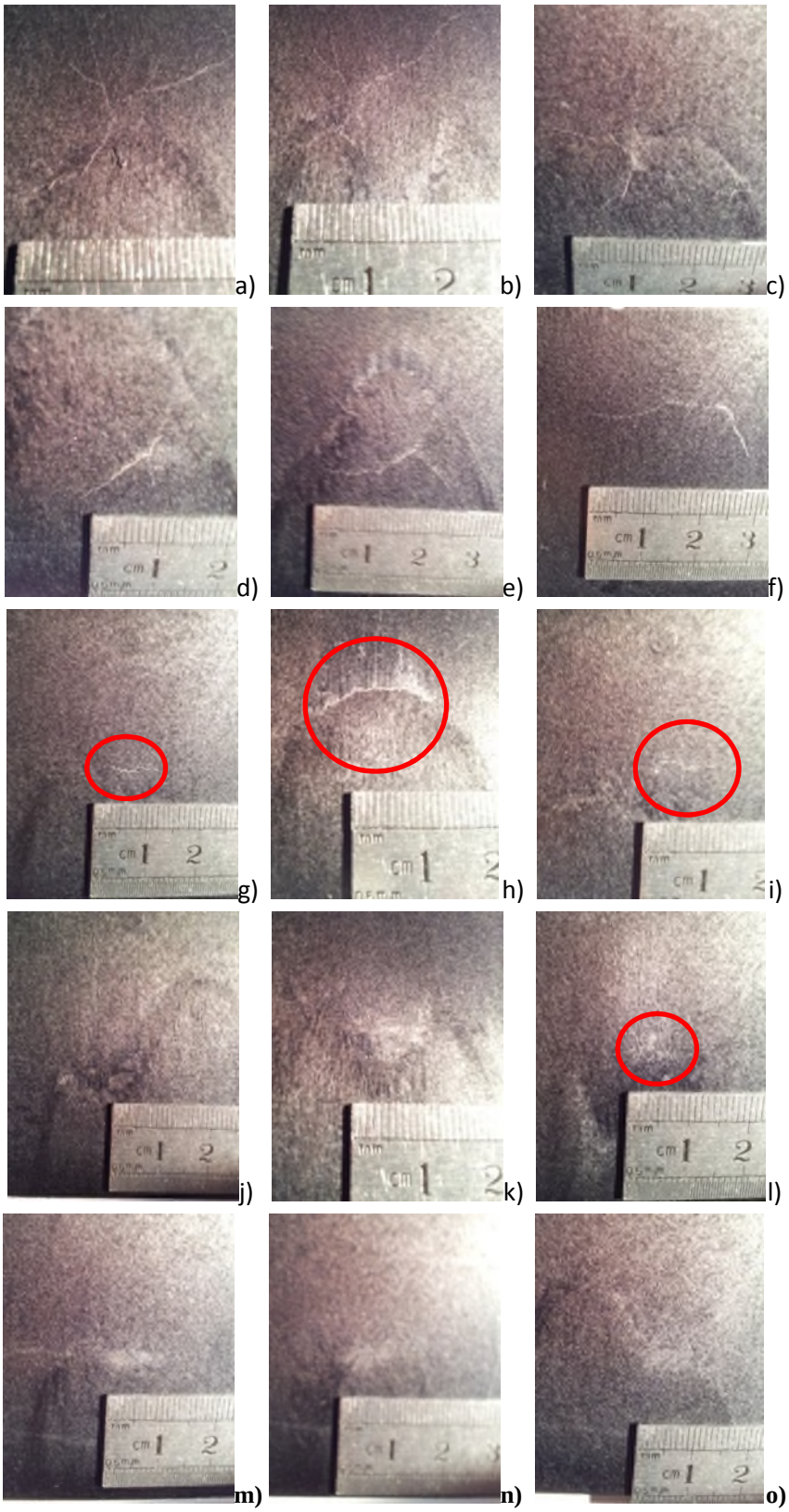

Figure 3-10 shows images of material B results from gas gun testing. Temperatures are slit up into groups: a-c -23°C; d-f 23°C; g-i 65°C; j-l 90°C; m-o 120°C

Table 3-4 Gas gun impacts on plaques across different temperatures and damage assessments on impacted plaques

Material	Temperature	Energy	Fracture length	Shape	Image
	°C	J	mm		
A-1	-20	7.52	35-36	X	Figure 3-9 image a
A-2	-20	7.58	38-40	X	Figure 3-9 image b
A-3	-20	7.59	20-32	T	Figure 3-9 image c
B-1	-20	8.22	33-40	X	Figure 3-10 image a
B-2	-20	7.79	30-40	X	Figure 3-10 image b
B-3	-20	7.41	30-30	X	Figure 3-10 image c
A-1	23	7.36	31-32	X	Figure 3-9 image d
A-2	23	7.12	30-35	Y	Figure 3-9 image e
A-3	23	7.18	30-37	X	Figure 3-9 image f
B-1	23	7.36	7-26	Y	Figure 3-10 image d
B-2	23	7.88	9-30	Y	Figure 3-10 image e
B-3	23	7.30	11-28	Y	Figure 3-10 image f
A-1	65	6.74	22	I	Figure 3-9 image g
A-2	65	6.68	24	I	Figure 3-9 image h
A-3	65	7.68	25	I	Figure 3-9 image i
B-1	65	7.61	13	I	Figure 3-10 image g
B-2	65	6.94	6	I	Figure 3-10 image h
B-3	65	7.70	13	I	Figure 3-10 image i
A-1	90	7.75	9	I	Figure 3-9 image j
A-2	90	8.21	17	I	Figure 3-9 image k
A-3	90	7.74	12	I	Figure 3-9 image l
B-1	90	7.56	No visual Damage		Figure 3-10 image j
B-2	90	8.17	No visual Damage		Figure 3-10 image k
B-3	90	8.09	2-3	T	Figure 3-10 image l
A-1	120	7.64	9	I	Figure 3-9 image m
A-2	120	7.21	5-6	X	Figure 3-9 image n
A-3	120	7.77	3	I	Figure 3-9 image o
B-1	120	7.29	No visual Damage		Figure 3-10 image m
B-2	120	7.65	No visual Damage		Figure 3-10 image n
B-3	120	7.47	No visual Damage		Figure 3-10 image o

3.3.5 Impact Failure Mechanism

The samples that failed as a surface crack propagated as a single tensile fracture. The rupture characteristic and size is a result of the energy that could not be dissipated through the material. The inclusion of different temperatures helped distinguish the impact performance of the two materials as surface rupture propagation and branching was reduced for each increase in temperature. Both materials reacted the same way to the increases of temperature but Material B showed and demonstrated a better impact performance to Material A. The improved impact performance (seen as reduced surface cracking) at elevated temperatures for Material B can be contributed to the elastomer modifier allowing the PA and elastomer matrix to strain more thus dissipates more impact energy, a similar finding to Mehrabzadeh and Burford with a PA11 with optimised amount of nitrile rubber [137]. This meant elastomer allowed the material to dissipate impact energy and effectively giving the material damping property. This damping property is likely to become more effective when the elastomer takes on more heat allowing the material to become more ductile. At temperatures below 23°C the elastomer no longer offers the material system any advantage over material A. To explain material B's drop off in impact performance compared to temperatures above 23°C, a brittle tough transition point that occurs in elastomer materials at low temperatures [138].

Although material A reacts the same as material B for impact testing when temperature is increased crack propagation goes down. Mechanical test results are completely different suggesting material A has a different energy dissipation characteristic. This may be an linked to the semi crystalline structure of PA's [139] where the crystalline structure is resisting strain increase of quasi-static nature of the tensile and flexural loading. Impact testing may not be experiencing this issue and reacts with amorphous structure instead. With an increase in temperature where the amorphous structure of PA becomes more plastic when it takes on more heat the semi crystalline structure maybe still resisting the tensile and flexural under quasi-static loading but impact testing

not experiencing this issue but reacts to the amorphous structure becoming more plastic allowing the sample to flex reducing impact damage. Material B may also have this effect of semi crystalline structure of PA but is unaffected as the elastomer allows the sample to flex. The increased flex found with material B could also be contributed to polymer chains having more freedom of movement due the elastomer used is likely to be amorphous. This would be expected as amorphous materials over their Tg become more plastic. Another effect of temperature in relation to the polymer chains have greater freedom of movement at elevated temperatures, allowing greater freedom of movement to dissipate impact energy. At lower temperatures polymer chains have freedom of movement.

The failure (surface fracture) from the impact testing conducted only shows up on the non-impacted face as a tensile rupture see Figure 3-11. The damage mode was initiated at the point of projectile impact as a result of the 10mm hemi-spherical point of the projectile acting as a focal point for impact energy. Energy that cannot be dissipated from the impact event resulted as a crack branching failure (load path). The extent of the branching can be linked to the amount of energy that cannot be dissipated meaning a high energy release will produce multiple branches and will be long in length, whereas a low energy release will result as a single branch small in length. Figure 3-11 illustrates the failure mechanism of the sample being hit by a projectile as a cross section. The sample deforms in a 3-point flexural manner but fails in a different way due to a larger surface area spreading the impact energy. Surface crack occurs when excess energy can no longer strain/flex the plaque sample causing a rupture on the non-impacting surface due to a tensile function. The more energy used the larger the surface crack and rupture becomes until total failure is reached.

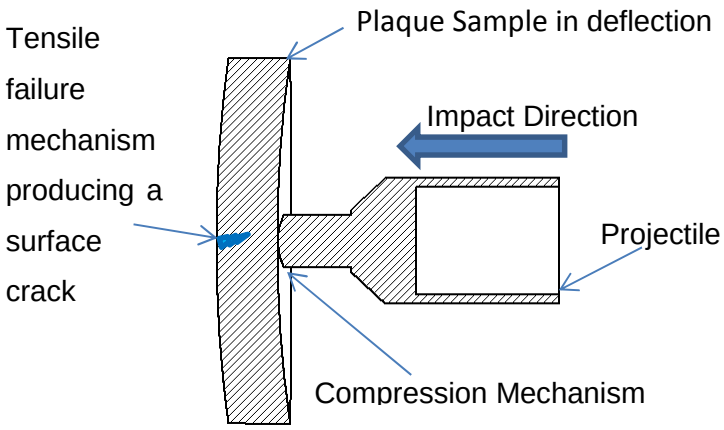

Figure 3-11 Cross section illustration of the failure mechanism

3.4 Conclusions and gaps in knowledge addressed

In this study, the influence of temperature on tensile and flexural properties of short glass fibre reinforced PA66 have been investigated. Several conclusions can be made from the results from the tensile, flexure and impact testing conducted which are as follows:

The use of material A would be better suited to structural applications as it demonstrated the least amount of deflection and remained close to the 5.2% strain range for each temperature tested for tensile and a 6% strain range for flexural. Whereas material B strain increased with an increase in temperature as to be expected due the addition of an elastomer, removing some of the stability that glass fibre offered to PA66. This would make Material B better suited to applications that require better impact resistance. Material A exhibits the best strength and modulus across each temperature tested. Material B exhibits the best deflection and maximum strain giving it a larger area in the stress/strain plots resulting in material B being tougher than material A. Testing conducted at 23°C gained the best toughness properties for both the materials whereas increases in temperature from 23°C up to 120°C reduced toughness properties for material A. Material B would have lost toughness when stress reduces, but levels out as strain increases with every temperature increase so toughness remains almost the same for each temperature increase. The test result also demonstrates the trade-off's in the mechanical properties of the two

materials when one of the materials has been impact modified with an elastomer. In this case mechanical strength is reduced for material B but gained much higher strain across all temperatures tested. Material B can be considered more ductile as maximum strain has a larger range when temperature is increased. Clear differences in material properties and plots can be observed in all results. The addition of an elastomer in a PA66 glass fibre matrix at elevated temperatures 90°C and 120°C has highlighted a surface ware issue which will affect its uses in translation and rotational applications.

SEM micrographs from fractured tensile samples demonstrated the elastomer in material B had better glass fibre adhesion allowing higher strain and extension which give the material system more toughness and which also improved with each increase in temperature as the elastomer became more effective. The addition of elastomer weakened material B's total strength compared to material A. Material A loses surface adhesion as temperatures were increased shown as long fibre pull out as well as cleaner fibres from pull out.

The influence of temperature on impact fracture of short glass fibre reinforced PA66 was investigated. The 7.5J impact energy proved to be an optimal energy when testing the two materials across the different temperatures. Material B exhibits the best impact performance at higher temperatures but is less affected by temperatures lower than 23°C due to a brittle transition point of the elastomer modifier. Both materials tested -20°C failed mainly with an X shape and similar size than any other temperature. This means there is no particular advantage for both materials if a low temperature application is required.

Chapter 3 adds to current knowledge epically to Eaton Ltd, as this work validates Eaton's material selection for an oil pan component material that operates at elevated temperature as part of its function. Impact performance at elevated temperatures using a gas gun to simulate a stone impact has only been studied at room temperature before this.

Chapter 4. Experimental, Melt compounding of 3-phase nanocomposites using a twin screw extruder

4.1 Introduction

Glass fibres (GF) are used to reinforce engineering thermoplastics such as polyamide (PA) which are extensively used under-the-bonnet as replacement to structural metal components [14], [15], [127]. Some under-the-bonnet components such as an engine oil pan are located close to the road surface which makes it subject to stone and other debris impacts. Such impacts can cause the failure of the 2-phase PA/GF composite grades. The latest development to address this issue is the addition of elastomers as a third phase to increase composite impact performance through increased material strain. This results in improvement in toughness of the material [8], [127]. Referencing back to Chapter 3 compares tensile stress/stain of PA66/GF with elastomer modified PA66/GF. In this example, the elastomer modifier reduces stress by 23.4% but increases strain response by 48.2% this trade-off improves the total toughness for the elastomer grade.

Studies into nano reinforcements could offer a similar performance improvement as a replacement to the elastomer phase. The addition of nano reinforcements can be introduced during the same compound process as glass fibres, this can minimize the processing costs. Current 2-phase nanocomposites when compared pure matrix exhibit enhanced mechanical and thermal properties, with improved barrier performance in PA6 and PA66 grades [17]–[20], [22], [23], [140]. Indeed, it is known that an addition of up to 5wt.% of inorganic nano-particles in polymers is enough for a considerable improvement in the material's mechanical properties compared to micro fillers, which require about >20wt.% [24]–[28]. A typical two phase polymer reinforced composite material system often consists of a polymer matrix and second reinforcing material which can be fibres or particles. The matrix holds the reinforcement while the reinforcing material improves different material properties of the matrix which in most cases is mechanical performance. To the best of author's

knowledge, there is lack of published literature in the area of effect of nano materials as a third phase to PA66 and GF composite. The interaction between matrix, GF and nano reinforcements could be minor or significant and may not offer an improvements, but have unintended negative effects instead.

In this study there are two types of nanoparticles of interest, organically modified montmorillonite (OMMT) and fumed silica (SiO_2). Both were readily available and can be cost effective as they are relatively cheap and could be easily added to the melt compounding process before or during the addition of glass fibres. The majority of published work that considers melt compounded PA nanocomposites [106], [141]–[145] are exclusively two phase considering OMMT, SiO_2 and other nanoparticles as a second phase reinforcement in PA matrices. Two papers that consider a matrix reinforced with fibres in the micro scale and nanoparticles as a third phase are; Mészáros et al. [106] who studied short basalt fibres (BF) and OMMT reinforcements in a PA6 matrix and Vlasveld et al. [141] studied woven glass or carbon fibres and SiO_2 in a PA6 matrix. Mészáros et al. [106] demonstrated extensive work showing PA6/BF/OMMT has improved by 13.3% tensile strength and modulus by and 9.8% over PA6/BF proving that nanoparticles can replace the elastomer phase. Cho and Paul investigated melt compounding nano clays into a PA6 matrices of which one was PA6 with 30% GF, similar to what is intended in this work. Limited results were given on their PA6-GF-organoclay, however results did show an improvement on modulus and yield strength by 48% and 31% respectfully over an PA-GF [146].

4.1.1 PA/OMMT nanocomposites

PA/OMMT nanocomposites are typically reinforced with OMMT in a range of 1-5wt.% [106], [101]–[105]. Studies found that PA66 with 3wt.% offered the highest tensile stress improvement of 15% compared to pure PA66 with a matrix saturation point somewhere between 3wt.% and 5wt.% with no significant difference [105]. Another study related to compounding of PA6/OMMT nanocomposite using a twin-screw extruder to mix each grade

found that composites containing 3wt% of OMMT in the PA6 matrix offered a 16% tensile strength and a 45% flexural strength improvement over pure PA6 [106].

4.1.2 PA/SiO_2 nanocomposites

PA/SiO_2 nanocomposites are typically reinforced with SiO_2 in a range of 1-5wt.% [17], [108]–[110]. Studies found the effect of SiO_2 surface modified with hexamethyldisilazane 1wt.% and 3wt.% offered tensile strength of PA66 increased by 7% with 3wt.% SiO_2. It was also observed that the tensile modulus increased significantly by 39% for both 1wt.% and 3wt.% SiO_2. The nanocomposites also exhibited an increase in the elongation at break by 58% for 1wt.% SiO_2 and 72% for 3wt.% SiO_2. Lu et al. explanation for this finding was an efficient load transfer with higher nanosilica concentration, which facilitates plastic deformation [108].

4.1.3 Compounding polymer matrix composites

Compounding using a twin screw setup is known to produce homogeneous melts when using micro filler materials, but the biggest challenge is the dispersion and exfoliation of nano fillers. Cho and Paul [146] found that a single pass compounding process using a twin screw extruder results in non-extensive exfoliation of clay in a PA6 matrix. They also found that a second pass can reduce amalgamation but undispersed tactoids are still easily observed. On the other hand, they also found slight improvement in the tensile strength and modulus of the organoclay composite produced by the second pass but no improvement in the elongation at break and Izod impact strength [146]. Other studies have found good exfoliation with some aggregates for PA/OMMT nano composites produced from a high concentration master batch, then diluted into grades [18], [106], [147]. A study by Stade [148] demonstrated fibre length reduction can occur for high fibre length/diameter ratios of the fibres and can also occur by extruding PA66 containing 30 and 50wt.% GF in a Buss compounding machine. Other processing variables that are also documented in other studies include processing speed, shear and screw setup. Lin et al. [149]

studied the structure development of MMT inside a PA66 matrix during melt mixing in twin screw extruder, with two screw configurations and two screw speeds (400 and 1000rpm). Configuration one included two kneading block sections and configuration two was setup with multi process element sections and one kneading block section. XRD studies found MMT compounded with screw configuration one exhibited better exfoliation than those from configuration two that can be contributed to increased shear from the increased processing speed. XRD studies also found that at higher screw rates (1000rpm), the [001] orientation characteristic peak of clay disappears, indicating better dispersion of clay with in the matrix material [149]. Both the configuration one and the 1000rpm screw rate contributed to improve the mixing efficiency as this creates high shear, which facilitates initial breakup of clay agglomerates. Benedito et al. [150] investigated the dispersion of multiwalled carbon nanotubes (MWCNT) into a polyurethane (TPU) matrix using two different screw designs, S1 and S2. Design S1 was setup for high-shear with kneading blacks and distributive elements and design S2 was setup with dispersive, distributive and back conveying elements. The results showed that the S1 design with processing speeds of 200 and 600rpm resulted in agglomeration densities of 0.16 and 0.15% respectfully [150]. This was a 50% improvement over the S2 design at 600rpm and a 70% improvement over the S2 at 200rpm. Although Lin et al. [149] and Benedito et al. [150] have worked with different matrices and nanoparticles, both studies reported that a twin screw extruder setup with kneading block sections and high screw speeds result in improved dispersion and exfoliation.

This study was set out to find if OMMT and SiO_2 can be compounded evenly that is to say dispersed and exfoliated into an existing PA66 matrix with GF. The influence of GF during compounding may help the dispersion of nanoparticles with possible negative effect of glass fibres reducing in length as well. It is considered that nano reinforcing materials in 2-4% loading can replace the elastomer and offer a similar performance. The addition of nano materials can be done during the glass fibre compounding phase, reducing compounding

costs compared to grafting of elastomer as an extra process cost. Other benefits could also be gained including reduced material weight, cost, wear, moisture absorption and improvements on thermal stability.

4.2 Materials

PA66 reinforced with 35wt.% glass fibre (PA66/GF), Radici grade Radilon A RV350LW 393 NER (henceforth denoted as RV350LW), used in this work was supplied by Vantage Polymers Ltd (UK). The first nanoreinforcement material was organically-modified montmorillonite Dellite 43B and was procured from Laviosa Minerals S.p.A. (Italy). Dellite 43B is montmorillonite modified with a quaternary ammonium salt (dimethyl benzylhydrogenated tallow ammonium). The second nanoreinforcement material is Aerosil R 812S, hydrophobic fumed silica (SiO_2) after treatment with hexamethyldisilazane (HMDS), and was procured from Evonik Industries (Germany).

4.3 Compounding and injection moulding

In this study a two-step melt compounding methodology was adopted (master batch followed by final grades) to disperse and exfoliate the nano fillers. A two-step melt compounding process will also enable high volume production at an industrial level. Figure 4-1 illustrates the inputs and outputs for the master batch followed by the grade processing. XRD and SEM characterisation studies were then conducted on injection moulded samples as this would represent the final fabrication route for short fibre reinforced components used in the automotive industry.

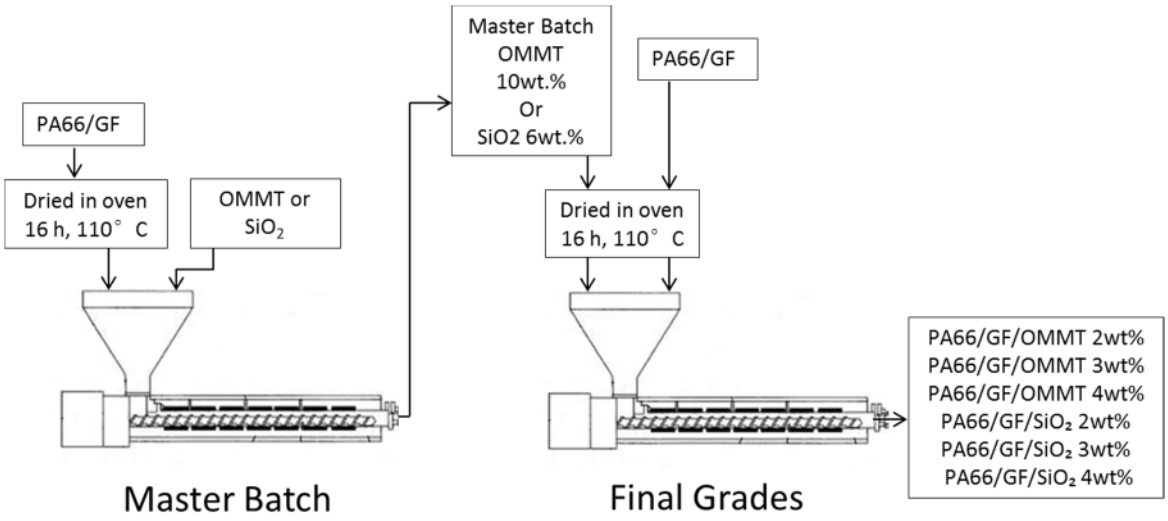

Figure 4-1: Flow diagram illustrating master batch and grades processing

4.3.1 Master batch processing

All master batch compounding was done by Ian Butterworth at Cranfield University. RV350LW pellets were dried in an oven for 16 hours at 110°C before processing. Each master batch was melt compounded using a Rondal 21mm benchtop twin screw extruder (UK). Figure 4-2 illustrates screw setup and gives details on mixing elements. Processing screw speed was maintained at 100rpm. From hopper to die, the barrel temperature was set to [235-285-285-285-260]°C, die temperature was set 25°C lower than the mid zones as a feasibility study showed thermal derogation of the PA matrix. Two master batches were produced, RV350LW having 10wt.% OMMT and RV350LW having 6wt.% SiO_2. RV350LW and the nanofillers were dry mixed by hand in glass sealable flasks in 1kg batches by agitating the flask for 3 minutes before adding to the extruder hopper. An ideal method to mixing the nanoparticles would been to mill the PA-GF pellets into a powered but this would have meant excessively damaging the glass fibres in the process.

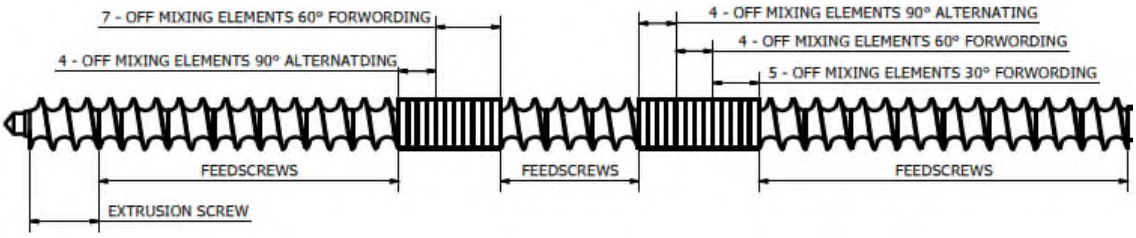

Figure 4-2: Screw configuration with details on mixing element setup.

4.3.2 Grade processing

All grade compounding was done by Ian Butterworth at Cranfield University. Table 4-1 references the grades compounded from the master batches and RV350LW base material. The same extruder, master batch processing setup and speed was used for the grade processing. All master batches pellets were dried in an oven for 16 hours at 110°C before dry mixing with RV350LW to dilute the master batches to the required grades.

Table 4-1: Grade compositions

Grades	Base Matrix	Wt.%	Nano filler	Wt.%
RV350LW	Radilon A RV350LW	0	-	-
M2	Radilon A RV350LW	98	Dellite 43B (OMMT)	2
M3	Radilon A RV350LW	97	Dellite 43B (OMMT)	3
M4	Radilon A RV350LW	96	Dellite 43B (OMMT)	4
S2	Radilon A RV350LW	98	Aerosil R 812S (SiO2)	2
S3	Radilon A RV350LW	97	Aerosil R 812S (SiO2)	3
S4	Radilon A RV350LW	96	Aerosil R 812S (SiO2)	4

4.3.3 Compounded test sample compression moulding

Compression moulding was done on a JBT 40T heated press (UK). The compression mould setup was done with two flat plates with a third mould pattern plate in between. The pattern plate produces bar samples (60x8x3mm). Each material grade was dried in an oven for 6 hours at 110°C before processing. Processing temperature was set to 280°C, before pressing a, soak time of 5 minutes was used to allow pellets to soften during pressing. Pressing was done at 10T and held for 3 minutes before switching to cooling. Samples were removed at 230°C to minimise thermal degradation to the samples. Also the cooling was not plumb to a chiller to have effective cooling.

4.3.4 Test sample injection moulding

Compounded nano grades were injection moulded by Polymer Training & Innovation Centre (UK), using Ferromatik Milacron K-Tec-110 to produce test samples. Temperature settings were at die [280, 285, 285, 285, 280]°C, 70°C at the hopper and tool temperature was set to 85°C. Cycle time was 22s with an injection speed of 180cm^3/s and injection pressure was 170bar for all material grades. Test samples were produced on a single family mould which included tensile, flexure and notched bars see Figure 4-3 for sample illustration. Plaques where done on a separate tool with a sample size of 60x60 by 2.1mm thickness.

XRD analysis and SEM scans in this work were conducted on the flexure bars length 120mm with a 12.5x3mm cross section. Sample conditioning was done to suit an off-the-shelf storage and end application service environment. Injection moulded samples were conditioned in non-moisture sealed packaging for more than 150 hours at 20 to 23°C, humidity was 60% to reach equilibrium for a workshop storage environment. This was beyond the outlined in ISO standard 291 (minimum of 88 hours for atmospheres 23°C/50% and 27°C/65%), due to PA's hygroscopic material characteristic.

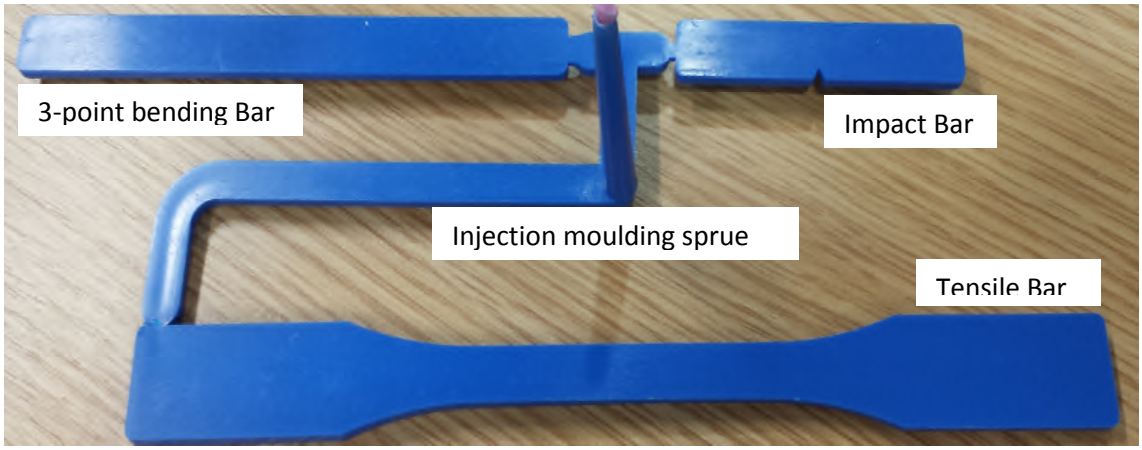

Figure 4-3: Image of the family mould impression

4.3.5 Scanning electron microscopy (SEM)

The samples were analysed on a Philips XL30 Field Emission SEM. Each sample was carbon taped to stages before being sputtered with gold palladium, except for the RV350LW sample that had been carbon coated for comparison. The carbon coated comparison was done to detach possible sputter coating decoration effect.

4.3.6 X-ray diffraction (XRD)

X-ray diffraction scans were done on a Siemens D5005 diffractometer which uses Cu Kα radiation (λ 0.1540nm) operating conditions 40kV and 30mA. Each material was scanned in 2θ range from 2 to 50° at a scanning rate of 1°/min. Sample scans were conducted on injection moulded composite grades including the RV350LW base material. Reference scans were also done on the Dellite and Aerosil in powder form. XRD was used to measure the Basal spacing. The Basal spacing can then be used to calculate inter layer distance which tells us if intercalation or exfoliation has been achieved. Basal spacing of OMMT layers (d) was calculated using the Bragg equation (2):

$$\lambda = 2d\ sin\theta \qquad \text{..... (2)}$$

4.4 Results and discussion

4.4.1 Processing of nanoparticles in the PA66/GF matrix

During the master batch processing of RV350LW + 10wt.% OMMT it was noted that the extruded nanocomposite master batch had become extremely brittle. As a result the extruded strands were easily snapped this means 10wt.% OMMT has significantly reduced the mechanical strain. This was an observation going from RV350LW trials to producing the first OMMT master batch. Okada and Usuki [104] also found that two phase nylon and clay hybrids with over 10wt.% OMMT became brittle, thus the behaviour of 3 phase nanocomposite master batch was in line with the two phase clay nanocomposite. Another notable difference was that all the OMMT grades could be done at higher processing speed without the extruder cutting out from high torque. Barick and

Tripathy [151] studied dynamic viscoelastic properties of pristine polyurethane and nanocomposites with different percentages of clay loading samples. Study found complex viscosity (g') of polyurethane/OMMT nanocomposite were higher than polyurethane matrix because the intercalated or exfoliated nanocomposite drags movement of polymer melt [151]. The low torque when processing the OMMT master batch would suggest a single pass will not intercalate or exfoliate OMMT particles. This could have also been affected by a high concentration of OMMT particles in the RV350LW. SEM image Figure 4-4(a) help demonstrate that the RV350LW/OMMT master batch has OMMT amalgamated clusters across the surface which was easily found at lower magnifications. Figure 4-4(a) also proves the existence of glass fibres in the PA66 matrix, most with lengths above 100µm after one compounding run. The reduction in GF length at this stage is likely to reduce mechanical strength properties of the compounded 3-phase nanocomposites (original glass fibre length between 500 to 600µm).

Master batch processing of RV350LW plus 6wt.% SiO_2 had no observable processing issues and was similar to processing RV350LW running at 100rpm maintaining a steady 50% torque. SEM image Figure 4-4(b) illustrates that the image of SiO_2 which had been compounded into the RV350LW had to be taken at a higher magnification to find amalgamated clusters across the surface of a master batch sample. Grade processing for 2, 3 and 4wt.% OMMT was similar to the master batch with the 2wt.% grade processing at higher constant torque.

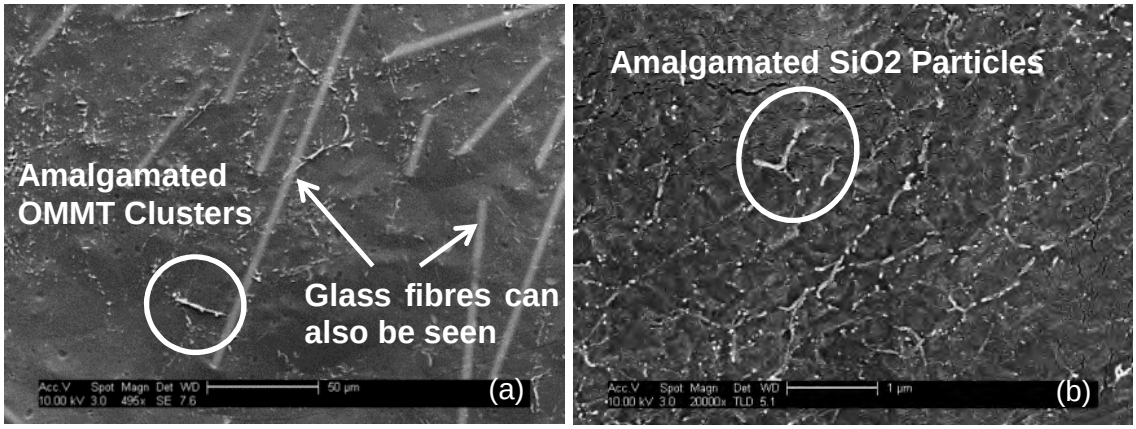

Figure 4-4: SEM images of (a) 10wt.% OMMT master batch and (b) 6wt. % SiO_2 master batch

4.4.2 SEM investigations

Initial SEM investigations were conducted on the surface injection moulded samples using lower magnifications and back scatter detection to determine if the two step compounding process had significantly reduced GF length. All images in Figure 4-5 is the GF have orientation. The orientation can be contributed to the injection moulding which has a flow direction. Figure 4-5 (a) clearly illustrates significantly longer fibres up to 540µm in length from a RV350LW sample that was injection moulded (average fibre length of 460µm counted from 100 fibres). Whereas Figure 4-5 (b) OMMT and Figure 4-5 (c) SiO_2 both represent 3wt.% grades that were compounded twice and injection moulded. OMMT and SiO_2 grades had far fewer long fibres when compared back to the RV350LW sample some of which have retained length of 300µm ± 40µm (12 out of 100 counted). However a significant amount of shorter fibres were found to have typical lengths of 60µm ± 15µm (72 out of 100 counted). The last 16 out of 100 fibres counted fell below 45µm in length. The reduction in fibre length from the compounding could translate to a reduction in mechanical strength for all of the nanocomposites grades as the GFs are the primary reinforcement for strength in a two phase PA/GF composite. This was due to long fibres having more surface area for the matrix to hold onto preventing fibre pull out. It would be reasonable to assume reduction in fibre length for the 3-phase nanocomposite is likely to result in extensive fibre pull out but this is also assuming there is no improvement of interaction of the matrix and nanoparticles to the GF surface. For instance the addition of nanoparticles in a PA matrix could promote an improved bond to the GF's. As a result increased fibre pull out strength on shorter fibre lengths would translate into an improved mechanical strength. This theory can be explained by comparing Figure 4-5(a) which has long consistent gaps filled in by matrix between the long fibres whereas Figure 4-5(b) and Figure 4-5(c) have scattered short fibres reducing the constant matrix areas. This would bring a positive effect if there is an improved bond between matrix and nanoparticle to GF which would improve mechanical strength due to more GFs sharing load. However this would have a negative

effect if there is no improvement on the bond between matrix and nanoparticles on the short fibres. This could result in excessive fibre pull out offering no strength improvement, relying on the matrix for strength which now effectively has short GFs acting as voids in the matrix which would reduce strain.

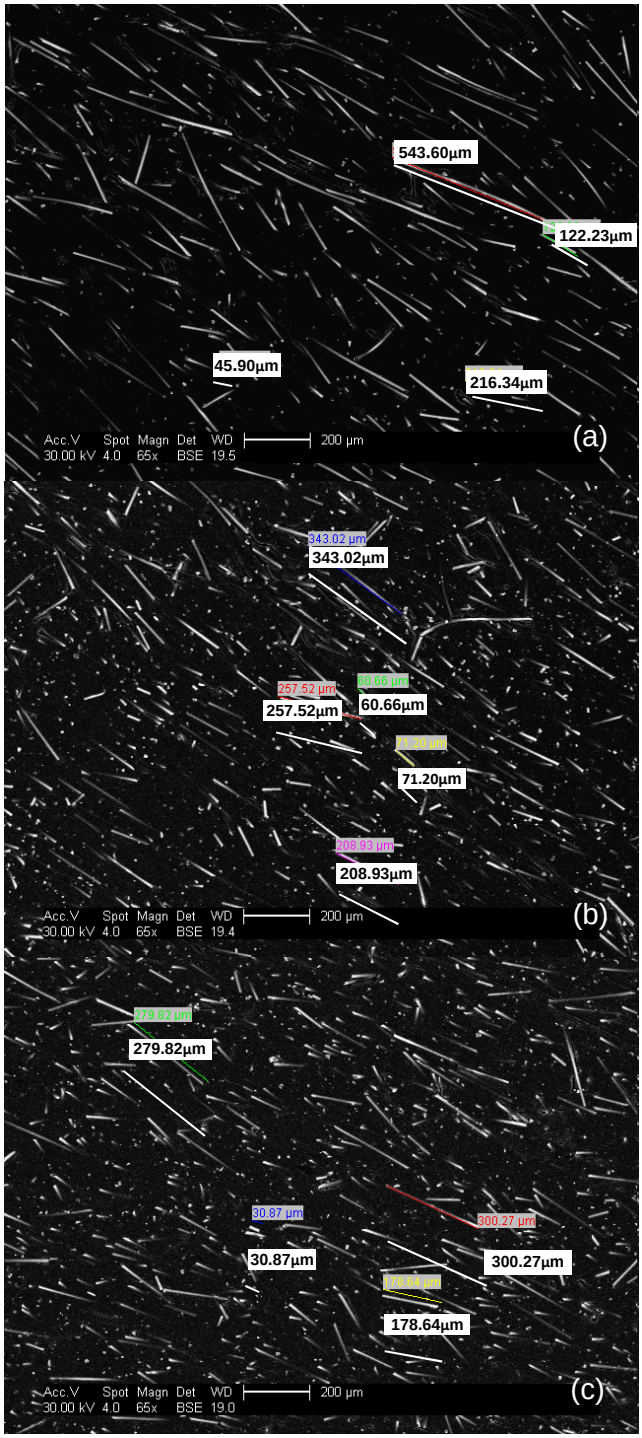

Figure 4-5: SEM backscatter images on grades (a) RV350LW (b) M3 (c) S2

SEM investigations were conducted on the OMMT and SiO_2 to characterise each nanomaterial before being compounded into the RV350LW grade. Figure 4-6(a) illustrates the typical size of the supplied OMMT particles and the Figure 4-6(b) demonstrates OMMTs naturally layered silicate structure at a higher magnification. This explains the OMMT in Figure 4-4(a) that can be easily seen at low magnification as the master batch compounding has most likely not intercalated and/or exfoliated the OMMT layers, but has broken down the clay stacks to smaller tactoids. Figure 4-6(c) illustrates SiO_2 as amalgamated clusters but at an increased magnification Figure 4-6(d) illustrates SiO_2 particles that can be seen more as loose structure with particles having a spherical shape. This loose structure could explain the better exfoliation and dispersion of the SiO_2 into the polymer matrix. For the polymer chains, it could be easier to penetrate between the SiO_2 particles and break the clusters. The SiO_2 amalgamated clusters could split up more easily explaining why higher magnification in Figure 4-4(d) was necessary to locate the SiO_2 in the PA matrix. Xu et al. [109] also described modified SiO_2 particles having a loose structure, and how silica modified with 3-aminopropyltriethoxysilane (APS) promotes PA66 grafting to the modified silica. Xu et al. [109] explained the PA66 grafting to the modified silica occurs during the melt process when compounding where the amine groups of the APS modifier are weakly attached to silica surface by physical absorption allowing the end carboxyl groups to react with the acylamino groups of the PA66 chains to form the interface structure based on hydrogen bonding and covalent bonding.

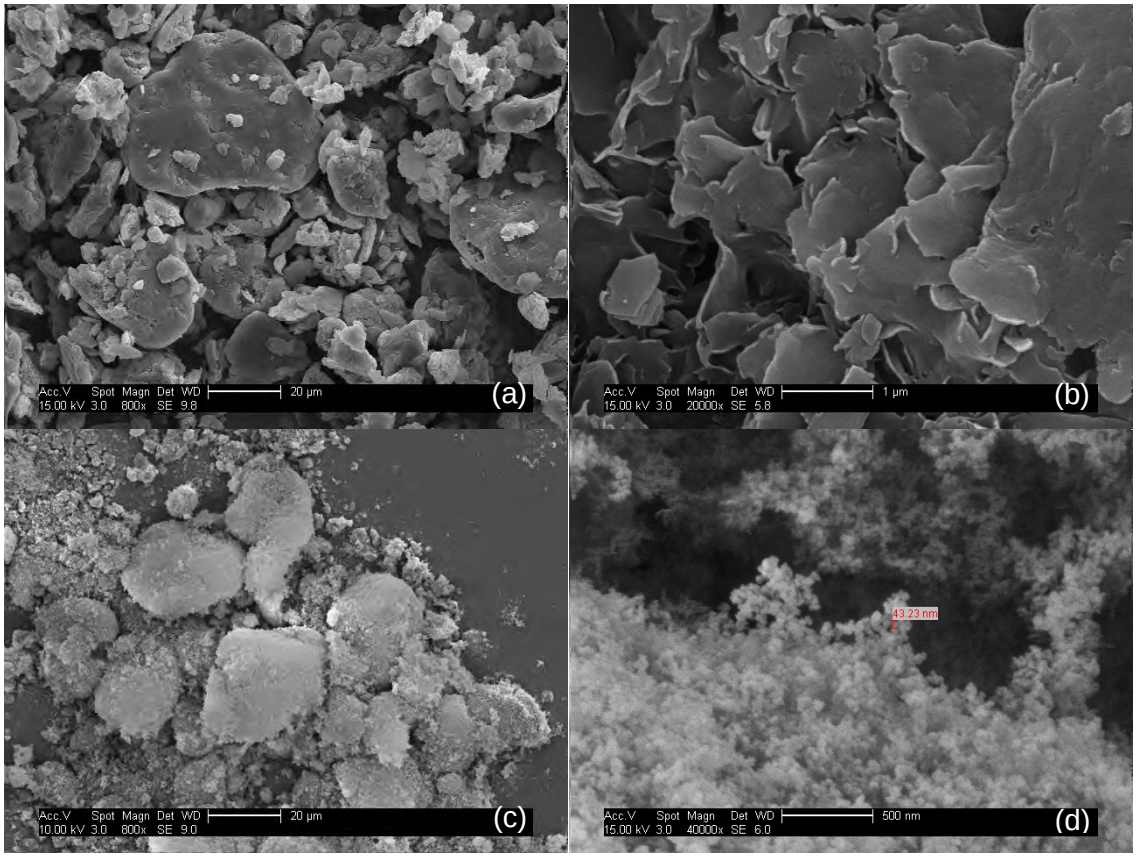

Figure 4-6: Reference scans for (a-b) MMT particles (c-d) SiO_2 particles.

RV350LW samples were also studied under the SEM to characterise the PA66 matrix without the compounded OMMT and SiO_2 nanoparticles. Figure 4-7(a) illustrates a marbling effect on the contrast of the PA66 surface with a consistent cracked surface appearance. The consistent cracked surface appearance at first was taken at face value assuming the sample surface was fractured with no influence to fracture direction. An explanation for the marbling surface effect on the test sample may have been a result of the plasma generated for the spluttering of gold palladium. Figure 4-7(b) was taken on another RV350LW sample that had been carbon coated. This proves that gold palladium spluttering can introduce a fracture effect in the nano scale on the surface of the PA66 matrix. Correspondence with Dyson at Quorum Technologies (e-mail correspondences available in Appendix A) recognised and explaned this was a coating effect related to the high current and low argon

pressure. Figure 4-8 links to the decoration surface effect of a gold target to current and argon pressure.

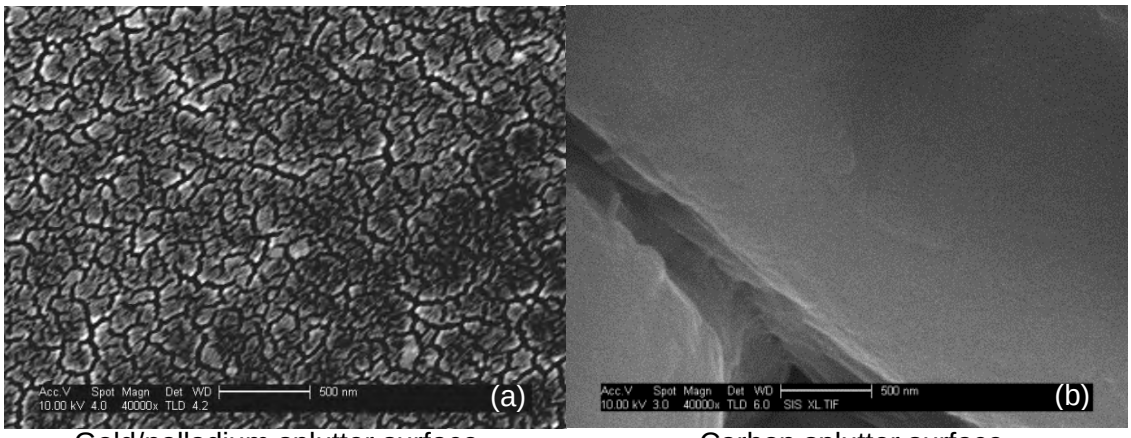

Gold/palladium splutter surface Carbon splutter surface

Figure 4-7: SEM images of RV350LW without nanoparticle reinforcement sputter surfaces: (a) Gold/palladium (b) carbon.

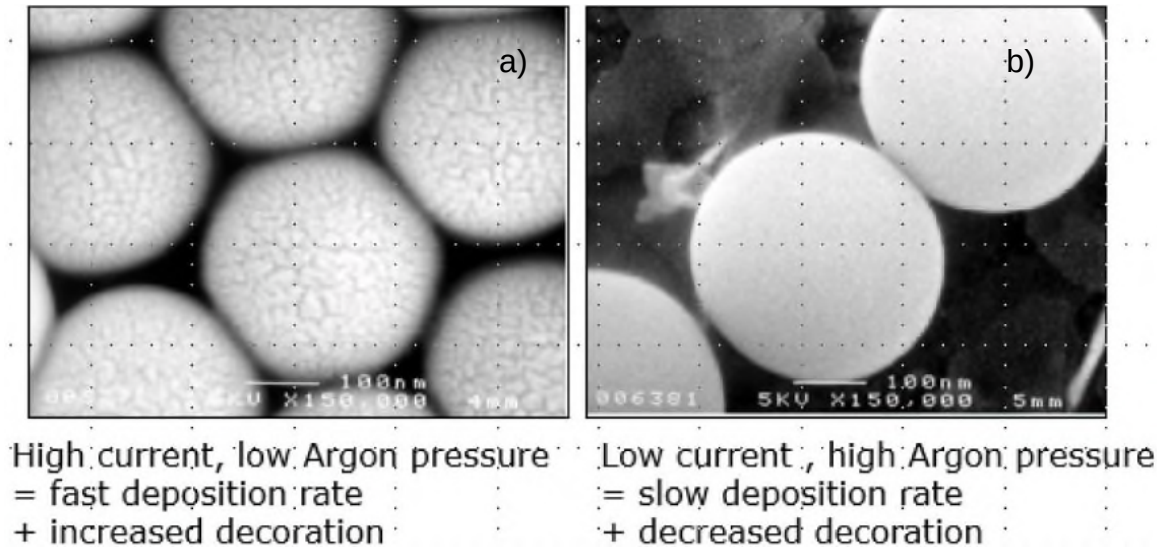

Figure 4-8: Sputter coating – decoration artefacts, linked to current and pressure

A recent study by Hou et al. [152] considers fractal patterns achieved under different sputter conditions using a gold target with high current and low argon pressure which gives a fine decoration effect in Figure 4-9. Figure 4-9(a) can be compared back Figure 4-7(a) in this work, which proves it's a sputter effect.

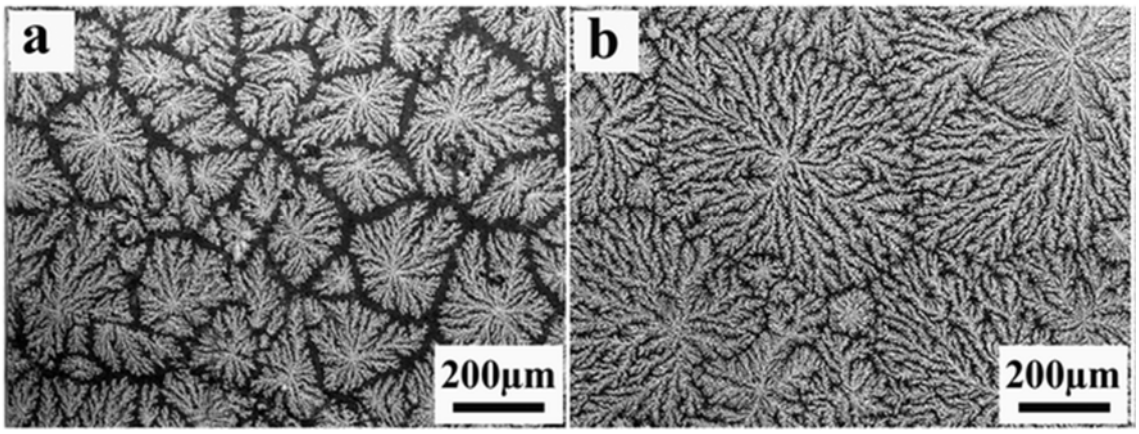

Figure 4-9: images of the gold-fractal patterns achieved under different conditions gold-sputtering durations of 8 min (a) and 12 min (b). Hou et al. with permission [152].

SEM investigations in Figure 4-10 on compounded OMMT material grades (RV350LW /OMMT samples) demonstrate the existence of nanoparticles in the matrix with even smaller clay stacks or tactoids when compared to OMMT master batch (Figure 4-4a). This means the OMMT grades have not been exfoliated and are likely to have limited intercalation between clay layers. The reduction in clay stacks or tactoids may offer some improvement to the OMMT nanocomposite grades but is unlikely to exploit the full reinforcement potential of OMMT.

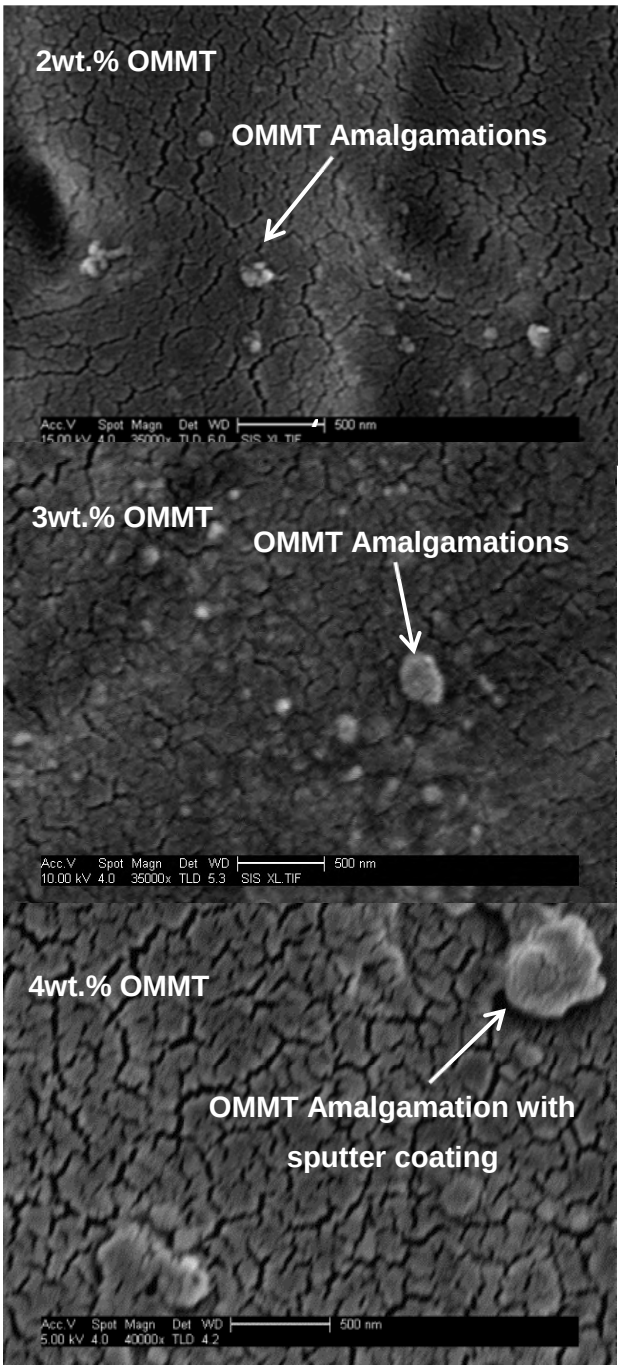

Figure 4-10: SEM scans for RV350LW/OMMT grades 2, 3 and 4wt.%

However, SEM investigations in Figure 4-11 on compounded SiO_2 material grades demonstrate better dispersion over all OMMT grades in Figure 4-10. SiO_2 at 4wt.% has limited amalgamations which can be considered as an improvement over the master batch in Figure 4-4b. Whereas SiO_2 at 2wt.% and

3wt.% demonstrate far less amalgamation with a fine scattering SiO_2 particles, this suggests that exfoliation has been achieved. The identification of SiO_2 particles is in agreement with studies conducted by Zhang et al. [110], SiO_2 particles where identified as bright particles in SEM images, see Figure 4-12.

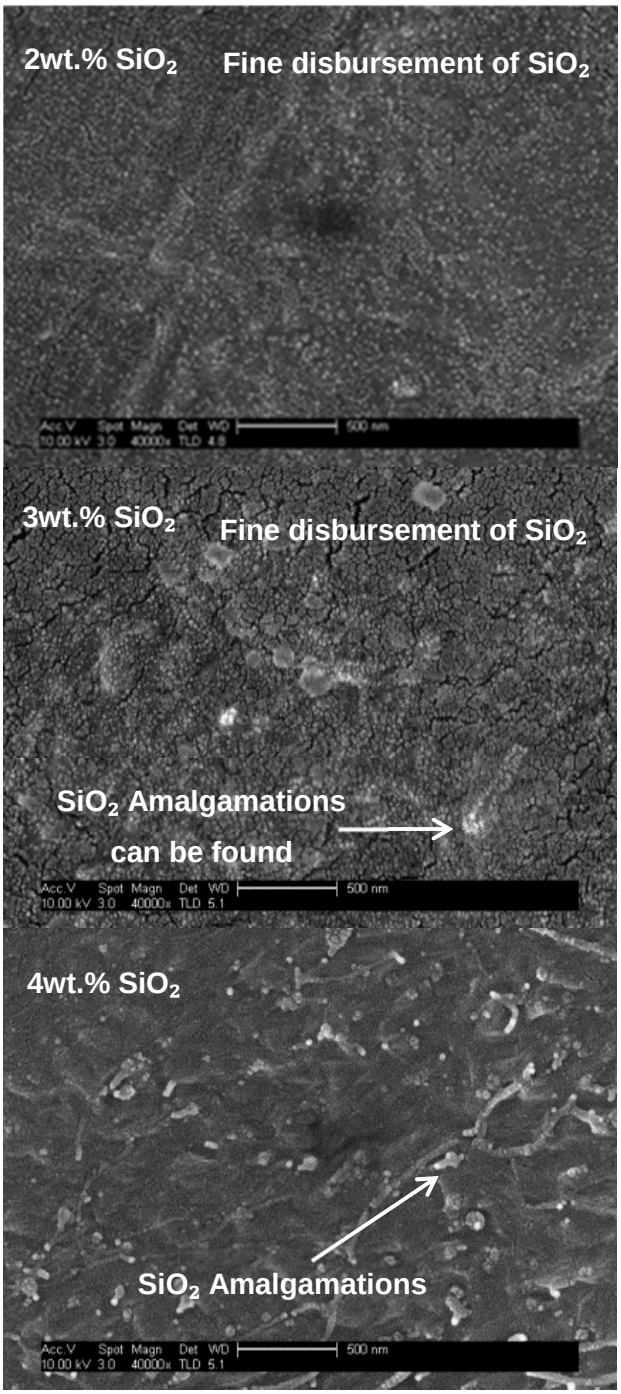

Figure 4-11: SEM scans for PA66/GF/SiO_2 grades 2, 3 and 4wt.%

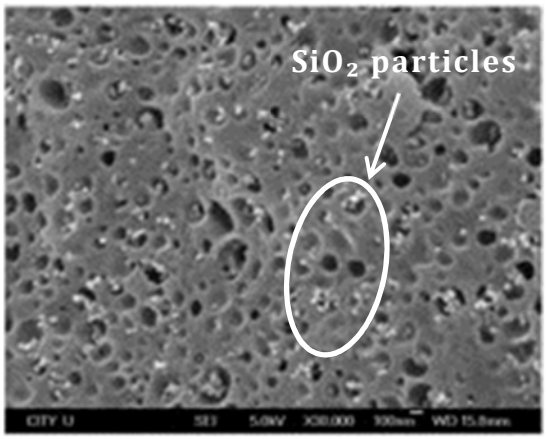

Figure 4-12: SEM image of PA6/elastomer/SiO_2 taken from Zhang et al. [110].

4.4.3 XRD investigations

XRD results for RV350LW, OMMT and SiO_2 nanocomposite grades in Figure 4-13a show the XRD patterns for OMMT nanocomposite grades have shifted to a lower angle than the OMMT reference. Table 4-2 gives the diffraction peaks for all OMMT materials and shows the interlayer spacing for all OMMT composite grades have increased to 1.01nm spacing which is a 4% improvement on supplied OMMT. This means the OMMT in each of the compounded nanocomposites has limited intercalation and has not been exfoliated. Lin et al. [149] found from XRD analysis that PA66/clay produced at higher screw rotation rate (1000 rpm), resulted in the disappearance of the clay's crystalline peak in the 001 orientation indicating better dispersion of clay. This was explained by the higher screw speed which creates higher shear and facilitates initial breakup of clay agglomerates. In this work, a 1000rpm processing condition was not possible as the extruders max screw speed was 300 rpm. Further work could consider 1000rpm as it is likely to improve the clays interlayer spacing but may also introduce a negative effect as glass fibres could get excessively damaged making the OMMT grades less comparable to the SiO_2 grades. Figure 4-13b show the XRD patterns for SiO_2 nanocomposite grades. The SiO_2 only had one distinguishable peak at 44.44° which did not show up for any of the SiO_2 nanocomposite grades. This tells us the spacing for

the SiO_2 particles is far from each other they can be considered exfoliated and well dispersed into the matrix which backs up the SEM images in Figure 4-11.

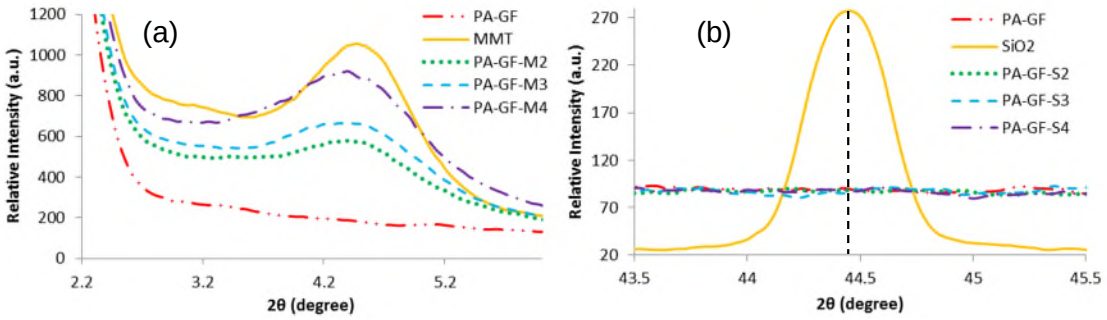

Figure 4-13: XRD patterns for composite grades: (a) OMMT; (b) SiO_2

Table 4-2: XRD diffraction peaks with basal and interlayer spacing for OMMT grades

	Nanomaterial content wt.%	Diffraction peak (2θ)	Basal spacing (nm)	Interlayer distance (nm)
RV350LW/OMMT	2	4.4	2.01	1.01
RV350LW/OMMT	3	4.4	2.01	1.01
RV350LW/OMMT	4	4.4	2.01	1.01
RV350LW	0	-	-	-
OMMT	100	4.48	1.97	0.97

4.5 Conclusions and gaps in knowledge

Several 3-phase nanocomposites were prepared using a twin screw extruder to melt compound OMMT and SiO_2 particles into RV350LW grade. Master batches of PA66/GF and nanoadditives were prepared and then used for the preparation of the nanocomposites. The following conclusions can be made on the compounding, SEM and XRD investigations.

Compounding 10wt.% OMMT into the existing RV350LW grade for a master batch grade can be achieved, there could be physical limitations when working with higher concentrations >10wt.%. In addition, the 10wt.% OMMT master batch had a brittle response for the compounded strands. Final OMMT grades at lower concentrations of 2, 3 and 4wt.% are far less brittle than the 10wt.% master batch. Compounding any additional SiO_2 into a master batch is

likely to have some losses to environment and hopper which should be monitored and factored in when diluting final grades.

SEM studies using back scatter demonstrates GFs will reduce in length from a two-step melt compounding process. The RV350LW reference grade demonstrated fibre lengths up to 540µm with compounded nano grades retained some long fibres between 300µm ±40µm. The shortest typical fibre length found on the compounded OMMT and SiO_2 nano grades was 60µm ±15µm. Further SEM investigations demonstrated compounded OMMT silicate layers broke down smaller clay stacks which show some dispersion in the RV350LW but OMMT cluster can still be identified. Compounded SiO_2 into RV350LW can be considered successful as grades can be seen to have a very good dispersion.

XRD investigations showed the RV350LW/OMMT grades became intercalated though the two-step melt compounding process which increased interlayer spacing to 1.01nm which was a 4% improvement on supplied OMMT. XRD characterisation on all the RV350LW/SiO_2 grades demonstrated exfoliation. It is believed that when the nanoadditives are well dispersed and/or completely exfoliated, they can provide high levels of reinforcement in the matrix properties. Therefore, it is likely that RV350LW/SiO_2 nanocomposites will have better mechanical properties than OMMT ones.

In this study the exfoliation of OMMT in RV350LW had limited success. A proven way to get exfoliation is to prepare the master batch then grades with the PA66 matrix [18], [105], [149], then add the GF afterwards this would also help retain GF length.

This chapter adds to knowledge as a two step compounding of OMMT and SiO_2 to produce a 3 phase nano composite can be achieved but requires process development to address OMMT dispersion and glass fibre breakage. Exfoliation SiO_2 can easily be achieved and maybe possible without producing a master batch first. Knowledge on the oversaturation point for SiO_2 when producing a master batch is will help others if a master batch is considered.

Chapter 5. Mechanical behaver of 3-phase nanocomposites at room temperature

5.1 Introduction

Standard room temperature testing of the 3-phase nanocomposites compounded in Chapter 4 has been tested in this Chapter. As room temperature (23°C) is the typical test conditioning for most mechanical testing standards this chapter detaches influencing factors such as temperature and aging affects, thus allows nano fillers in loading content in wt.% to be the focus of this study. It is also expected the reduced fibre length found in Chapter 4's SEM studies will have an effect on total mechanical strength when comparing the compounded nano grades.

5.1.1 Infrared thermography

The technology allows operators to validate normal operations and, more importantly, locate thermal anomalies (abnormal patterns of heat invisible to the eye) which indicate possible faults, defects or inefficiencies within a system or machine asset [153], [154]. In this work a Hi-speed FTIR camera is used to detect infrared radiation (heat) in this case heat generated from a high power flash, heat is dissipated though an object that has homogeneous matrix (heat transfer known as conduction). Surface and subsurface fractures will have space for air or gas between the fractures, heat will transfer though convection. Convection will show up as a hot spot (air holds heat) thus highlighting a fracture in a homogeneous material that conducts evenly as light travels in a straight line. This is useful technique to replace and address the limitation of the C-scan used in previses work, where full fractures would produce too much vibration (background noise) to be read accurately.

5.2 Materials and sample preparation

RV350LW and nano grades see Table 5-1 were prepared as outlined in previous chapter; refer to sections 4.2 (Materials), 4.3.2 (Grade processing) and 4.3.4 (Test sample injection moulding). Three types of test samples were

produced by injection moulding from a single family mould: tensile bar geometry and dimensions linked to 1B dumbbell in ISO 527 with a 3mm thickness, flexure bars length 127mm with a 12.5 by 3mm cross section similar to ASTM D790. Notched bars length 64mm with a 12.5 by 3mm cross section, notch type C in ISO 179. Square plaque shape 60x60 by 2mm thickness as outlined in ISO 6603 were produced separately. Material sample conditioning was done to suit an off-the-shelf storage environment. All samples were left in a workshop in non-moisture sealed boxes for more than 150 hours at 20 to 23°C, humidity was 60% to reach equilibrium for a workshop storage environment. This was beyond the outlined in ISO standard 291 (minimum of 88 hours for atmospheres 23°C/50% and 27°C/65%), for PA's due to having a hygroscopic material characteristic.

Table 5-1: Recap on compounded material grades compositions found in Chapter 1

Grades	Base Matrix	Wt.%	Nano filler	Wt.%
RV350LW	Radilon A RV350LW	100	-	-
M2	Radilon A RV350LW	98	Dellite 43B	2
M3	Radilon A RV350LW	97	Dellite 43B	3
M4	Radilon A RV350LW	96	Dellite 43B	4
S2	Radilon A RV350LW	98	Aerosil R 812S	2
S3	Radilon A RV350LW	97	Aerosil R 812S	3
S4	Radilon A RV350LW	96	Aerosil R 812S	4

5.3 Mechanical testing and characterisation

5.3.1 Mechanical and impact test Methodology

Tensile and flexure testing were conducted on an Instron 5500R universal test machine. Tensile testing was conducted following ISO standard 527, testing speed for all specimens was 1 mm/min. Flexure testing was conducted following ISO standard 178 and all specimens were tested at 2 mm/min.

Charpy impact testing was conducted to ISO standard 179, on a Zwick D-790 desktop pendulum setup with a 1j hammer attachment. Testing span was calculated as 4 times width from the notch of the sample which equalled 50mm.

Gas gun impact testing was conducted using 10mm hemi-spherical projectile weighting 22g using previous works conducted by Mouti et al. [7], [8], [13] as a guide and test procedure for gas gun testing. The testing was done using different impact energies 2, 2.5, 3 and 3.5 joules for all specimens tested. The required projectile velocity for each of the impact energies was calculated using equation (1).

v = Velocity E = Energy M = Mass of projectile

$$v = \sqrt{\frac{E}{\frac{1}{2} \cdot m}} \quad \text{..... (1)}$$

Specimen setup was done using an angle plate to hold the plaque fixture normal to the gas gun barrel at a 400mm distance. Plaque fixture held plaque samples leaving a 50x50mm window as the exposed impact area. Gas gun setup can be seen in Figure 3-3a-c in Chapter 3. The impacts were reproduced at least five times per test for each material using a new plaque for each shot. Any miss fired shots were retaken on new plaques. This was verified using high speed camera footage to check that each shot was straight and hit central to the plaque. All mechanical tests were done at 23°C. This temperature was checked before starting and during each test using a K-type thermocouple on the sample surface.

5.3.2 Scanning Electron Microscopy (SEM)

The samples were analysed on a Philips XL30 Field Emission SEM. Samples were carbon taped to sample stages before being sputter coated with gold-palladium.

5.3.3 Hi-speed camera setup

High speed camera footage was taken for every shot during gas gun testing using a Photron fastcam SA4 with a macro lens. Photron fastcam viewer (PVR) Ver.3.0 was used to record, playback and edit footage.

5.3.4 Infrared thermography

High speed infrared (IR) camera FLIR SC7600 was set to 20fps, 50Hz/sec in mid-wave (3-5.5μm). Setup also included a Thermoscope 2 high power flash unit with total of 25kj output with an estimated 2kj reaching the sample surface. Data capture and results were processed using MOSAIQ 4.0, the software calculates information logarithmically to generate the IR images with intensity scale.

5.4 Results and Discussion

5.4.1 Mechanical properties

Mechanical test results from tensile and flexure testing can be found in Table 5-2. It was observed that the type of nanoparticles and the loading also had an effect on each nanocomposite. The samples with 2% OMMT and 3% SiO_2 retained the tensile stress at break most with 22.9% and 24.7% losses respectively. These grades also retained the flexure stress at break most with 15.3% and 14.4% losses respectively. The OMMT optimum at a 2wt.% loading was not exactly expected when comparing work done by Chung et al. [105]. They found PA66 with OMMT at a 3wt.% loading offers an optimum tensile strength of 75 MPa a 17% improvement on Pure PA66. Although it is possible that the interaction of OMMT and (shorter) GF in a 3-phase composite could have shifted the optimum OMMT loading down to 2wt.%. The limited exfoliation of OMMT in this work is also an influencing factor when comparing to Chung et al. [105]. The SiO_2 optimum at a 3wt.% loading was in agreement when comparing to a 2-phase nanocomposite by Xu et al. [109]. They found PA66 with SiO_2 at a 3wt.% loading offers an optimum tensile strength of 79 MPa (10% improvement on Pure PA66). It was expected that strain at break would be where the OMMT and SiO_2 nanomaterials grades would differ significantly. OMMT would reduce strain and SiO_2 grades would increase it, this is in agreement for tensile and flexure results in Table 5-2.

It was also expected that both tensile and flexure stress at break would reduce for all compounded nanogrades when compared to PA66-GF. This expectation was based on compounding glass fibre breakage found in Figure 4-5 which was likely to translate in a reduction in mechanical strength for all of the nanocomposites grades as the GF's are the primary reinforcement for strength in a PA/GF composite. Thomason [155] studied GF length in a PA66 matrix found mechanical test results for short GF (340μm) exhibited a slightly greater loss in tensile strength than the equivalent long GF (520μm), and consequently there is a greater advantage of long GF over short GF in a PA-GF composite.

Tensile and flexure tests show OMMT reduces strain for each increase in loading. As a result 4% OMMT reduces the tensile and flexure strain at break by 30% and 26% respectively. The reduction in strain would have been considered a benefit if the stress for each OMMT grades were equal to or better than the PA-GF reference. This would have demonstrated a material that would strain less at a higher loading allowing better dimensional stability for a component. It is possible that OMMT filled grades could achieve this if the GF length was maintained after compounding.

Tensile and flexure results show SiO_2 grades to increase in strain with 4% SiO_2 offering the highest strain with 20% and 34% improvement on PA/GF for tensile and flexure respectively. Again due to GF breakage SiO_2 grades do not reach the fully intended toughness through strain intended. Figure 5-1 compares all material grades as a percentage of toughness with PA-GF used as a 100% normalised reference to allow nano grades to be rated. Each OMMT grade can be seen to significantly reduce composite toughness, whereas SiO_2 grades maintained best toughness. This was to be expected for the SiO_2 grades as an improvement in strain performance has resulted in an improvement in toughness. Flexural toughness for $SiO_2$2% and $SiO_2$4% offers a 7.6% and 1.5% improvement respectively, but had a negative effect on tensile toughness for $SiO_2$2% and $SiO_2$4% by reducing it by 16.8% and 24.6% respectively. $SiO_2$3%

was predicted to have the best material toughness of the SiO_2 grades but has reduced by 4.5% and 3.6% for tensile and flexure moduli. If the GF length was maintained during compounding it is more than likely that all the SiO_2 grades would have a significant improvement on toughness. OMMT grades retain the best modulus for both tests especially for flexure where OMMT4% shows a 3% improvement with reduced scatter on PA-GF. SiO_2 has reduced modulus for all SiO_2 grades as a result of the reduced stress and increased strain.

Table 5-2: Mechanical test results from tensile and flexure testing

	Tensile Properties			Flexural Properties		
	Stress at break (MPa)	Strain at break (%)	Modulus (GPa)	Stress at break (MPa)	Strain at break (%)	Modulus (GPa)
PA-GF	183.1 ± 1.7	2.9 ± 0.1	11.0 ± 0.6	292.5 ± 10.6	4.7 ± 0.1	9.1 ± 0.2
OMMT2%	141.1 ± 3.1	2.5 ± 0.2	10.7 ± 1.0	247.7 ± 6.1	4.4 ± 0.2	8.6 ± 0.8
OMMT3%	126.1 ± 2.1	2.4 ± 0.2	9.7 ± 0.5	233.0 ± 2.3	4.1 ± 0.2	9.0 ± 0.1
OMMT4%	120.4 ± 5.7	2.0 ± 0.1	10.1 ± 0.3	223.1 ± 2.2	3.5 ± 0.1	9.4 ± 0.1
$SiO_2$2%	115.9 ± 0.7	3.4 ± 0.1	8.4 ± 0.2	213.9 ± 2.5	6.2 ± 0.3	7.6 ± 0.1
$SiO_2$3%	137.9 ± 2.1	3.2 ± 0.2	9.2 ± 0.2	250.4 ± 2.1	5.5 ± 0.2	8.5 ± 0.1
$SiO_2$4%	97.8 ± 1.2	3.4 ± 0.1	8.2 ± 0.4	190.1 ± 1.2	6.3 ± 0.2	7.0 ± 0.1

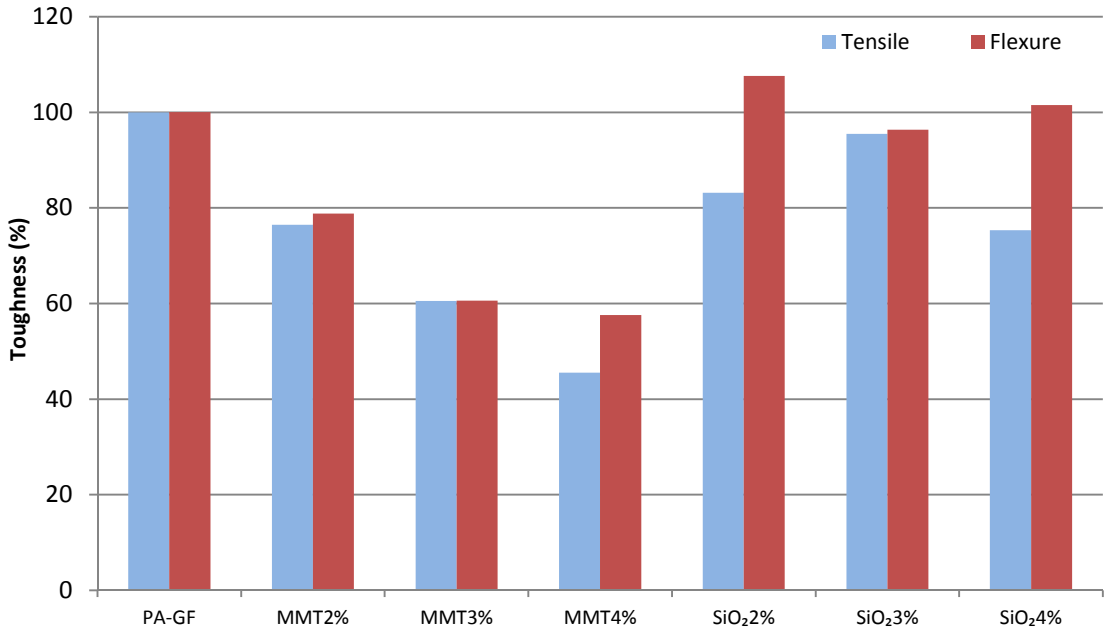

Figure 5-1: Tensile and flexural stress vs strain results calculated into toughness (toughness has been normalised to PA-GF, 100% as reference grade value)

5.4.2 Charpy dynamic impact testing

Figure 5-2 compares notched Charpy impact results for compounded nano grades and PA-GF. The notched Charpy impact performance for all nano grades in Figure 5-2 fell far below expectation when comparing to PA-GF impact strength of 14.5 ± 1.0 kJ/m^2. 3% SiO_2 retained the best impact performance of 7.5 ± 0.8 kJ/m^2 but translates into a 48% reduction in the notched Charpy impact performance to the PA-GF grade. It was expected that the impact performance for SiO_2 grades would be reduced by 5 to 10% when compared to the PA-GF reference. To understand why the tensile and flexure toughness comparison has failed and to accurately predict the notched Charpy impact each of mechanical properties were compared.

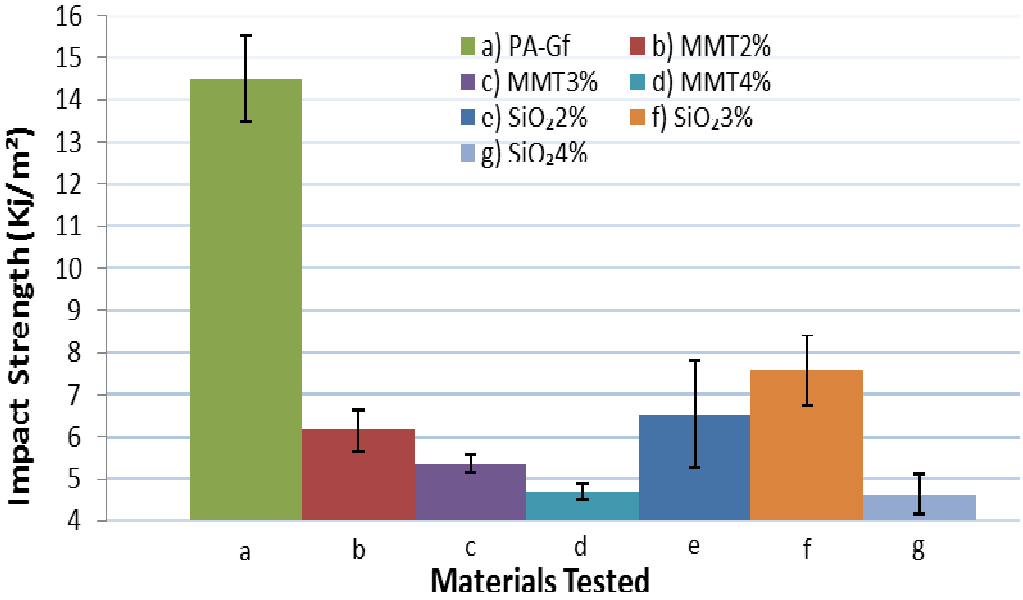

Figure 5-2: Notched Charpy impact on all material grades

5.4.3 Gas gun dynamic impact testing

Results from gas gun impact can be seen in Table 5-3 with pass and failure criteria's reference in Figure 5-3. Table 5-3 shows impacts at energies above 2.5J results in all materials grades to fail. Impacts conducted at 2.5J shows PA-GF and PA-GF-E material grades to withstand the impact. Also 2.5J impacts no

longer cause any of the nano grades to fail as a hole through the full thickness of the sample. For Impacts at 2J the 2wt.% and 3wt.% nano grades for both materials pass, whereas 4wt.% nano grades fracture only on the non-impacted surface. The poor performance of the 4wt.% nano grades is in agreement with results in Figure 5-2 as these grades also had the lowest impact performance for the Charpy.

Table 5-3: Gas gun test results for different impact energies tested

	Impact Energy 3.5J		**Impact Energy 3J**		**Impact Energy 2.5J**		**Impact Energy 2J**	
Material	Result	Failure	Result	Failure	Result	Failure	Result	Failure
PA-GF	Fail	2	Fail	2	Pass	-	Pass	-
PA-GF-E	Fail	2	Fail	1	Pass	-	Pass	-
OMMT2%	Fail	3	Fail	3	Fail	1	Pass	-
OMMT3%	Fail	3	Fail	3	Fail	2	Pass	-
OMMT4%	Fail	3	Fail	3	Fail	2	Fail	1
$SiO_2$2%	Fail	3	Fail	3	Fail	1	Pass	-
$SiO_2$3%	Fail	3	Fail	2	Fail	1	Pass	-
$SiO_2$4%	Fail	3	Fail	3	Fail	2	Fail	1

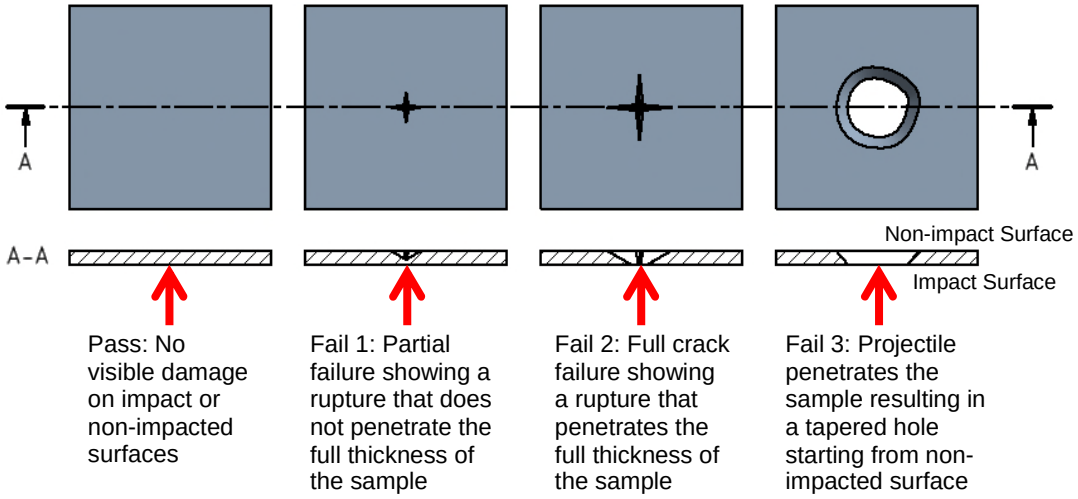

Figure 5-3: Illustrating the typical results and cross section of samples reference to failure criteria in Table 5-3

The failure propagates on the non-impacted surface as a tensile rupture as illustrated Figure 5-4(b), which can be seen as a surface crack by visual inspection. The failures illustrated in Figure 5-3 of types 2 and 3 can be identified by visual inspection on the impact and non-impacted surfaces. The type 1 failure is likely to go unnoticed due to being on the inside surface that is not visually checked on most components and will only be noticed if the fracture propagates to a full rupture of the sample thickness. The worst case scenario is the same area gets hit for the second time resulting in a type 2 or 3 failure.

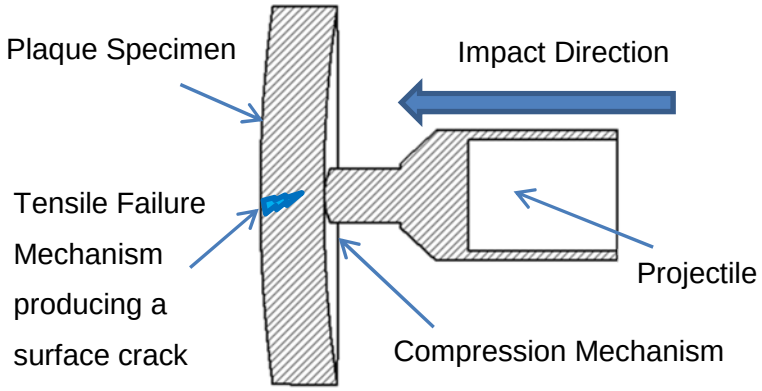

Figure 5-4: Gas gun impact cross section of the failure mechanism

There was an expectation that the BASF elastomer modified PA-GF-E grade would have had significant improvement on impact resistance when compared to the Radici PA-GF grade. This expectation was due to the elastomer modifier would allow the PA-GF-E grade to stain and thus allow impact energy to be dissipated instead of been released as a fracture. Figure 5-5 was created using tensile test data for BASF's PA-GF and PA-GF-E grade from previous work [156] with a third plot comparing Radici's PA-GF grade tested in this work. Figure 5-5 clearly shows a trade-off between stress and strain with a PA-GF grade having a greater mechanical stress that can with stand a 2.5J impact, whereas the PA-GF-E was specifically developed by BASF to dissipate the impact energy through strain and begins to fail between 2.5 and 3J. A study by Thomason [55] found that PA66-GF composites that have longer

GF lengths (500µm) have a significant improvement on composite notched impact and instrumented multi-axial impact tests when compared to shorter GF lengths (300µm). Hassan et al. [60] worked on two GF lengths materials short GF (50-550µm) and long GF (50-1250µm) at different volume fractions in a PA66 matrix. Their results also demonstrate improved tensile strength and impact properties for all long GF composites for each fibre volume. This would suggest all the nano grades and the PA-GF-E could benefit from longer fibres to retain mechanical strength and increase the strain to improve overall impact performance.

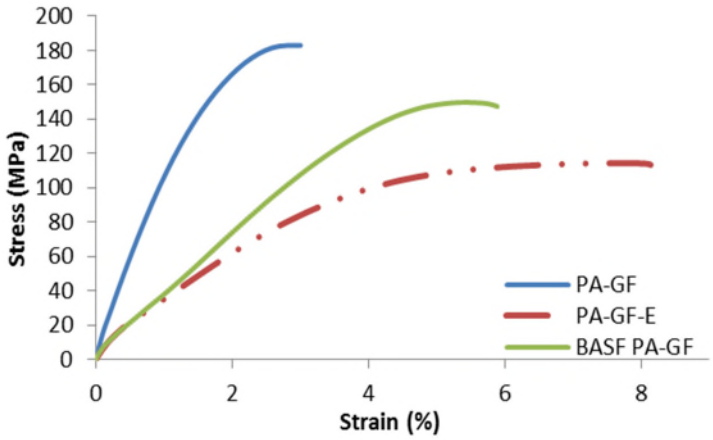

Figure 5-5: Illustrating the tensile performance difference between Radici PA-GF Vs BASF grades PA-GF and PA-GF-E

5.4.4 Surface analysis on fractures

Micrographs of fractured surfaces tensile samples were taken on SEM for each material grade given in Figure 5-6. Figure 5-6 (a) shows the fracture surface of the PA-GF reference grade. PA66 matrix can be observed to have a brittle fracture surface with crazing. The interaction between GF and matrix can be considered poor due to long and clean fibre pull-out. Figure 5-6 (b) shows the fracture surface of the OMMT2% grade. PA66 matrix can be observed to have a similar brittle fracture surface with increased crazing as PA-GF in Figure 5-6 (a). The interaction between GF and matrix with the addition of OMMT can be seen on the pulled out glass fibre surface which now have a thin textured coating of matrix. Figure 5-6 (c) shows the fracture surface of the 3% OMMT

grade. The PA66 matrix has become slightly porous and textured with a 3% addition of OMMT. This may explain why there has been a further drop in mechanical strength compared with OMMT2%. However 3% addition of OMMT shows to greatly improve the bond between matrix and GF as pulled out GFs have a thick coating of matrix. The improvement of the matrix bounding to glass fibres could be contributed the OMMT's surface treatment which has been polarised to interact better within a PA66 matrix. Figure 5-6 (d) shows the fracture surface of the OMMT4% grade. Matrix can be observed to have a textured brittle fracture surface with crazing similar to PA-GF in Figure 5-6 (a). The interaction between GF and matrix is slightly less than other additions of OMMT, but can be considered an improvement on PA-GF grade. This would suggest that if GF length was retained, the improved matrix interaction would result in a strength improvement for the OMMT grades.

Figure 5-6 (e) shows the fracture surface of the $SiO_2$2% grade. Matrix can be observed to have a stepped and not so brittle fracture matrix surface with crazing. The stepping could be linked to the crazing where the matrix has somewhat peeled from itself following different crazing contours. A peeled matrix would suggest the SiO_2 particles have made the matrix more plastic and can be linked to increased strain results for the $SiO_2$2% grade. The interaction between GF and matrix can be considered as very good due to very short fibre pull out and fibre being pulled out having a coating of matrix. Figure 5-6 (f) shows the fracture surface of the $SiO_2$3% grade. Matrix can be observed to have some stepping and less crazing compared to Figure 5-6 (e) where the fracture surface seems to be more brittle. The most notable difference is that the fibre pull out is longer than the other SiO_2 grades in Figure 5-6 but $SiO_2$3% grades have retained better mechanical strength. This would suggest SiO_2 has an influence on the matrix mechanical strength. Figure 5-6 (g) shows the fracture surface of the $SiO_2$4% grade. Matrix can be observed to have a stepped and not so brittle fracture surface with crazing. The interaction between GF and matrix is very good with almost no fibre pull out across the majority of the surface but with some areas with very short fibre pull out.

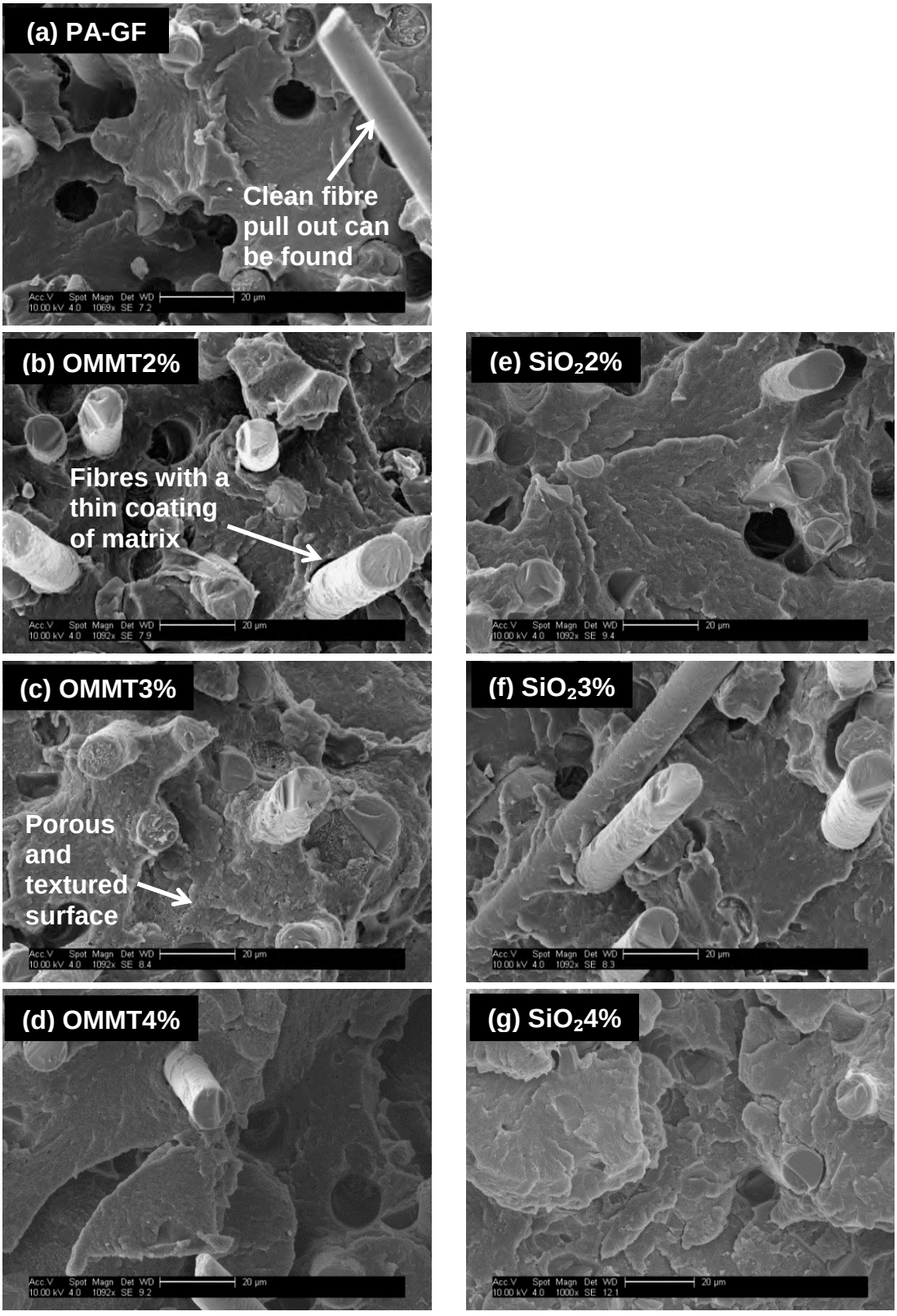

Figure 5-6: SEM images taken from the fracture surfaces after tensile tests (a) PA-GF; (b) OMMT2%; (c) OMMT3%; (d) OMMT4%; (e) $SiO_2$2%; (f) $SiO_2$3%; (g) $SiO_2$4%

To summarise the PA-GF reference grade demonstrated a brittle fracture surface and crazing with long clean fibre pull out. The clean fibre surface suggests a poor bond between matrix and fibre where the PA-GF grade cannot utilise the full tensile strength of the GF. If there was a good bond between matrix and GF, SEM images would show very short fibre pull out with extensive broken fibres. The SEM studies on all nanomaterial grades have affected the matrix fracture surface such as texture and crazing. The effect and relation between matrix and the addition of nanoparticles has improved the bond between matrix and GFs for all nano grades tested. However, this was not translated into the mechanical behaviour. This would suggest that if GF length of the nano grades was retained to the same length as the fibres in the PA-GF reference, there could have been significant mechanical property improvement for each nano grade over the PA-GF grade. Some reasoning why PA-GF and SiO_2 grades have fibre pull out compared to the OMMT grades could be linked to OMMT stiffening effect from its silicate layers has made the matrix more brittle. The other function OMMT appears to have is improved matrix bonding to the fibres. This shows as almost no fibre pull where the matrix is failing round the fibres. This would suggest OMMT could offer superior strength performance if the glass fibres where longer to allow better load transfer from improved matrix bounding.

5.5 Conclusions and contribution to knowledge

Tensile and flexure tests demonstrate that each type of nanoparticle and loadings in wt.% has an effect on an existing PA-GF composite. This adds to current knowledge as the 3-phase nanocomposites are not common off the shelf materials. Also one of the phases is glass fibre in the micro scale so any room temperature mechanical testing is going to add to new knowledge. Nano grades OMMT2% and $SiO_2$3% retain the best tensile and flexure stress this is also an unknown what quantity of nano addition would have an effect if any. This knowledge helps anyone looking to take this work further by narrowing down how much nanoparticle addition is needed when using OMMT or SiO_2.Tensile and flexure strain reduced for OMMT grades with increase in

weight percent, whereas SiO_2 offers increased strain above the reference PA-GF grade. Mechanical and impact testing highlight that the nanocomposites fail primarily at reduced stress for both tensile and flexure testing. As a result impact performance is significantly reduced when compared to the PA-GF reference material. GF length throughout this work has been identified as a significant influencing factor for all tests. The reduction of stress and impact performance for all nano grades can be contributed to the reduced GF length. Gas gun impact testing of PA-GF and PA-GF-E also further verified the benefit from longer GF in the PA-GF grade which had a similar impact performance to the PA-GF-E grade. Results for SiO_2 nanocomposites may realistically be a suitable replacement to an elastomer but will require processing optimisation to retain GF lengths as a consideration for possible further work. The three phase nano composite grades compounded as a part of this study do not offer any distinctive mechanical or impact performance benefits to improve the current PA-GF and PA-GF-E micro scale composites. However all tests in this work were conducted at 23°C which is the typical test conditioning for most mechanical testing standards. Further work on these materials will consider testing at elevated temperature conditions related to an under-the-bonnet application. It is possible the nanocomposites may offer an improved thermal/mechanical performance when compared to PA-GF and PA-GF-E grades.

Chapter 6. Experimental, Thermo-mechanical testing of 3-Phase nanocomposites

6.1 Introduction

An engine oil pan is a classic example of a component that is subjected to elevated temperatures and which also has a structural requirement. The same elevated temperature conditions of 23, 65, 90, 120˚C were repeated for comparison purposes and to fulfil the criteria in Chapter 3. The current PA-GF and PA-GF-E grades tested in Chapter 3 demonstrate increased strain performance and, in turn, offer improved impact performance when temperature is increased. However, the effect of elevated temperatures on the mechanical and dynamic response to a 3-phase composite that has both a micro and nano fillers is yet to be fully established. It's hoped that OMMT reinforcement will retain better stress and modulus performance when temperature is increased to the PA-GF reference. Work by Liu et al. compounded and tested PA6 with 4.2wt.% OMMT with comparison to a pure PA6. And found at temperatures of 62 to 112°C PA6-OMMT grade showed improved flexural strength and modulus with no trade off in notched impact strength [157]. The improvement found by Liu et al. has likely come from OMMT layered silicate structure within PA6 matrix reducing polymer chin movement at higher temperatures resulting in improved load capacity when compared to a pure PA6 matrix. Its regularly documented SiO_2 will increase mechanical strength, elongation at break and impact strength response in a PA matrix [97], [158]–[160]. It hoped SiO_2 grades at elevated temperatures will also have increased strain response similar to material B can be gained. The nanocomposites demonstrated performance loss due to reduced GF length in Chapter 5, but they may still demonstrate improved mechanical properties retention over the PA-PF base grade. Comparisons back to material B should also be considered as it is this grade that is intended to be improved on.

Therefore this chapter repeats the same testing as Chapter 3 but considers the compounded nano grades in Chapter 4 to study the influence nano fillers on thermal performance.

6.2 Materials

RV350LW and nano grades were prepared as outlined in chapter 4; refer to sections 4.2 (Materials), 4.3.2 (Grade processing). Section 4.3.4 (Test sample injection moulding) gives details on the tensile, flexure and plaque test samples standards and dimensions. BASF Ultramid A3W7G-OSI (material B) was also included as a second reference and represents the current baseline used in industry. Material B was injection moulded into new plaque samples so that the same plaque thickness can be compared to the PA-GF and nano grades.

6.3 Thermomechanical testing and characterisation

6.3.1 Test conditioning

Thermal test conditioning using environmental chambers was performed as outlined in section 3.2.5 (Thermal conditioning). Temperature tests conditions of 23, 65, 90 120°C were repeated for tensile, flexure and gas gun impact. Also, before running each test a soak time of +1 hour was given to equipment and the fixtures to ensure test setup had stabilised. Materials were also given a soak time (10-15 minutes) to ensure the core (and not just the surface) of each sample was at temperature. Temperature was checked on all mechanical test samples before starting each test using a k-type thermocouple on the sample surface (except for the plaque samples). Plaque samples required the impact surface to be unobstructed by the thermocouple, this meant the fixture was monitored by the thermocouple instead and an inferred thermometer was used to verify sample surface temperature before each shot.

6.3.1 Mechanical and impact test Methodology

Tensile and flexure testing were conducted on an Instron 5500R universal test machine. Tensile testing was conducted following ISO standard 527, testing

speed for all specimens was 1 mm/min. Flexure testing was conducted following ISO standard 178 and all specimens were tested at 2 mm/min.

Gas gun impact testing was conducted using 10mm hemi-spherical projectile weighting 22g. The testing was done using temperature as the variable with 3.5 Joule being the fixed input for all specimens tested. Setting the impact energy to 3.5 Joules allowed fracture damage to be tracked across all temperatures and materials tested as well as conserving test samples. The required projectile velocity for the impact energy was calculated using equation (1). Specimen setup was done the same as section 3.2.4 with the high speed camera setup to verify each shot was straight and hit central to the plaque.

6.3.2 Hi-speed camera setup

High speed camera footage was taken for every shot during gas gun testing using a Photron fastcam SA4 with a macro lens. Photron fastcam viewer (PVR) Ver.3.0 was used to record, playback and edit footage.

6.3.3 Infrared thermography

High speed infrared (IR) camera FLIR SC7600 was set to 20fps, 50Hz/sec in mid-wave (3-5.5μm). Setup also included a Thermoscope 2 high power flash unit with total of 25kj output and with an estimated 2kj reaching the sample surface. Data capture and results were processed using MOSAIQ 4.0. The MOSAIQ software calculates information logarithmically to generate the IR images with intensity scale.

6.4 Results and Discussion

6.4.1 Tensile and flexure testing

Tensile and 3-point bending results can be found in Table 6-1, Table 6-2, Figure 6-1(a-b) and Figure 6-2(a-b) for all materials and temperatures tested in this chapter. Plotted data in Figure 6-1(a-b) and Figure 6-2(a-b) illustrates that tensile and flexure strength reduces whereas strain increases for all materials when temperature is increased. This was expected for the nano grades when

considering thermomechanical performance, however the OMMT grades tested at 23°C did have a reduced strain when comparing to the PA-GF reference. The reduction in tensile strain for the OMMT grades at 23°C is in agreement with results found in literature for 2-phase PA-OMMT nanocomposites. This is due to the OMMT layered stack structure stiffening the PA matrix thus reducing composite strain [161]–[163]. However OMMT grades tested above 23°C (65 to 120°C) in this work no longer sees the OMMT offering the reduction strain, where strain becomes greater with each temperature increase when compared to the PA-GF reference. As the end application is for an oil pan operating between 65 to 90°C the increased strain can be considered a benefit for dissipating energy from a stone impact scenario. When comparing the micro grades Radici PA-GF to the results for BASF material A in Figure 3-4 (found in chapter 3), the strain slightly decreased with temperature increase. To explain why the BASF material A strain shows little effect when testing at elevated temperatures compared to the Radici PA-GF grade, could be linked to heat stabilizer additives used this will be different between manufactures.

Comparing PA-GF against all the nano grades in Table 6-1, tensile stress has reduced for all nano grades. Nano samples OMMT2% and $SiO_2$3% retained the best tensile stress at break for all temperatures tested, difference was between (22 to 25%) and (24 to 29%) losses respectively. Table 6-2 OMMT2% and $SiO_2$3% also retained the best flexure stress at break for all temperatures tested, difference was between (15 to 19%) and (14 to 21%) losses respectively. As discussed in Chapter 5 it was expected that both tensile and flexure stress at break would reduce for all compounded nano grades when compared to a reference PA66-GF.

In Table 6-1 and Table 6-2, tensile and flexure modulus have also reduced for all nano grades with OMMT2% and $SiO_2$3% retaining the best modulus of the two nano materials used for all temperatures tested. OMMT2% retained the best modulus for all the nano grades tested with (2 to 32%) and (5 to 23%) losses for tensile and flexure modulus respectively for all temperatures tested. $SiO_2$3% retained the best modulus for the SiO_2 grades (16 to 38%) and (7 to

33%) losses for tensile and flexure modulus respectively for all temperatures tested.

Tensile and flexure strain in Figure 6-1(a-b) and Figure 6-2 (a-b) clearly shows a significant increase for elevated temperatures with the aforementioned exception for all OMMT grades at 23°C which was below the tensile and flexure strain for PA-GF. The greatest increase in strain can be seen in Figure 6-1b and Figure 6-2b for all SiO_2 grades and temperatures tested with OMMT2% and OMMT3% offering the highest strain for the OMMT grades in Figure 6-1a and Figure 6-2a. OMMT2% gains the highest strain of the OMMT grades tested with (14 to 52%) and (15 to 32%) increases for tensile and flexure modulus respectively for all temperatures tested above 23°C. $SiO_2$4% demonstrates the highest strain for the SiO_2 grades (20 to 127%) and (23 to 53%) increases for tensile and flexure modulus respectively for all temperatures tested, including 23°C.

Table 6-1: Tensile testing with different temperature conditions with nano grades compared to PA-GF as a reference

		PA-GF	OMMT2%	OMMT3%	OMMT4%	$SiO_2$2%	$SiO_2$3%	$SiO_2$4%
23°C	Stress (MPa)	183.1 ±1.7	141.1 ±3.1 23% reduction	126.1 ±2.1 31% reduction	120.4 ±5.7 34% reduction	115.9 ±0.7 37% reduction	137.9 ±2.1 25% reduction	97.8 ±1.2 47% reduction
	Strain (%)	2.86 ±0.1	2.52 ±0.2 12% reduction	2.38 ±0.15 17% reduction	2.00 ±0.1 30% reduction	3.37 ±0.08 18% Increase	3.23 ±0.17 13% Increase	3.43 ±0.14 20% Increase
	Modulus (MPa)	10953 ±600	10698 ±1039 2% reduction	9703 ±524 11% reduction	10112 ±258 8% reduction	8421 ±184 23% reduction	9152 ±166 16% reduction	8223 ±420 25% reduction
65°C	Stress (MPa)	119.7 ±3.2	91.6 ±0.8 23% reduction	83.3 ±2.5 30% reduction	81.4 ±2.2 32% reduction	74.1 ±0.5 38% reduction	87.2 ±2.9 27% reduction	64.1 ±1.2 46% reduction
	Strain (%)	5.13 ±0.25	5.86 ±0.42 14% Increase	5.58 ±0.46 9% Increase	4.65 ±0.1 9% reduction	8.79 ±0.45 71% Increase	7.25 ±0.34 41% Increase	10.99 ±0.16 114% Increase
	Modulus (MPa)	6326 ±110	4674 ±61 26% reduction	4959 ±148 22% reduction	5093 ±125 19% reduction	2981 ±67 53% reduction	4675 ±133 26% reduction	2648 ±147 58% reduction
90°C	Stress (MPa)	111.3 ±1.7	83.7 ±1.9 25% reduction	74.7 ±1.4 33% reduction	74.5 ±0.9 33% reduction	66.0 ±0.5 41% reduction	78.5 ±1.6 29% reduction	55.0 ±1.5 51% reduction
	Strain (%)	5.37 ±0.44	6.90 ±0.62 28% Increase	6.38 ±0.38 19% Increase	5.32 ±0.15 1% reduction	9.56 ±0.48 78% Increase	7.63 ±0.26 42% Increase	10.31 ±1.58 92% Increase
	Modulus (MPa)	5326 ±323	3888 ±165 27% reduction	3819 ±100 28% reduction	4072 ±89 24% reduction	2266 ±53 57% reduction	3579 ±48 33% reduction	1642 ±46 69% reduction
120°C	Stress (MPa)	90.8 ±3.1	70.7 ±1.8 22% reduction	61.3 ±1.6 32% reduction	63.6 ±1.7 30% reduction	58.7 ±0.8 35% reduction	69.6 ±0.8 23% reduction	47.1 ±1 48% reduction
	Strain (%)	4.7 ±0.11	7.14 ±0.63 52% Increase	7.57 ±0.58 61% Increase	6.94 ±0.27 48% Increase	9.54 ±0.35 103% Increase	7.69 ±0.59 64% Increase	10.65 ±0.81 127% Increase
	Modulus (MPa)	4837 ±140	3283 ±85 32% reduction	2848 ±81 41% reduction	3282 ±82 32% reduction	1950 ±40 60% reduction	2997 ±42 38% reduction	1340 ±40 72% reduction

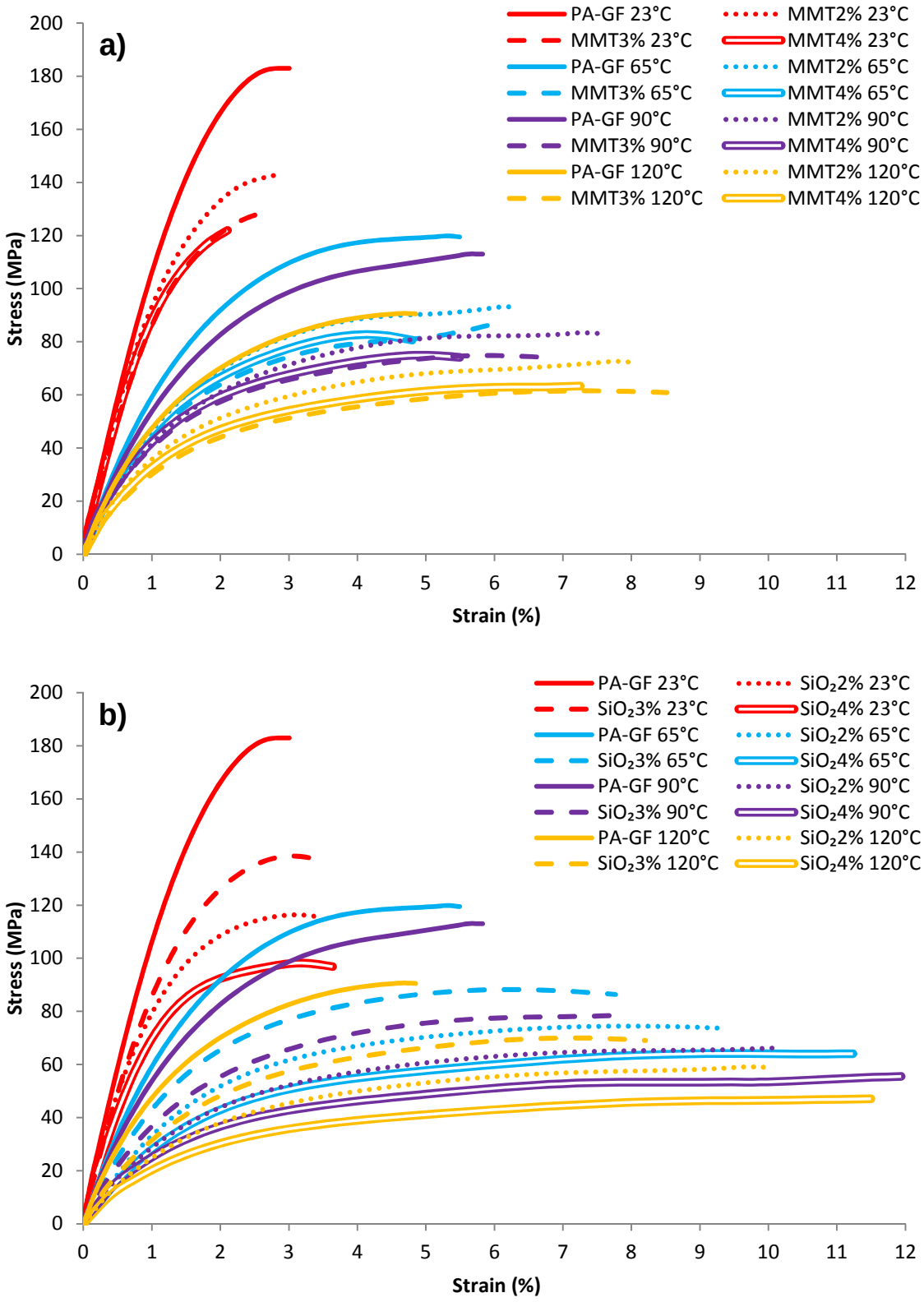

Figure 6-1: Plotted tensile stress/strain on material grades; a) OMMT and b) SiO_2 with different temperature conditions

Table 6-2: 3-point bend testing with different temperature conditions with nano grades compared to PA-GF as a reference

		PA-GF	OMMT2%	OMMT3%	OMMT4%	$SiO_2$2%	$SiO_2$3%	$SiO_2$4%
23°C	Stress (MPa)	292.5 ±10.6	247.7 ±6.1 15% reduction	233 ±2.3 20% reduction	223.1 ±2.2 24% reduction	213.9 ±2.5 27% reduction	250.4 ±2.1 14% reduction	190.1 ±1.2 35% reduction
	Strain (%)	4.7 ±0.09	4.41 ±0.18 6% reduction	4.09 ±0.17 13% reduction	3.48 ±0.12 26% reduction	6.17 ±0.29 31% Increase	5.46 ±0.15 16% Increase	6.29 ±0.22 34% Increase
	Modulus (MPa)	9094 ±201	8597 ±772 5% reduction	9049 ±42 0.5% reduction	9377 ±89 3% Increase	7570 ±11 17% reduction	8469 ±115 7% reduction	7027 ±28 23% reduction
65°C	Stress (MPa)	206.6 ±4.9	168.7 ±3 18% reduction	155.9 ±5.1 25% reduction	152.8 ±1.3 26% reduction	138.7 ±1.8 33% reduction	169.6 ±2.8 18% reduction	118.1 ±4 43% reduction
	Strain (%)	6.49 ±0.07	7.46 ±0.19 15% Increase	7.48 ±0.46 15% Increase	6.66 ±0.07 3% Increase	10.56 ±0.31 63% Increase	8.39 ±0.07 29% Increase	11.37 ±1.45 75% Increase
	Modulus (MPa)	5245 ±87	4465 ±40 15% reduction	4218 ±26 20% reduction	4367 ±35 17% reduction	3161 ±182 40% reduction	4137 ±353 21% reduction	3017 ±108 42% reduction
90°C	Stress (MPa)	184.8 ±2.3	150.6 ±1.2 19% reduction	136.5 ±2.4 26% reduction	136.7 ±2 26% reduction	125.1 ±1.9 32% reduction	152.8 ±0.9 17% reduction	97.6 ±2.1 47% reduction
	Strain (%)	5.88 ±0.08	7.63 ±0.26 30% Increase	7.92 ±0.36 35% Increase	6.5 ±0.25 11% Increase	10.11 ±0.6 72% Increase	8.38 ±0.03 43% Increase	12.45 ±1.11 112% Increase
	Modulus (MPa)	4661 ±286	3856 ±52 17% reduction	3338 ±41 28% reduction	3855 ±47 17% reduction	2678 ±66 43% reduction	3451 ±24 26% reduction	2305 ±75 51% reduction
120°C	Stress (MPa)	164.1 ±1.9	132.6 ±1.4 19% reduction	115.8 ±2.2 29% reduction	117.9 ±2.1 28% reduction	107.4 ±0.3 35% reduction	130 ±2.8 21% reduction	86.2 ±2.2 47% reduction
	Strain (%)	5.98 ±0.26	7.87 ±0.34 32% Increase	8.68 ±0.29 45% Increase	8.04 ±0.35 34% Increase	10.67 ±0.32 78% Increase	8.78 ±0.48 47% Increase	12.91 ±0.92 116% Increase
	Modulus (MPa)	4258 ±78	3299 ±44 23% reduction	2858 ±28 33% reduction	2960 ±31 30% reduction	2360 ±7 45% reduction	2870 ±26 33% reduction	2022 ±40 53% reduction

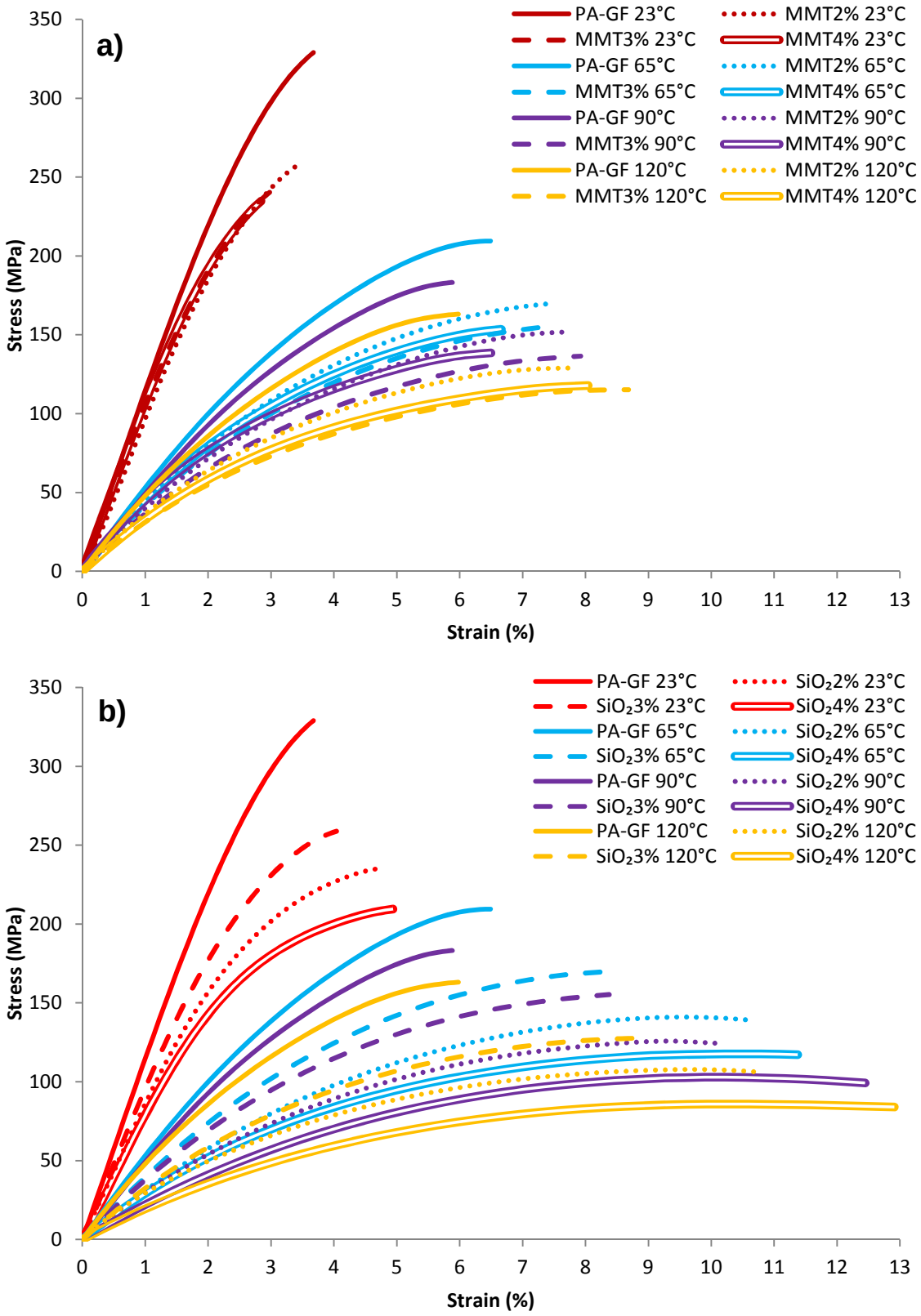

Figure 6-2: Plotted 3-point bending stress/strain on material grades; a) OMMT and b) SiO_2 with different temperature conditions

Although OMMT2% and $SiO_2$4% offer the greatest increase to strain of the two nano materials used, $SiO_2$4% comes with a significant trade-off to strength and modulus to all other nano grades. It can be said the SiO_2 grades have the same trade-off in stress-strain found in material B whereas OMMT grades offer better modulus and stress while retaining strain with not a significant improvement over the reference PA-GF grade. As the whole point of this work is to develop a new material system to replace the elastomer in material B, Figure 6-3a-d was plotted using tensile data to evaluate if any of the SiO_2 nano grades were suitable replacements.

When comparing all the SiO_2 grades to material B in Figure 6-3a-d, $SiO_2$2% and $SiO_2$3% stand out as a starting point for further development to replace material B for all temperatures tested. The $SiO_2$2% grade has a similar strain response to material B for all temperatures except 120°C which is 17% less than material B. But increases in temperature causes $SiO_2$2% tensile strength to drop from 14% to 19% at temperatures between 65 to 120°C respectively. The $SiO_2$3% grade has a similar stress response to material B for all temperatures tested. But $SiO_2$3% has a trade-off when tensile strain is considered, where strain falls below material B as much as 22% to 24% for temperatures between 23 to 90°C and 33% for 120°C. However, $SiO_2$4% is the only grade that can match and even surpass material B at temperatures 65 and 90°C for tensile strain, but is significantly defiant when it comes to tensile strength by as much as 26% to 35% between temperatures of 65 to 120°C, which is the operating range that the material is expected to function at. It is unlikely that, even if the glass fibre length could be retained for the $SiO_2$4% grade, it could offer enough mechanical strength to be a viable replacement for material B.

Glass fibre length was an issue going into this chapter with no reference materials predicting accurately how much mechanical strength each nano grade has lost. Figure 6-4 has been recreated from data by Thomason [54] who worked on glass fibre length in PA66 matrix at 30wt.% and 40wt.% fibre loadings. Data in Figure 6-4 illustrates a 7% improvement on 0.45mm fibres

over 0.34mm fibres (22% difference in fibre length) at 30wt.% fibre loading and a 14% improvement on 0.52mm fibres over 0.31mm fibres (40% difference in fibre length) at 40wt.% fibre loading. Figure 6-4 can also be used to predict that long fibres in a 35wt.% would have a 11% improvement. The SEM investigation in Chapter 1 with an average fibre length of 460µm was found in the RV350LW reference grade (35wt.% fibre loading). The compounded nano grades had the highest concentration of glass fibres with a length of 60µm ±15µm, which is a more than seven times greater reduction in fibre length and a five times reduction compared to material B 300µm fibre length, which is still a ten times magnitude difference than the fibres studied by Thomason. As $SiO_2$2% is the closest match to material B and now knowing there is a seven times fibre length reduction due to compounding, a 20% improvement to tensile stress to try and match material B would not be too much of an over prediction based on Thomason's findings for the 40wt.% grades with 14% improvement when long fibres are compared.

Figure 6-5 illustrates what $SiO_2$2% would look like if a 20% improvement to tensile stress was added and compared to the material B. At 23°C $SiO_2$2% is likely to exceed material B tensile strength with negligible difference in strain. At temperatures 65 and 90°C both materials are likely to be very similar, whereas 120°C material B is going to have up to 20% strain but, due to the application $SiO_2$2%, should still be an attractive alternative if compounding costs can produce the nano phase cheaper than adding elastomer third phase. Not forgetting that the 20% improvement on tensile stress will be a conservative expectation if glass fibre length was retained during compounding.

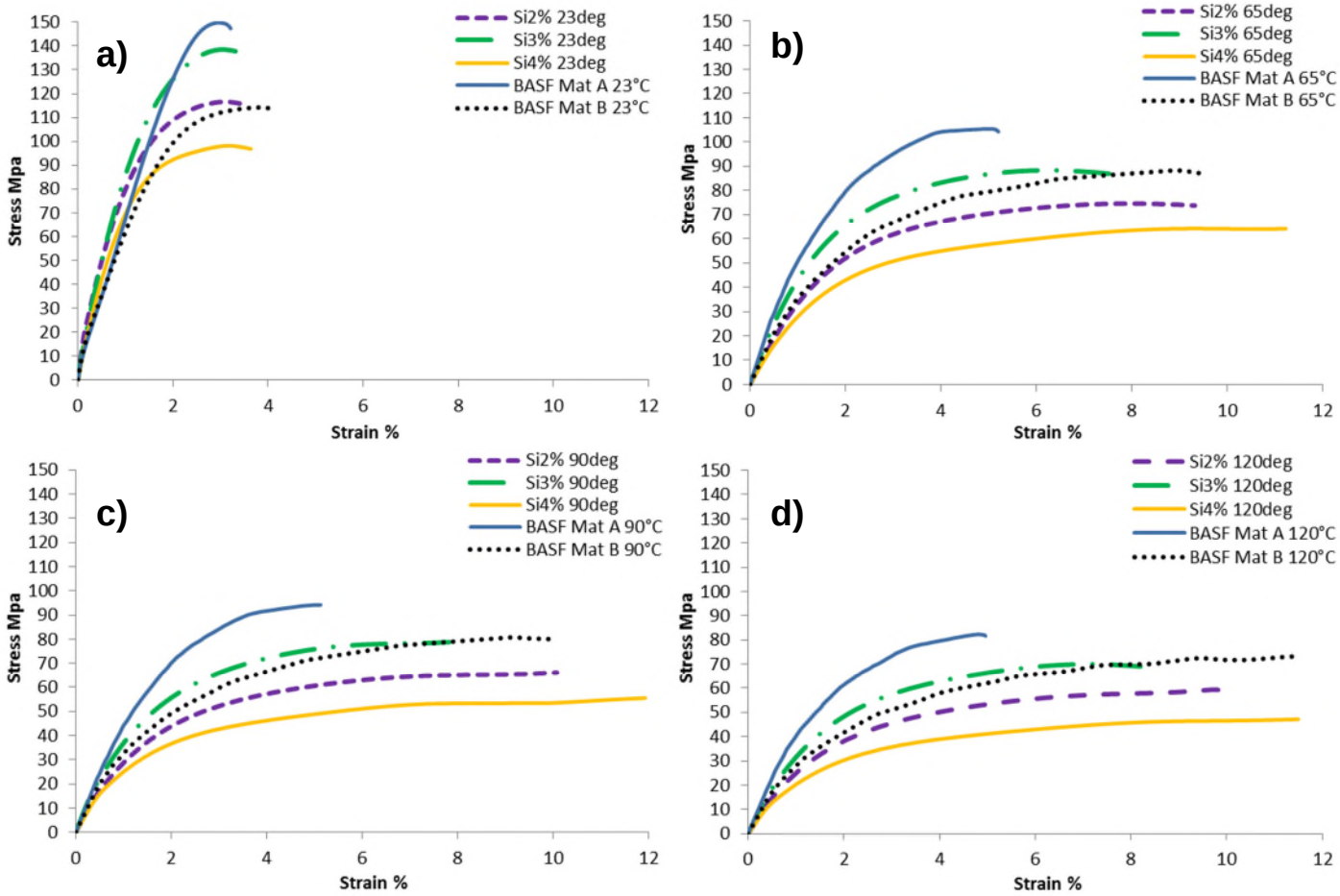

Figure 6-3: SiO_2 nano grade plotted against BASF Material A and B with a projection on what a $SiO_2$2% may look like is glass fibre length was retained from the compounding process

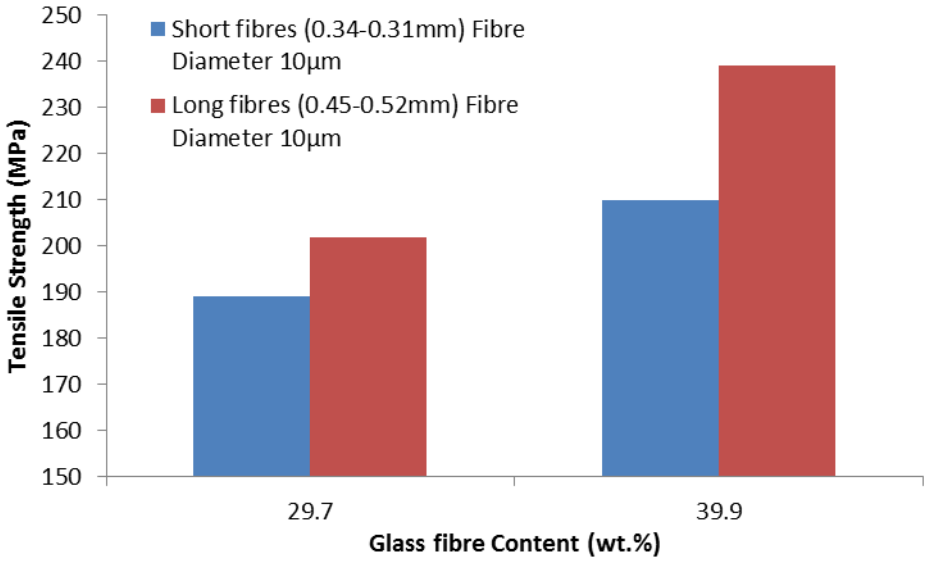

Figure 6-4: Plot illustrating the effect of glass length in a PA66 matrix recreated from work by Thomason [54]

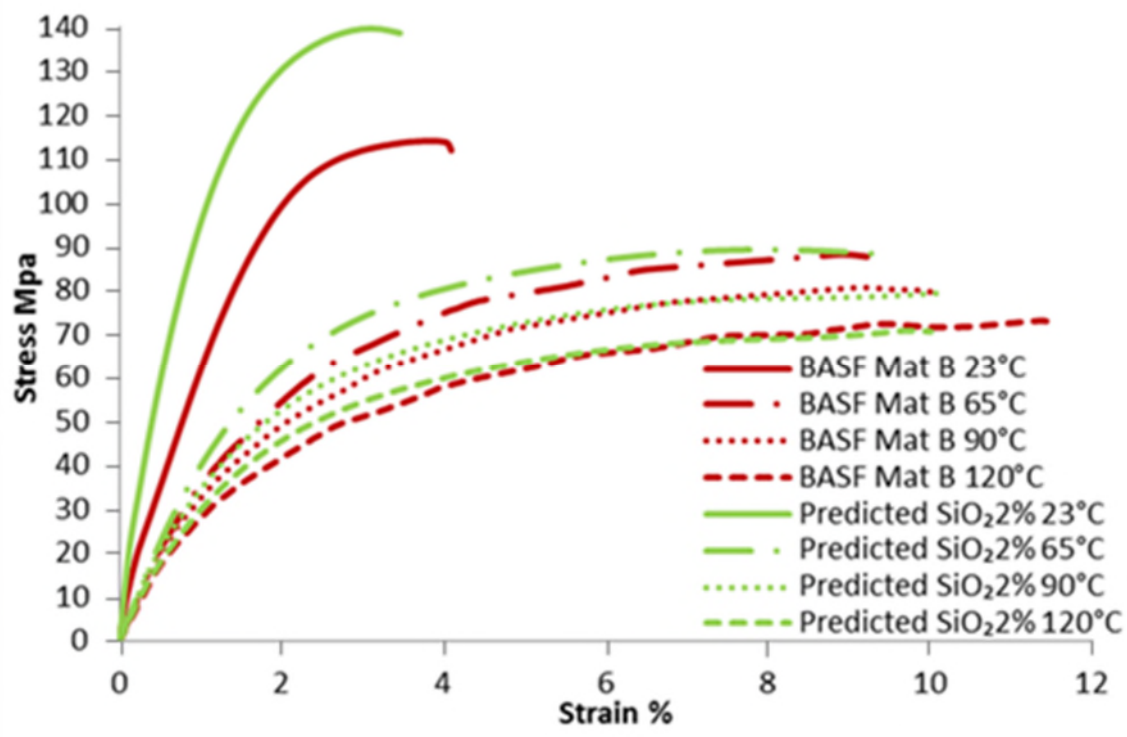

Figure 6-5: BASF material B with re-plotted $SiO_2$2% predicted 20% extra stress performance

6.4.2 Gas gun impact testing

Gas gun impacting results can be found in Table 6-3 with pass and failure criteria's reference in Figure 6-6. Results generated in Table 6-3 was conducted using an impact at energy of 3.5j ±0.33j which is within a 10% tolerance for shot repeatability. The 3.5j impact energy can be considered to be suitable impact energy to use in as it captured the influence of temperature on impact response. Failure assessment was done with images taken from thermography Figure 6-7 on PA-GF illustrates how thermography can be used to accurately capture fracture damage and size on the impacted and non-impacted surfaces. Figure 6-7 also demonstrates how fracture damage reduces when temperature is increased from 23°C to 120°C.

The results at 23°C for all nano grades tested fall into the worst case scenario with all samples failing as a whole (type 3 fail), whereas the PA-GF and material B references failed as a fracture on both surfaces (type 2 fail). As fracture failures can be measured on both PA-GF and material B using thermography it was expected material B would have reduced fracture length than the PA-GF grade. This was not the case with both materials having similar fracture lengths between 33mm ± 4mm across the 5 samples tested per material. To explain why the Radici PA-GF grade can match material B's impact performance and why material A falls short, can be found by comparing mechanical performance. PA-GF has a tensile strength of 183 MPa and material A is 150 MPa with a similar strain around 3% to each other which meant the PA-GF grade has a 16% greater tensile strength thus having a better impact performance over material A. It was expected that the PA-GF would perform better due to longer GF length offering a significant mechanical stress performance over the nanocomposite grades. It was also expected that all OMMT grades at 23°C would have poor impact performance due to reduced mechanical strain when compared to the PA-GF, material B references and SiO_2 grades. Although the SiO_2 grades have increased mechanical strain over the PA-GF reference the significant reduction stress has outweighed the strain increase. Using the predicted data plotted for $SiO_2$2% and Mat B at 23°C in

Figure 6-5, Figure 6-8 was created to illustrate that the predicted $SiO_2$2% would sit in the middle of Mat B and PA-GF thus the $SiO_2$2% with longer GF is likely to have a type 2 fail impact response. As the predicted $SiO_2$2% is a conservative prediction it is possible that a SiO_2 grade with full fibre length retention will outperform Mat B's impact performance at 23°C.

65°C testing now divides the two nanocomposites grades from each other, where OMMT grades failed as a type 3 and the SiO_2 grades failed as a type 2. Fracture length for $SiO_2$4% was the greatest at 41mm ±4mm, $SiO_2$2% 39mm ±3mm and $SiO_2$3% 28mm ±4mm. The reduction in the SiO_2 grades failure type can be contributed to the greater mechanical strain response for the SiO_2 grades seen in Figure 6-1 and Figure 6-2. However, saying this, the strain response for most of the OMMT grades is now surpassing the PA-GF reference grade. The increased strain does improve the OMMT grades toughness but the further reduction in mechanical stress has out weighted the increased strain benefit to improve impact performance. The PA-GF and material B reference grades continue as a type 2 fail with reduced fracture propagation to 23mm ±3mm for PA-GF and 21mm ±3mm for material B.

All grades tested at 90°C are now showing increased impact performance with OMMT grades failed as a type 2 fracture. Fracture length for OMMT4% was the greatest at 42mm ±3mm, OMMT3% 37± 2mm and OMMT2% 37mm ±2mm. SiO_2 grades continue as a type 2 failure with reduced fracture propagation with $SiO_2$4% 20mm ±2mm, $SiO_2$2% 18mm ± 3mm and $SiO_2$3% 18mm ±2mm. The PA-GF and material B reference grades now fail on the back surface of the plaque as a tensile rupture (fail type 1) as illustrated in Chapter 3 impact failure mechanism. At this point it could be argued using $SiO_2$2% with predicted 20% extra stress performance is going to give a similar impact performance as the PA-GF and material B grades. Figure 6-8 illustrates the predicted $SiO_2$2% with matching material B for mechanical performance.

Material grades at 120°C are still showing increase impact performance with OMMT grades still failing as a type 2 fracture. Fracture length for OMMT4%

showed the greatest at 33mm ±4mm, OMMT3% 26± 2mm and OMMT2% 24mm ±2mm. $SiO_2$4% now fails as a type 1 fracture with a fracture length of 5mm ±2mm. $SiO_2$4% had two impacted plaques that passed with one plaque having a 2.8mm type 1 fracture. $SiO_2$4% also had two plaques that had subsurface damage picked up in the thermography images. Subsurface damage can be seen in Figure 6-9 showing up as a bright spot up to 8mm in diameter on non-impacted image. This suggests a 3.5j impact is just over the top limit for the $SiO_2$4% grade. Thermography images taken on grades PA-GF, material B, $SiO_2$2% and $SiO_2$3% showed no surface or subsurface damage on all impacted plaques. It can be said PA-GF, material B, $SiO_2$2% and $SiO_2$3% grades can all withstand 3.5j impact at 120°C.

Table 6-3: Gas gun test results using an environmental chamber to condition material samples

		Impact Energy 3.5j ±0.33															
		PA-GF		Material-B		OMMT2%		OMMT3%		OMMT4%		$SiO_2$2%		$SiO_2$3%		$SiO_2$4%	
		Result	Failure	Result	Failure	Result	Failure	Result	Failure	Result	Failure	Result	Failure	Result	Failure	Result	Failure
Temperature	23°C	Fail	2	Fail	2	Fail	3	Fail	3	Fail	3	Fail	3	Fail	3	Fail	3
	65°C	Fail	2	Fail	2	Fail	3	Fail	3	Fail	3	Fail	2	Fail	2	Fail	2
	90°C	Fail	1	Fail	1	Fail	2	Fail	2	Fail	2	Fail	2	Fail	2	Fail	2
	120°C	Pass	-	Pass	-	Fail	2	Fail	2	Fail	2	Pass	-	Pass	-	Fail	1

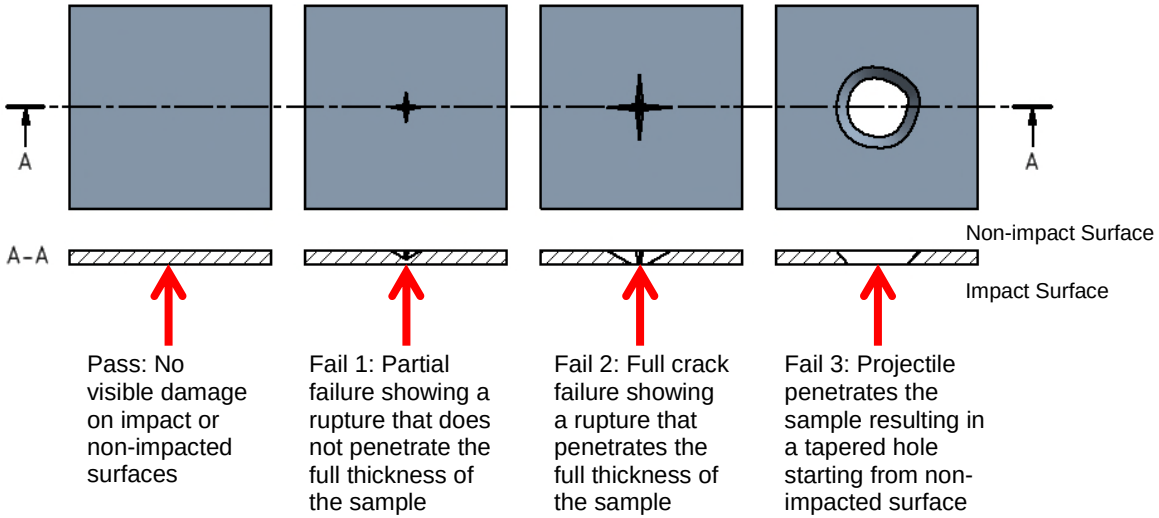

Figure 6-6: Illustrating the typical results and cross section of samples reference to failure criteria in table above

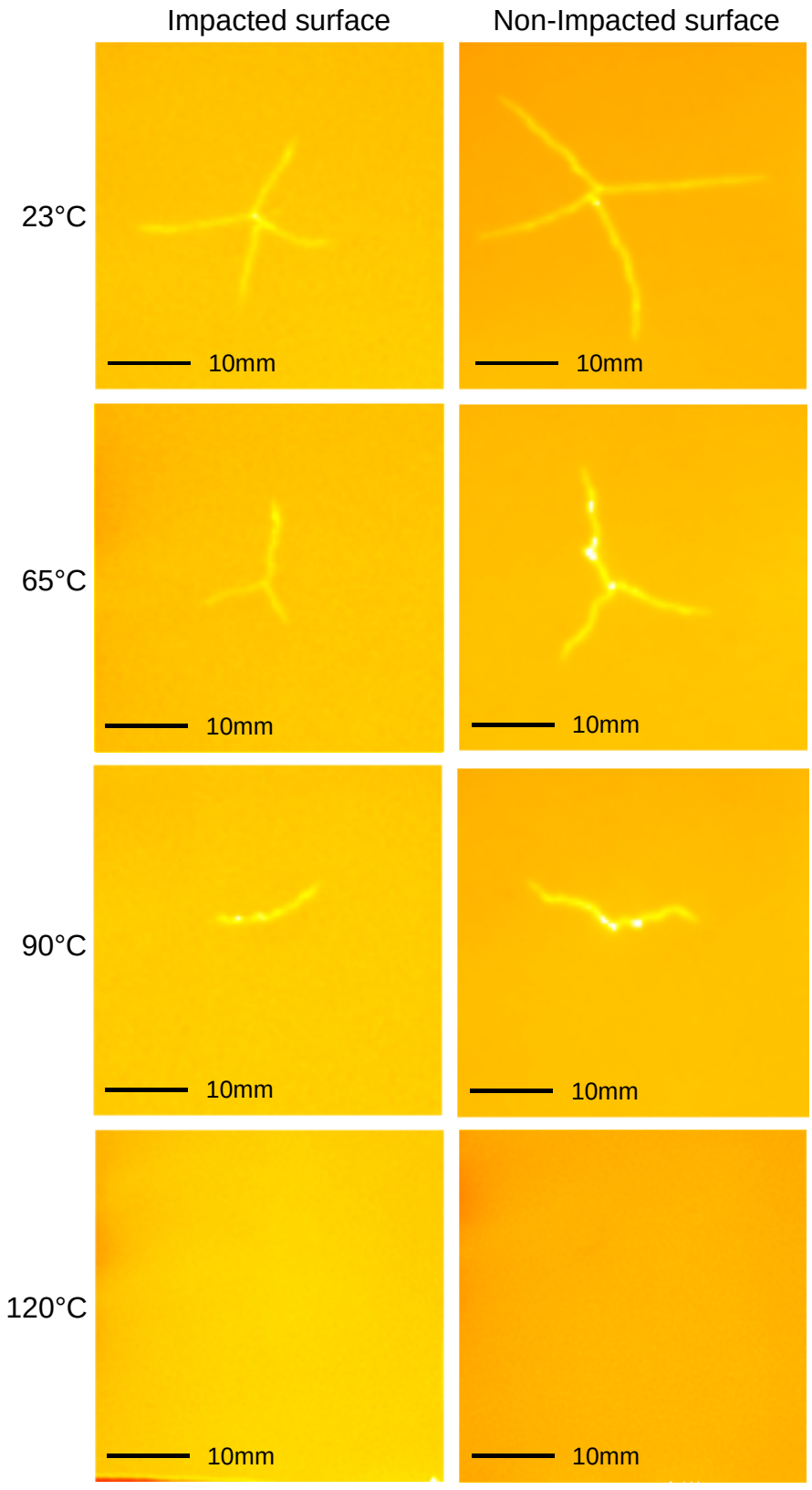

Figure 6-7: Cropped thermography images of impacted PA-GF plaque samples with impacted and non-impacted surfaces vs temperature

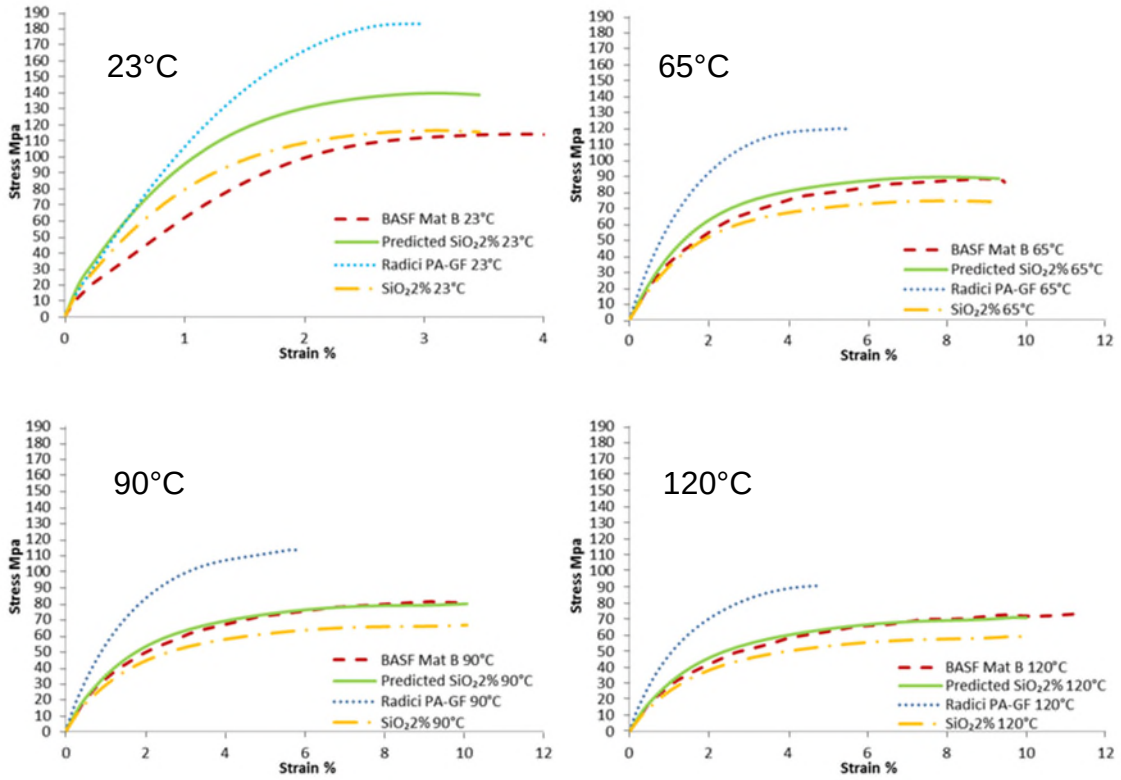

Figure 6-8: Plotted BASF mat B, predicted $SiO_2$2% in reference to Radici PA-GF

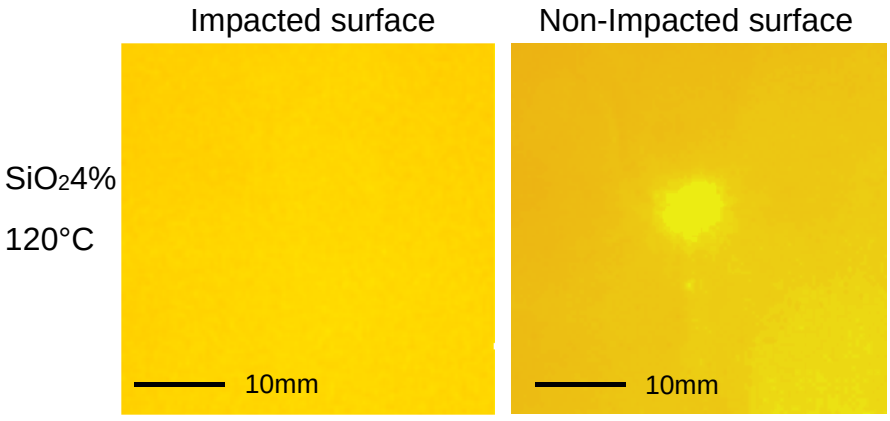

Figure 6-9: Thermography images of one of the $SiO_2$4% plaques with subsurface damage at 120°C

6.5 Conclusions and gaps in knowledge

In this study the influence of temperature on tensile and flexural properties of 3-phase nanocomposites has been investigated addressing gaps in current knowledge. As 3-phase nanocomposites are not commonly available this demonstrates the importance of the effects of temperature often over looked when selecting a new material that has an application above room temperature (23°C). This knowledge will be very important to automotive manufactures that will have need for the materials to operate at elevated temperatures.

Tensile and flexure testing plots show that mechanical strength reduces when temperature is increased, whereas mechanical strain increases with elevated temperatures. The types of nano particle and loading at each temperature had a clear effect on mechanical and impact performance.

As expected none of the nano grades could match or surpass the PA-GF reference grade for mechanical stress at any temperature tested. However, the nano grades did offer a significant improvement on mechanical strain especially when testing at temperatures above 23°C.

All of the nano grades studied would not suit the oil pan application in their current state. However, the predicted $SiO_2$2% with a conservative 20% improvement on mechanical stress matches the tensile plots of material B at different temperatures. Further work should consider retaining 540μm GF length found in PA-GF for nano grades $SiO_2$2% and $SiO_2$3%.

Evaluating impact damage on plaques which have only been impacted at one impact energy, it was observed that thermograph can clearly characterise fracture damage and was better than optical and visual observation.

The impact testing in this chapter does clearly illustrate one material that can be used to replace the current material B and that is the PA-GF reference. Not only does the PA-GF match the material B for impact performance in this chapter it out performs it for mechanical strength which will suit it for high stress applications under-the-bonnet.

Chapter 7. Experimental, Thermo-aging of 3-Phase nanocomposites

7.1 Introduction

All modern vehicles are built from a wide range of materials each having different properties to suit different component applications. Certain components will have an expected working life based on their application and environment. For instance none stressed components such as interior trim, door panels, seats, rear and side windows are typically expected to last the full life of the vehicle with an allowance to age and ware over time. Non stressed components can fail if used under conditions outside their normal service life, such as excessive use, mistreatment or as a result from a crash. Components that subjected to different types of loading and strain will wear to failure over time. But are expected to be replaced only a few times in a 10 year period such as bearings, cam belt, bushes and tyres. When considering the elastomer materials used for cam belt, bushes and tyres, there is often an expected shelf life before fitting to a vehicle where the material properties degrade over time and will cause the component to fail sooner due to aging. Components found under-the-bonnet are expected to operate at elevated temperatures. Chapter 6 testing results demonstrate a reduction in mechanical strength and increase in strain performance due to thermal effect on the matrix phase in PA-GF and nano grades. As the intended application for the PA-GF and nanocomposite grades is for an oil pan component, there is an expectation for the component to last the life of the vehicle and to operate at elevated temperatures. Thermal aging of reinforced and none reinforced PA6 and PA66 has been a subject to many studies from 90˚C to 170˚C documenting mechanical performance to degrade more quickly [164]–[167]. Thermal aging the composite PA materials at 140˚C for 1000 hours will accelerate the aging process and will allow each grade to be compared and rated. Further sampling to be taken out between the 1000 hours on a weekly basis will help map any effect on mechanical performance as a cross section of material performance over time.

This chapter was set out to benchmark an existing PA-GF grade with the six nano grades compounded in Chapter 1 and characterised mechanical performance over a six week thermal aging study.

7.2 Materials

RV350LW and nano grades were prepared as outlined in Chapter 1; refer to sections 4.2 Materials, 4.3.2 Grade processing. Section 4.3.4 Test sample injection moulding gives details on the tensile, flexure and plaque test samples standards and dimensions.

7.3 Thermo-aging, testing and characterisation experimental

7.3.1 Test sample aging

Before thermal aging was started all test samples where dried in the environmental chamber at 80°C for 24 hours. Dried samples where then labelled up weeks 0 to 6 for each material grade and placed in desiccator for up to 20 hours. The 20 hours in the desiccator was to keep the samples dry while allowing the environmental chamber to reach and stabilise at 140°C ready for the thermal aging to start. Thermal aging was conducted for total of 1008 hours with sampling taken at 168 hours to suit a working week for sample removal. Removed samples were place back into the desiccator to allow the samples to cool and to not absorb moisture before testing. Testing was done within 4 days of the thermal aging at 23°C.

7.3.2 Mechanical and impact test Methodology

Tensile and flexure testing were conducted on an Instron 5500R universal test machine. Tensile testing was conducted following ISO standard 527, testing speed for all specimens was 1 mm/min. Flexure testing was conducted following ISO standard 178 and all specimens were tested at 2 mm/min.

Charpy impact testing was conducted to ISO standard 179, on a Zwick D-790 desktop pendulum setup with a 4, 2 and 1j hammer attachments. Testing

span was calculated as 4 times width from the notch of the sample which equalled 50mm.

Gas gun impact testing was conducted using 10mm hemi-spherical projectile weighting 22g. The testing was done using impact energies of 2 and 3 joules to try and capture a border range of failure for each material over weeks tested. The required projectile velocity for the impact energy was calculated using equation (1). Specimen setup was done the same as section 3.2.4 with the high speed camera setup to verify each shot was straight and hit central to the plaque.

7.3.3 Scanning Electron Microscopy (SEM)

The samples were analysed on a Philips XL30 Field Emission SEM. Sample were carbon taped to sample stages before being sputter coated with gold-palladium.

7.3.4 Hi-speed camera setup

High speed camera footage was taken for every shot during gas gun testing using a Photron fastcam SA4 with a macro lens. Photron fastcam viewer (PVR) Ver.3.0 was used to record, playback and edit footage.

7.4 Results and discussion

7.4.1 Quasi static mechanical testing

Tensile and 3-point bending results can be found in Table 7-1, Table 7-2 Figure 7-1(a-f) and Figure 7-2(a-f) for all materials verses weeks tested in this chapter. Plotted data in Figure 7-1(a-f) and Figure 7-2(a-f) helps visualise tensile/bending stress, strain and modulus over time in weeks.

The PA-GF reference grade shows no significant change in tensile strength and modulus from the thermal aging. Tensile strength starts at 211.3MPa at week0 and ends with a 3% loss at week6 with no real effect in between. Tensile modulus starts at 11.2GPa at week 0 and ends with a 3% loss at week6 also no real effect in between. Tensile strain reduces during thermal aging starting at

4.16% at week0 and ends with 3.55% a 15% loss by week6. Tensile strain also shows an anomaly at week5 with an increase back to starting strain of 4.14% seen in weeks 0 and 1. The anomaly seen in week5 can also be seen for all other material grades tested suggesting there may be an issue with the testing itself. Test speed and lab temperature during testing was checked from notes with no issues obversed to influence the testing. The conditioning of the samples during week5, there was a ≤6 hour power cut 2 days before sample removal. This was considered acceptable as the temperature drop during the power outage was from 140°C to 118°C which was 16% (highest loss) at the sixth hour. But now considering week5 had a ≤6 hour loss during aging it can be seen in all materials tested for the tensile testing. Tensile modulus for PA-GF grade shows a small drop of 3% from week 0 to week 6 this can be considered an insignificant change for 6 weeks of aging.

Tensile testing of the aged OMMT grades has reduced the tensile strength performance of OMMT2%, OMMT3% and OMMT4% by 14%, 17% and 18.8% respectfully from week 0 to week 6. Aging has also reduced tensile strain performance of OMMT2%, OMMT3% and OMMT4% by 25% 35.7% and 33.2% respectfully from week 0 to week 6. Tensile modulus can be considered unaffected by the aging for any of the OMMT grades as the average deviation was below 2% for all the OMMT grades tested, which better than the PA-GF and SiO_2 grades. From the aging of the OMMT grades the 2% OMMT grade retains the best tensile strength and stain from the 6 week aging.

Tensile testing of the aged SiO_2 grades has had minimal effect on the tensile strength performance of $SiO_2$2%, $SiO_2$3% and $SiO_2$4% which have reduced by 1.2%, 5.8% and 4.4% respectfully from week 0 to week 6. Aging did reduced tensile strain performance of $SiO_2$2%, $SiO_2$3% and $SiO_2$4% grades by 17.4% 16% and 27.7% respectfully from week 0 to week 6. Tensile modulus can be considered unaffected by the aging for any of the SiO_2 grades as the average deviation was below 3% for all the SiO_2 grades tested. All the SiO_2 grades retained tensile strength and strain properties better than the OMMT

grades. Tensile modules from week 0 to week 6 showed no significant change on all material grades tested and would suggest aging has no effect.

The 3-point bending results at first glance shows an improvement for the PA-GF reference grade, with flexural strength improving from 325 MPa week 0 to 345 MPa in weeks 1 and 2. If week 0 was considered to be a true representative result then flexural strength is mostly retained during thermal aging finishing at 332MPa at week 6 a 2% improvement. Results show an initial gain from week 1 and week 2 before beginning drop back down gain. The initial gain is also visible for all the nano grades tested suggests the gain is linked to the thermal ageing removing further moisture with in the PA matrix. 3-point strain reduces during thermal aging starting at 3.67% at week0 and ends with 3.27% a 11% loss by week6. 3-point modulus starts at 11GPa at week 0 and ends with 11.5 a 4% gain at week6. PA-GF modulus only increases after week 3, this is also similar to all other grades tested.

3-point testing of the aged OMMT grades has reduced the tensile strength performance of OMMT2%, OMMT3% and OMMT4% by 4.8%, 14.9% and 18% respectfully from week 0 to week 6. Aging has also reduced tensile strain performance of OMMT2%, OMMT3% and OMMT4% by 21.7% 31.2% and 29.4% respectfully from week 0 to week 6. 3-point modulus shows a small improvement for the OMMT2%, OMMT3% and OMMT4% by 2.4%, 1.9% and 3.7% respectfully from week 0 to week 6. From the aging of the OMMT grades the 2% OMMT grade retains the best tensile strength and stain from the 6 week aging.

3-point bend strength of the aged SiO_2 grades has $SiO_2$2% and $SiO_2$3% has increase by 3.9% and 3.2% respectfully from week 0 to week 6. The $SiO_2$4% grade showed a 3.5% reduction in flexural strength from week 0 to week 6. Aging did reduced 3-point strain performance of $SiO_2$2%, $SiO_2$3% and $SiO_2$4% grades by 21.7% 20.5% and 34.2% respectfully from week 0 to week 6. However aging did increase 3-point modulus of the SiO_2 grades for $SiO_2$2%, $SiO_2$3% and $SiO_2$4% by 8.9% 4.7% and 10.4% respectfully from week 0 to 6.

Table 7-1: Tensile testing on aged material grades

		Week 0	Week 1	Week 2	Week 3	Week 4	Week 5	Week 6
PA-GF	Stress (MPa)	211.3 ±2.0	215.9 ±1.9	211.9 ±3.6	213.2 ±3.0	214.7 ±3.9	214.9 ±3.8	205.5 ±10
	Strain (%)	4.16 ±0.14	4.14 ±0.22	3.97 ±0.38	3.64 ±0.09	3.57 ±0.18	4.14 ±0.27	3.55 ±0.33
	Modulus(MPa)	11,176 ±325	11,392 ±197	11,034 ±129	11,117 ±316	11,183 ±128	10,916 ±68	10,822 ±167
OMMT2%	Stress (MPa)	162.8 ±3.6	159.3 ±5.8	155.7 ±2.9	153.3 ±7.2	151.3 ±0.7	148.7 ±17.3	139.9 ±5.6
	Strain (%)	2.88 ±0.23	2.89 ±0.23	2.79 ±0.15	2.58 ±0.04	2.31 ±0.05	2.88 ±0.12	2.16 ±0.19
	Modulus(MPa)	10,389 ±402	10,610 ±241	10,406 ±119	10,472 ±344	10,226 ±87	10,240 ±141	10,264 ±181
OMMT3%	Stress (MPa)	145.5 ±2.4	142.1 ±0.7	135.2 ±1.3	136.4 ±0.5	129.3 ±1.8	136.8 ±1	120.8 ±2.2
	Strain (%)	2.72 ±0.17	2.63 ±0.16	2.28 ±0.04	2.16 ±0.03	1.91 ±0.08	2.19 ±0.06	1.75 ±0.05
	Modulus(MPa)	10,366 ±489	10,250 ±204	10,259 ±205	10,447 ±130	10,239 ±52	10,149 ±126	10,203 ±99
OMMT4%	Stress (MPa)	138.9 ±6.6	136.1 ±2.5	129.2 ±4.1	128.8 ±1.8	120.0 ±2.3	129.5 ±2.4	111.4 ±2.9
	Strain (%)	2.29 ±0.11	2.30 ±0.09	2.03 ±0.09	1.89 ±0.08	1.63 ±0.04	1.92 ±0.08	1.53 ±0.08
	Modulus(MPa)	10,507 ±210	10,521 ±171	10,523 ±181	10,653 ±134	10,546 ±89	10,412 ±149	10,311 ±92
$SiO_2$2%	Stress (MPa)	133.7 ±0.8	133.5 ±2.6	134.0 ±0.6	136.6 ±0.9	136.7 ±0.3	137.6 ±0.8	132.1 ±1.1
	Strain (%)	3.86 ±0.09	3.66 ±0.19	3.64 ±0.16	3.39 ±0.12	3.26 ±0.08	3.57 ±0.23	3.19 ±0.16
	Modulus(MPa)	8,919 ±259	8,824 ±102	8,819 ±78	9,021 ±105	8,959 ±129	8,822 ±51	8,774 ±184
$SiO_2$3%	Stress (MPa)	159.1 ±2.4	158.0 ±0.7	154.5 ±4.8	159.2 ±1.2	159.1 ±0.6	148.8 ±24.1	149.9 ±4.3
	Strain (%)	3.69 ±0.19	3.55 ±0.17	3.53 ±0.17	3.40 ±0.14	3.28 ±0.08	3.39 ±0.44	3.1 ±0.15
	Modulus(MPa)	9,877 ±1482	9,738 ±82	9,422 ±306	9,741 ±137	9,771 ±83	9,352 ±144	9,582 ±127
$SiO_2$4%	Stress (MPa)	112.8 ±1.3	114.0 ±0.9	112.9 ±1.2	116.1 ±0.7	114.1 ±1.9	113.6 ±4.5	107.8 ±2.4
	Strain (%)	3.43 ±0.14	3.29 ±0.25	3.21 ±0.11	3.00 ±0.07	2.74 ±0.22	2.91 ±0.42	2.48 ±0.19
	Modulus(MPa)	8,305 ±157	8,235 ±142	8,213 ±149	8,358 ±203	8,351 ±78	8,184 ±97	8,092 ±94

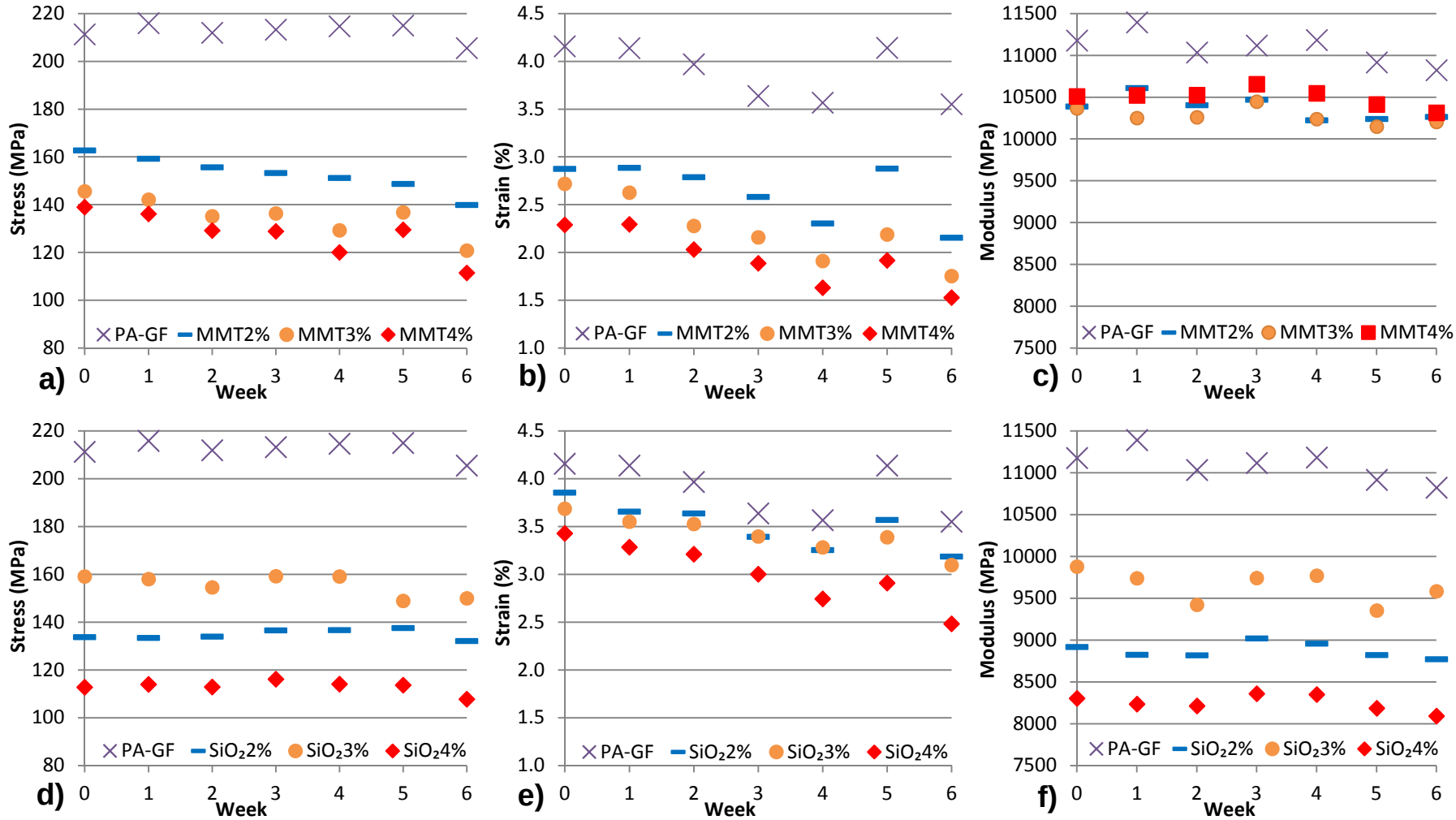

Figure 7-1: Plotted tensile testing on aged material grades; a), b) and c) OMMT; d), e) and f) SiO_2 grades

Table 7-2: Three-point bending testing on aged material grades

		Week 0	Week 1	Week 2	Week 3	Week 4	Week 5	Week 6
PA-GF	Stress (MPa)	325.2 ±6.1	344.9 ±2.9	345.4 ±3.6	336.4 ±3.8	332.2 ±4.3	326.8 ±6.3	331.9 ±3.8
	Strain (%)	3.67 ±0.01	3.68 ±0.07	3.65 ±0.07	3.48 ±0.07	3.41 ±0.07	3.23 ±0.1	3.27 ±0.1
	Modulus(MPa)	11,054 ±61	11,051 ±268	11,079 ±114	11,241 ±177	11,348 ±183	11,289 ±246	11,494 ±578
OMMT2%	Stress (MPa)	238.7 ±1	250.0 ±9.8	247.4 ±8.4	236.0 ±6.5	226.3 ±10.3	228.9 ±4.1	227.3 ±2.9
	Strain (%)	2.86 ±0.03	2.84 ±0.05	2.68 ±0.1	2.48 ±0.09	2.57 ±0.43	2.31 ±0.11	2.24 ±0.04
	Modulus(MPa)	10,190 ±44	10,045 ±288	10,175 ±170	10,594 ±263	10,477 ±208	10,539 ±374	10,432 ±480
OMMT3%	Stress (MPa)	228.3 ±0.9	229.5 ±4.9	227.7 ±2.1	204.4 ±5.8	192.0 ±3.2	194.0 ±3.8	194.2 ±2.2
	Strain (%)	2.82 ±0.06	2.59 ±0.09	2.51 ±0.04	2.15 ±0.09	1.97 ±0.04	1.97 ±0.04	1.94 ±0.02
	Modulus(MPa)	10,137 ±39	10,097 ±154	10,108 ±80	10,321 ±174	10,231 ±300	10,286 ±219	10,326 ±326
OMMT4%	Stress (MPa)	217.3 ±1.2	216.0 ±5.7	212.0 ±7	187.7 ±12.5	179.6 ±4.5	181.0 ±3.4	178.2 ±4.9
	Strain (%)	2.45 ±0.05	2.30 ±0.1	2.21 ±0.12	1.88 ±0.12	1.77 ±0.06	1.75 ±0.06	1.73 ±0.06
	Modulus(MPa)	10,201 ±19	10,194 ±315	10,324 ±88	10,605 ±181	10,855 ±368	10,850 ±378	10,578 ±135
$SiO_2$2%	Stress (MPa)	230.9 ±2.1	244.0 ±2.6	246.1 ±3.5	245.4 ±3	239.6 ±3.2	234.8 ±4.6	239.9 ±3.1
	Strain (%)	4.23 ±0.08	3.83 ±0.13	3.79 ±0.11	3.74 ±0.1	3.53 ±0.13	3.24 ±0.06	3.31 ±0.09
	Modulus(MPa)	8,605 ±15	8,624 ±184	8,610 ±326	8,898 ±167	9,128 ±267	9,203 ±201	9,374 ±276
$SiO_2$3%	Stress (MPa)	259.7 ±6.9	274.2 ±4.8	277.4 ±4.3	272.9 ±6.3	264.4 ±6	263.2 ±5.8	267.9 ±2.3
	Strain (%)	4.04 ±0.2	3.58 ±0.15	3.58 ±0.08	3.50 ±0.16	3.34 ±0.11	3.23 ±0.1	3.21 ±0.08
	Modulus(MPa)	9,723 ±26	9,750 ±135	9,771 ±134	9,825 ±131	9,837 ±191	9,966 ±298	10,179 ±241
$SiO_2$4%	Stress (MPa)	199.9 ±0.5	215.3 ±2.2	214.4 ±4.4	205.8 ±7.8	205.1 ±1	196.8 ±12.3	192.9 ±10.3
	Strain (%)	4.09 ±0.09	3.68 ±0.06	3.52 ±0.2	3.20 ±0.27	3.18 ±0.03	2.91 ±0.39	2.69 ±0.25
	Modulus(MPa)	8,075 ±32	8,283 ±107	8,312 ±122	8,340 ±237	8,411 ±112	8,648 ±277	8,918 ±127

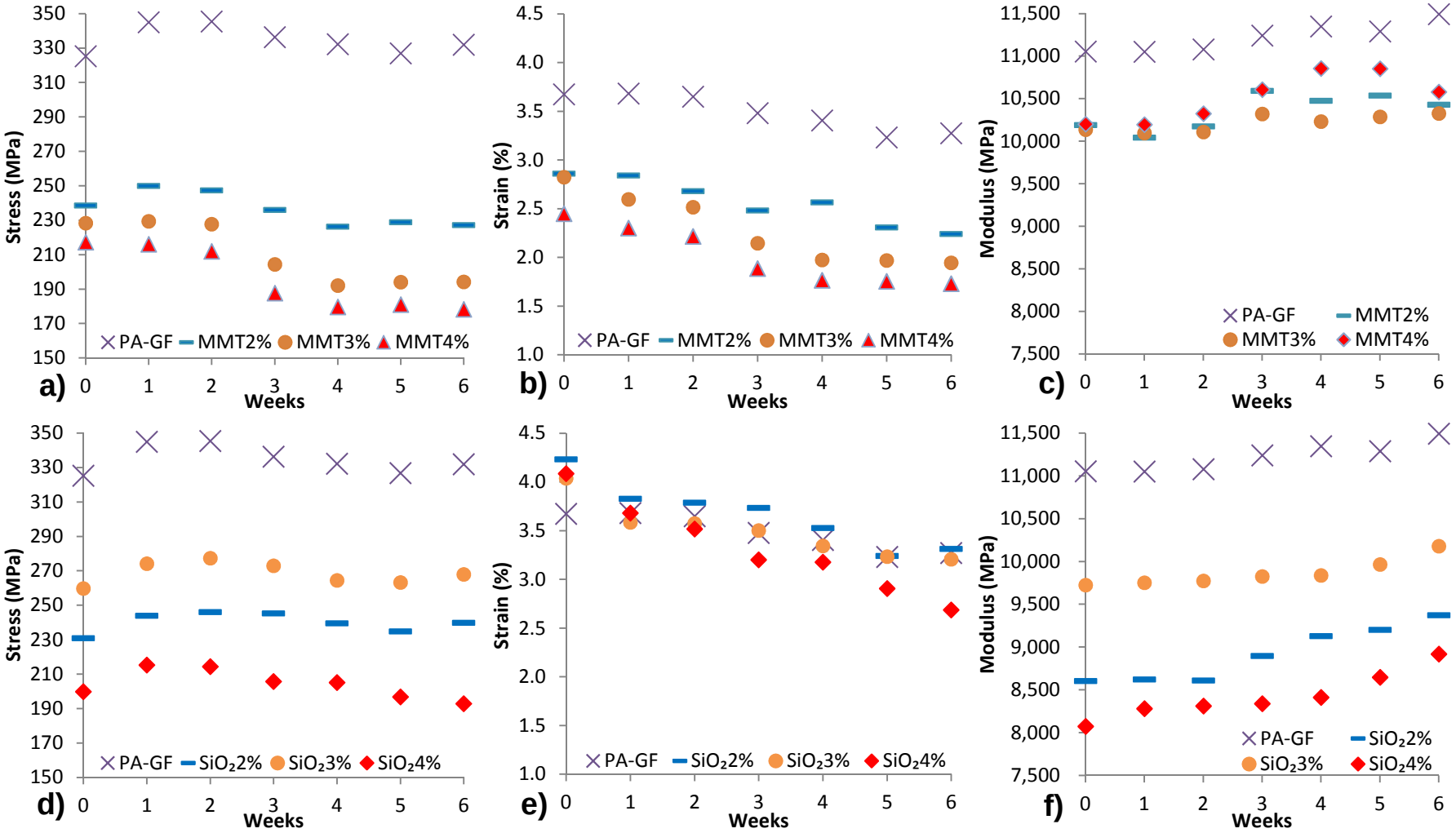

Figure 7-2: Plotted Three-point bending testing on aged material grades; a), b) and c) OMMT; d), e) and f) SiO_2 grades

7.4.2 Charpy notched impact testing

Notched Charpy impact results can be found in Table 7-3 and Figure 7-3 for all materials verses weeks tested in this chapter. Table 7-3 has been included to show the standard deviations which would not have come across easily on Figure 7-3 due to the nano results are very close and are on top of each other. All material grades tested break into two pieces having a similar function as the 3-point bending with non-impacted side which initiates as tensile rupture which then develops though the width of the sample until it fails.

The results in Figure 7-3 clearly shows the PA-GF grade is toughest, failing at higher impact energies when compared to the nano grades which are failing at lower impact energies suggesting that they are brittle. The lower failure energies can be contributed to the reduced fibre length for the compounded nano grades as discussed in Chapter 1. SEM images in Figure 7-4 show the typical fracture surface from the Charpy testing. The left image of the PA-GF grade with long fibre pull-out up to 100µm, whereas the right hand image is a $SiO_2$4% grade to illustrating the typical fracture surface found on each of the nano grades with minimal fibre pull-out up to 30µm. As the Charpy impact failure mechanism starts as tensile failure the PA-GF grade benefits from the longer fibres supporting a greater load thus an improved impact resistance.

As expected from the tensile and 3-point bending results the thermal aging in Table 7-3 shows reduces the impact performance over the six week aging. Not all of the grades see this effect early on in the aging with most grades seeing effect after the first three weeks, it is likely that all grades lose mechanical and impact performance equally around the three week period but is hidden in the deviation scatter. The three week period before properties begin to degrade can be contributed to the thermal stabilisers used in the PA-GF reference grade to help the polymer matrix decomposing from accelerated heat aging. However the degradation of performance from week0 to week6 is likely to be a result from the aging annealing the crystalline structure for the PA66 matrix, this would explain why all grades are experiencing degradation of

performance over time. The PA-GF grade at week 0 is 13.3j and reduces by 9% at week 6. The OMMT grades OMMT2%, OMMT3% and OMMT4% at week 0 start at 5.3, 5.4 and 4.7j and by week 6 have reduced by 9.4, 20.4 and 8.5% respectfully. The OMMT losses are similar to the PA-GF reference except for the OMMT3% grade. The OMMT3% grades reduction by 20.4% at first glance could have a discrepancy in the results for week 0, but considering reduction from week 1 to week 6 works out 14%, week 0 can be considered a representative result. The SiO_2 grades $SiO_2$2%, $SiO_2$3% and $SiO_2$4% at week 0 start at 4.9, 7.6 and 4.0j and by week 6 have reduced by 10.2, 13.1 and 15% respectfully. When comparing the SiO_2 grades losses to PA-GF, OMMT2% and OMMT4% grades the SiO_2 losses become grater at higher percent additions of SiO_2. The percent of SiO_2 addition should be factored into the life cycle of the material if the application features impact performance. However when comparing the nano results in Figure 7-3 the $SiO_2$3% grade clearly shows the best impact performance of any of the nano grades tested. Although none of the nano grades can match or outperform the PA-GF grade for impact performance, it can be said each nano grade material and content loading in percent does have its own effect on impact performance. Further work should focuse on a PA-GF using SiO_2 with loadings between 2 and 3% while retaining glass fibre length.

Table 7-3: Notched Charpy impact on aged material grades with standard deviation

		PA-GF	OMMT 2%	OMMT 3%	OMMT 4%	SiO_2 2%	SiO_2 3%	SiO_2 4%
Week	0	13.3j ±0.4	5.3j ±0.2	5.4j ±0.2	4.7j ±0.2	4.9j ±0.3	7.6j ±0.8	4.0j ±0.3
	1	12.9j ±0.4	5.4j ±0.4	5.0j ±0.1	4.7j ±0.1	4.8j ±0.3	7.1j ±0.5	3.8j ±0.3
	2	12.9j ±0.6	5.2j ±0.2	4.9j ±0.4	4.7j ±0.2	4.9j ±0.2	6.8j ±0.5	3.7j ±0.2
	3	13.0j ±0.8	5.2j ±0.3	4.6j ±0.2	4.6j ±0.5	4.8j ±0.2	6.6j ±0.7	3.7j ±0.3
	4	12.5j ±0.7	5.1j ±0.3	4.4j ±0.2	4.4j ±0.3	4.8j ±0.3	6.4j ±0.7	3.7j ±0.3
	5	11.9j ±0.8	5.0j ±0.2	4.4j ±0.1	4.2j ±0.2	4.8j ±0.1	6.5j ±0.4	3.5j ±0.4
	6	12.1j ±0.4	4.8j ±0.1	4.3j ±0.2	4.3j ±0.1	4.4j ±0.2	6.6j ±0.4	3.4j ±0.4

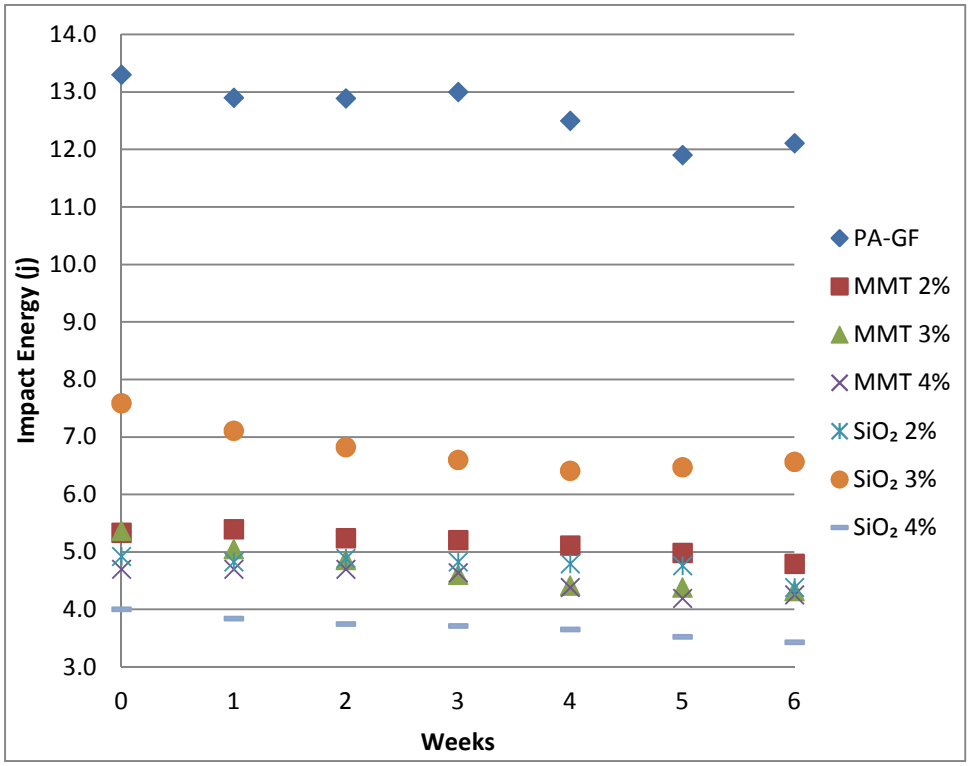

Figure 7-3: Plotted Notched Charpy impacts on aged material grades

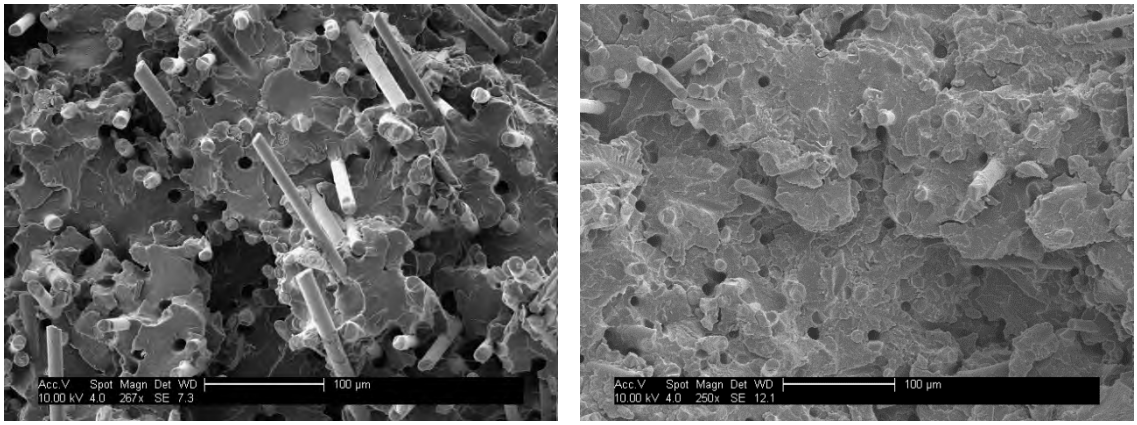

Figure 7-4: SEM images of fractured Charpy samples; Left PA-GF; Right $SiO_2$4%

7.4.3 Gas gun impact testing

Gas gun impact results can be found in Table 7-4 for all materials tested with failure assessment. Failure assessment was done by eye for obverse fractures and thermography images taken on majority of small fractures. Pass and fail criteria can be found in Figure 6-6 in the previous chapter. Two impact energies where selected 2 and 3j to gain an indication where the different failure criteria's can be seen for each material grade tested. The 2j ± 0.14 and 3j ± 0.19 impact energies are within ±7% and ±6.3% tolerance respectfully for shot repeatability. The 2j impacts capture initial failure and different failure types for most nano composite grades over the 6 week aging. 3j was suitable energy to capture initial failure and different failure types for PA-GF and $SiO_2$3%. Across all material grades impact tested, the trend found in mechanical test can also be seen material performance reduces over weeks aged. Figure 7-5 illustrates with images of $SiO_2$4% impacted at 2j and demonstrates how fracture damage increases the longer the material sample is aged 0 to 6 weeks from a type1 rupture to a type3 hole.

The results in Figure 7-5 shows the PA-GF grade has the best impact performance for both impact energies tested with the 2j impact tests resulting in no failures for the full 6 weeks of aging. 3j impacts on PA-GF between weeks 0 to 2 now fails as a type1 failure and weeks 3 to 6, failure increases to a type2. PA-GF failure point is going to be somewhere between 2 and 3j. 2j impact on OMMT2%, OMMT3% and $SiO_2$2% give the same type1 failure between weeks 0 to 2 and type2 weeks 3 to 6 with one discrepancy with OMMT3% week1 showing a fail type 2 in-between a type1 on week0 and week2. On further investigating of the results and notes taken gives average impact energy of 2.18j for OMMT3% at week1, this means the impacts where on high end of the impact repeatability. Figure 7-6 illustrates why shot repeatability needs to be improved on 2j impacts and further work should consider improving the gas gun's shot repeatability within a ±2.5% tolerance (±0.05j on a 2j impact). This may include replacing the pressure gauge on the gas gun with a gauge with

higher resolution or to test more samples and selected the ones that are within tolerance.

2j impact on OMMT4% has least impact performance out of any of the nano grades which fail as a type2 in weeks 0 to 2 and as a type3 week 3 to 6. $SiO_2$3% offers the best impact performance out of all the nano grades tested, passing on weeks 0 to 3 and failing as a type1 on weeks 4 to 6. $SiO_2$4% offer the least amount of impact performance of any of the SiO_2 grades, with week 0 starting as a type1 failure, weeks 1 to 4 type2 and week 5 to 6 type3. 3j impacts on all OMMT grades, $SiO_2$2% and $SiO_2$4% resulted in a full failure (type 3) for all aged samples. 3j impacts on $SiO_2$3% between weeks 0 and 3 shows an improvement with a failure type 2, this improvement over other nano grades can be linked to $SiO_2$3% having better mechanical strength with a good mechanical stain responses to dissipate the impact energy. Week 4 to 6 $SiO_2$3% fails as a type3 the same as all other nano composites. It's a clear indication that none of the nano grades would be a suitable replacement for PA-GF grades used for automotive applications.

When comparing the tensile and 3-point bending strength results Figure 7-1(a and d) and Figure 7-2(a and d) to gas gun impact results in Table 7-4, results show grades that have the best impact performance are also the same grades that have the best mechanical strength. This suggests the primary mechanical property linked to impact performance is strength as discussed in chapters 5 and 6. It can be argued at this point the predicted $SiO_2$2% grade in Figure 6-8 could offer an improved impact performance over a 6 week aging and would justify further work to be done on SiO_2 grades close to the 2% loading.

Table 7-4: Gas gun test results using samples that have been thermal aged from 0 to 6 weeks

		Impact Energy 2j ±0.14													
		PA-GF		OMMT2%		OMMT3%		OMMT4%		$SiO_2$2%		$SiO_2$3%		$SiO_2$4%	
		Result	Failure	Result	Failure	Result	Failure	Result	Failure	Result	Failure	Result	Failure	Result	Failure
Week	0	Pass	-	Fail	1	Fail	1	Fail	2	Fail	1	Pass	-	Fail	1
	1	Pass	-	Fail	1	Fail	2	Fail	2	Fail	1	Pass	-	Fail	2
	2	Pass	-	Fail	1	Fail	1	Fail	2	Fail	1	Pass	-	Fail	2
	3	Pass	-	Fail	2	Fail	2	Fail	3	Fail	2	Pass	-	Fail	2
	4	Pass	-	Fail	2	Fail	2	Fail	3	Fail	2	Fail	1	Fail	2
	5	Pass	-	Fail	2	Fail	2	Fail	3	Fail	2	Fail	1	Fail	3
	6	Pass	-	Fail	2	Fail	2	Fail	3	Fail	2	Fail	1	Fail	3
		Impact Energy 3j ±0.19													
		PA-GF		OMMT2%		OMMT3%		OMMT4%		$SiO_2$2%		$SiO_2$3%		$SiO_2$4%	
		Result	Failure	Result	Failure	Result	Failure	Result	Failure	Result	Failure	Result	Failure	Result	Failure
Week	0	Fail	1	Fail	3	Fail	3	Fail	3	Fail	3	Fail	2	Fail	3
	1	Fail	1	Fail	3	Fail	3	Fail	3	Fail	3	Fail	2	Fail	3
	2	Fail	1	Fail	3	Fail	3	Fail	3	Fail	3	Fail	2	Fail	3
	3	Fail	2	Fail	3	Fail	3	Fail	3	Fail	3	Fail	2	Fail	3
	4	Fail	2	Fail	3	Fail	3	Fail	3	Fail	3	Fail	3	Fail	3
	5	Fail	2	Fail	3	Fail	3	Fail	3	Fail	3	Fail	3	Fail	3
	6	Fail	2	Fail	3	Fail	3	Fail	3	Fail	3	Fail	3	Fail	3

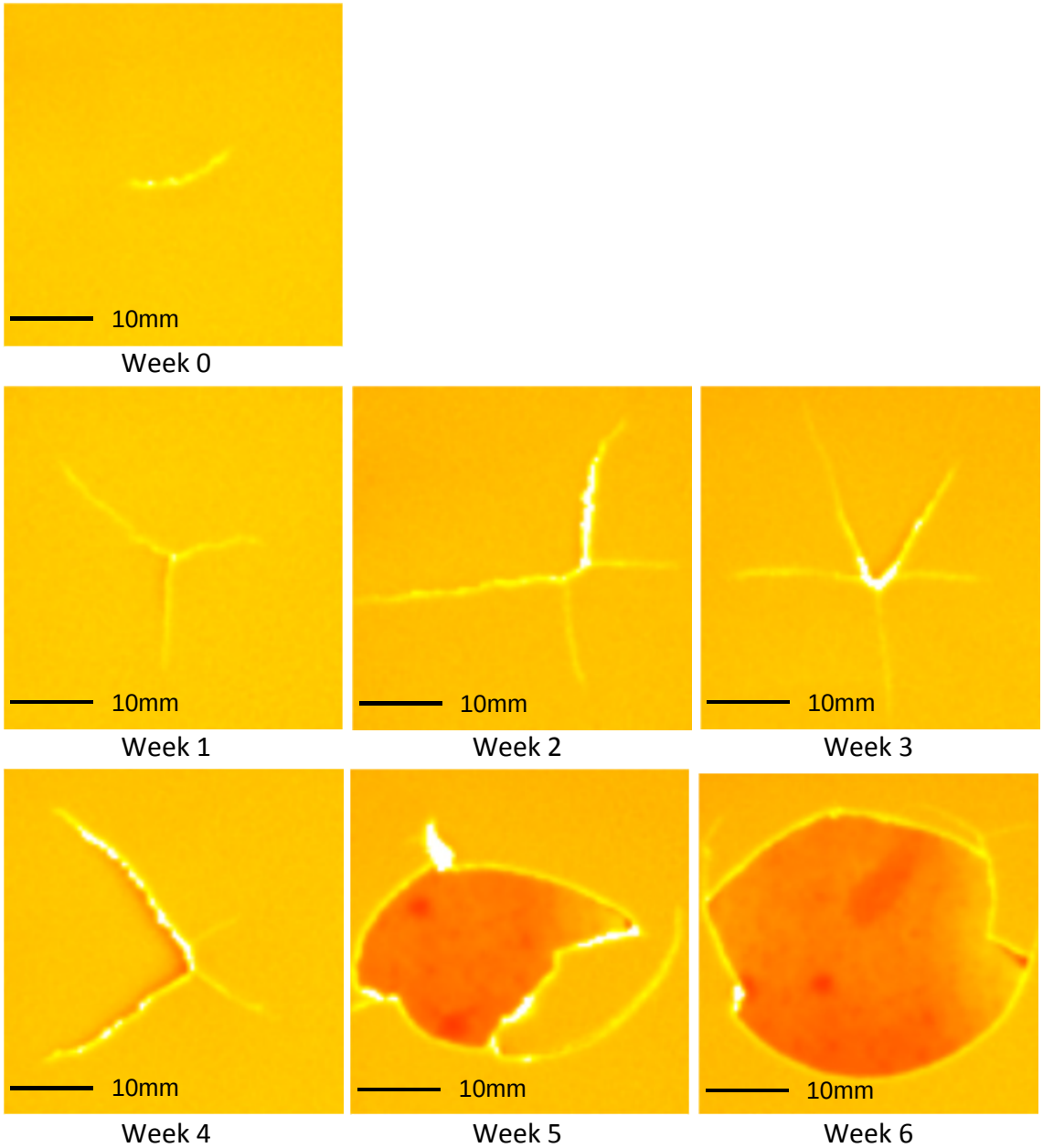

Figure 7-5: Cropped thermography images of impacted $SiO_2$4% plaque samples at 2j illustrating failure types 1, 2 and 3 influence by the aging.

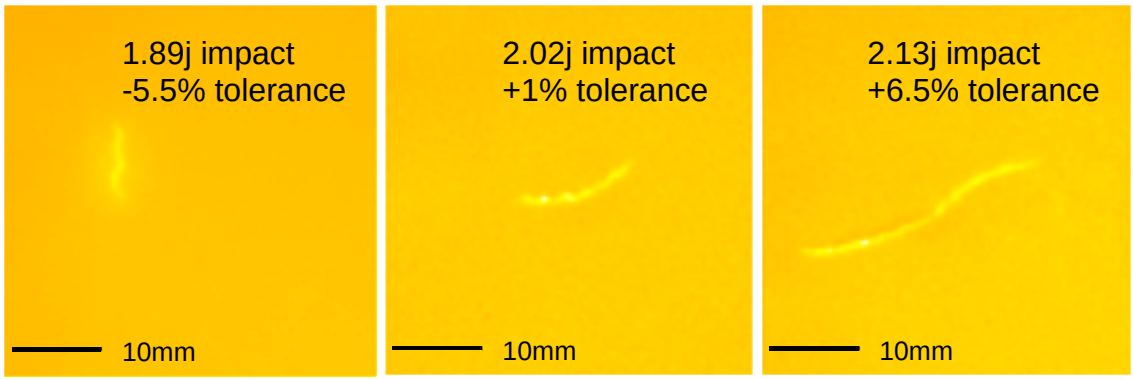

Figure 7-6: Images showing why shot repeatability needs to be improved on 2j impacts

7.5 Conclusions, contribution to knowledge and further work

The results from the tensile and 3-point bending tests mainly show mechanical properties retained similar gains and losses for nano grades when comparing to the PA-GF reference grade. Therefore, it can be concluded that the addition of nano particle reinforcement will not significantly reduce the existing life span of PA-GF though mechanical property degradation. $SiO_2$2% retains the best mechanical performance of any of the nano composites but still need further work to retain both tensile and flexural strength to be a viable replacement to Radici PA-GF reference grade and material B.

The 6 hour power cut, 2 days before sample removal illustrated a possible relaxation for all the material grades tested. This was primarily seen in the tensile strain returning to the same strain found in weeks 0, 1 and 2. Whereas flexure strain showed for all material grades had a reduction of around 1 to 3% for week5 when compared to week6 which is small inconsistency.

Contribution to Knowledge in this chapter demonstrates 3-phase nanocomposites will not decay any differently to the commercial grade tested. Knowledge is specific to adding SiO_2 and OMMT to a PA-GF, when thermal aging considered. This adds value to industry confidence on material selection when compared to current commercial available.

Further work should consider cycling in the thermal aging to see if other mechanical properties can be retained during aging, as this will help simulate

the automotive application. Other further work should consider improving shot repeatability within a ±5% tolerance to allow fracture results to be measured and compared more accurately when using thermography. The issue with the ±7% and ±6.3% shot repeatability for 2j and 3j impacts respectfully can be seen in Figure 7-6.

Chapter 8. Conclusions and further work

8.1 Conclusions of the thesis

Benchmark testing on the short glass fibre reinforced PA66 was continued from Monti [128], on BASF grades Ultramid A3HG7 (material A) and Ultramid A3WG7-OSI (material B). New testing considered the effect of temperature on the performance of each material. Studies found material A would be better suited to structural applications as it demonstrated the least amount of strain for each temperature tested for both tensile and flexural tests. Whereas material B strain increased with increase in temperature due the addition of an elastomer. This would make Material B better suited to applications that require better impact resistance trough increased strain. Material A exhibits the best strength and modulus across each temperature tested. Material B exhibits the best maximum strain giving it a larger area in the stress/strain plots resulting in material B being tougher than material A. Material B would have lost toughness when stress reduces, but levels out as strain increases with every temperature increase so toughness remains almost the same for each temperature increase. SEM micrographs from fractured tensile samples demonstrated the elastomer in material B had better glass fibre adhesion allowing higher strain and extension which give the material system more toughness and which also improved with each increases in temperature as the elastomer became more effective. Material A loses surface adhesion as temperatures were increased shown as long fibre pull out as well as cleaner fibres from pull out. Temperature also demonstrated a clear effect on both materials when subjected to 7.5J impact event. Material B exhibits the best impact resistance at higher temperatures but is less affected by temperatures lower than 23°C due to a brittle transition point of the elastomer modifier. A recommendation to keep using material B is advised as it offers the best impact performance.

As an alternative to material B, nano fillers were investigated as replacement to the elastomer used. A two-step melt compounding process achieve good results for SiO_2 with some limitations for OMMT. Compounding

worked well by producing a higher concentration master batch first, then diluting to the final grades. SEM studies using back scatter detection tells us GFs will reduce in length from a two-step melt compounding process. Compounded SiO_2 into PA-GF was successful as grades have good dispersion within the matrix. XRD investigations showed the PA-GF-OMMT grades became intercalated though the two-step melt compounding process which increased interlayer spacing on supplied OMMT. A twostep compounding technique was successful for SiO_2 but can consider not suitable for dispersing OMMT.

Room temperature (23°C) mechanical testing of 3-phase nanocomposites demonstrate that each type of nanoparticle and loadings in wt.% do have an effect on an existing PA-GF composite. Nano grades OMMT2% and $SiO_2$3% retain the best tensile and flexure stress. Tensile and flexure strain reduce for OMMT grades for increases of weight percent, whereas SiO_2 offers increased strain above the reference PA-GF grade. Mechanical and impact testing highlight that the nanocomposites fail primarily at reduced stress for both tensile and flexure testing. The reduction of stress and impact performance for all nano grades can be contributed to the reduced GF length. Gas gun impact testing of Radici PA-GF and BASF PA-GF-E also further verified the benefit from longer GF in the PA-GF grade which had a similar impact performance to the PA-GF-E grade.

The influence of temperature on tensile and flexural properties of 3-phase nanocomposites investigations shows mechanical strength reduces when temperature is increased, whereas mechanical strain increases with elevated temperatures. The types of nano particle and loading at each temperature had a clear effect on mechanical and impact performance. None of the nano grades could match or surpass the PA-GF reference grade for mechanical stress at any temperature tested, this due to the loss in glass fibre length from the compounding process. However, the nano grades did offer a significant improvement on mechanical strain especially when testing at temperatures above 23°C. This trade off found in the mechanical testing did translate in the SiO_2 nano grades catching up with PA-GF reference. All of the nano grades

studied would not suit the oil pan application in their current state. However, a predicted $SiO_2$2% with a conservative 20% improvement on mechanical stress matches the tensile plots of material B at different temperatures. Further work should consider retaining 540µm GF length found in PA-GF for nano grades $SiO_2$2% and $SiO_2$3%.

Thermal aging study indicates no distinctive to advantage to using nano reinforcements over the base PA-GF matrix. However it also tells us using nano reinforcements will not result in 3-phase composite that degrades any quicker for mechanical performance and impact losses over the PA-GF reference grade.

The results from the tensile and 3-point bending testing mainly show mechanical properties to be retained for nano grades when comparing to the PA-GF reference grade. This tells us the addition of nano particle reinforcement is not going to significantly reduce the existing life cycle of PA-GF though mechanical property degradation. $SiO_2$2% retains the best mechanical performance of any of the nano composites but still need further work to retain both tensile and flexural strength to be a viable replace the Radici PA-GF reference grade and material B.

The 6 hour power cut, 2 days before sample removal illustrated a possible strain relaxation for all the material grades tested. This was primarily seen in the tensile strain returning to the same strain found in weeks 0, 1 and 2. Whereas flexure strain showed for all material grades had a reduction of around 1 to 3% for week5 when compared to week6 which is small inconsistency. Further work should consider cycling in the thermal aging to see if other mechanical properties can be retained during aging, as this will help simulate the automotive application.

One action that can be taken from this work is to consider Radici PA-GF as a replacement to the current BASF material B, as it has a similar impact performance with improved mechanical strength which will suit it for high stress applications under-the-bonnet.

8.2 Contributions of the present work

From previse work from Zakaria Mouti PhD thesis [13], he suggested several areas that can be investigated as further work. This included elevated temperature testing and thermal aging which can be used by Eaton for their validation of the oil pan product.

Benchmark testing done in Chapter 3, addresses the temperature testing gap in knowledge related to the specific elastomer grade at elevated temperatures and validates Eaton's material selection for an oil pan component material.

Compounding 3-phase nanocomposites with an existing micro filler is a gap in knowledge addressed in the Chapter 4. Being able to compound 3-phase nanocomposites using a twin screw extruder and two step compounding to disperse OMMT and SiO_2 is a process that can be scaled up for industry. This chapter not only demonstrates compounding can be an achieved in a twin screw extruder it also demonstrates what dispersion and exfoliation can be achieved.

Room temperature mechanical testing in Chapter 5 addresses then unknown mechanical performance and series of 3-phase nanocomposites will have when nanofillers are used with glass fibres for property reinforcement. Results also illustrates that each compounded grade have an optimal performance near the 2 and 3wt.%.

Chapter 6 addresses further gaps in knowledge related to mechanical performance when nanograde s are subjected to elevated temperatures. This knowledge is very important to automotive manufactures that will have need for the materials to operate at elevated temperatures.

It was unknown what influence aging will have on the nanocomposites Vs a commercial grade, epically nanocomposites that has both micro and nano reinforcements. This gap in Knowledge addresses in chapter 7 demonstrates nanocomposites will not decay any differently to the commercial grade. This

adds value to industry confidence on material selection as a replacement. Following on from this work the testing conducted in this work has been used as a guide to develop other tests on gearbox oil pans for the Ultran project [168].

8.3 Suggestions for further work

8.3.1 Gas gun impact and thermography

Gas gunshot repeatability become an issue at very low impact energies this was due to compounding issues related to the gas gun itself which was designed for higher velocities only. Suggestions to improve the gas gun for lower and high velocity shot repeatability are as follows:

1) Replace the pressure gauge being used to one that has a high reading resolution. The current pressure gauge reads in 0.1bar, a replacement pressure gauge that reads in 0.02 or 0.05 with improve this by 2 to 5 times.
2) Fit a second regulator to help the first regulator, for instance expecting the one regulated to reduce 300bar down to 50bar is not a problem but going down to 1bar is difficult to active for lower velocity shots.
3) Manufacture more projectile shuttles, all to the same weight and consider a way maintain the projectile shuttles once damaged. Also have a test barrel with velocity measurement, just to drop the projectiles though to ensure the shuttles is not dragging inside the barrel.
4) Consider testing more samples and tack out the samples that don’t get impacted at the right velocity.

8.3.2 Micro and nano scale compounding line using a twin screw extruder that could be scaled up into industry

Further work should consider sourcing a single compounding line that can compound both nano and glass fibre at different points down the screw length whilst still retaining glass fibre length is essential. The idea of a single compounding line screw setup is to save the cost of compounding PA and nano, then re-compounding to add the glass fibres. The screw configuration will have to feed both nano and polymer together into a series of mixing elements to start dispersing the nano into the polymer matrix. An ideal setup will have a far longer screw for extra physical and ultra-sonic mixing zones for nano dispersion. Ultra-sonic dispersion is becoming more common when dispersing nano fillers in state-of-the-art compounding setups. Ultra-sonic dispersion is proven to be especially effective when a nano structure is made up of layered stacks as seen in clay and grapheme [169]–[171]. The ultra-sonic waves get in-between the layered structure and increases the gap allowing the polymer matrix to fill the gaps thus increasing exfoliation see Figure 8-1. After the mixing elements, glass fibres can be added and should at this point help keep mixing and dispersing the nano filler while still retaining glass fibre length unlike the compounding conducted in chapter 4 in this work. Figure 8-2 illustrates the compounding line screw configuration with ultra-sonic dispersion is likely to look for an ideal setup.

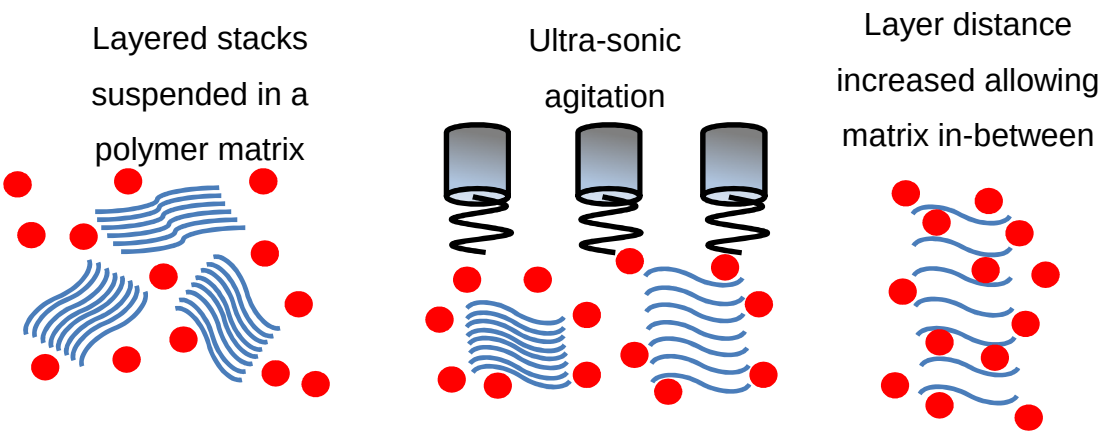

Figure 8-1: Images left to right show how use of ultra-Sonic's can increase the gap between a layered structure

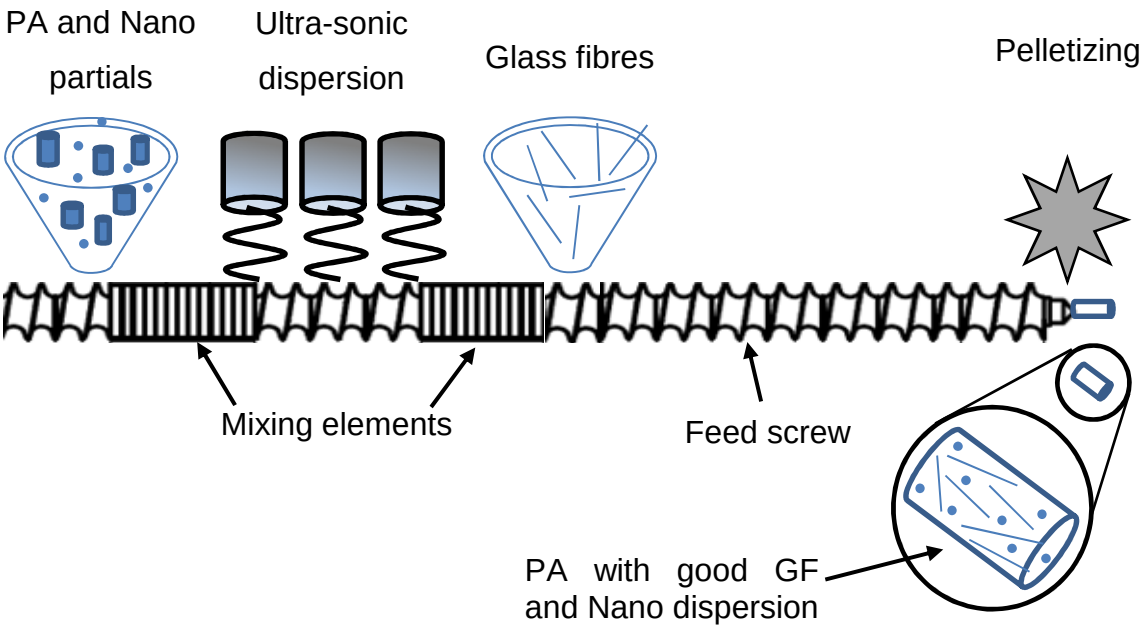

Figure 8-2: Suggested compounding line screw configuration and ultra-sonic dispersion

8.3.3 Simulation of materials in LS-DYNA

Thermal test data gained from this work can be used to develop materials that consider thermal effects such as MAT_225 (PIECEWISE LINEAR PLASTIC THERMAL). Further work should also look into developing materials cards that are more suited to polymers. Such cards consider different strain rates such as MAT_89 (PLASTICITY POLYMER) or MAT_123 (MODIFIED PIECEWISE LINEAR PLASTICITY). This will require more mechanical testing at different strain rates. Inputting different strain rates curves to the material card will improve the accuracy of the dynamic simulation of the stone impact.

8.3.4 High strain rate testing

Tensile and 3-point bending are often tested at quasi-static speeds due to most testing standards require slower test speeds. This means most test frames are servo mechanical which suits them the slow test speeds only. Sourcing a suitable testing frame that can achieve similar rates as the gas gun impact will help develop a high rate or strain dependant material cards as well as validating

any existing cards. A suitable test frame that can achieve faster test rates is the Instron VHS 8800. The Instron VHS is a servo hydraulic test frame can achieve test speeds from 1m/s up to 20m/s see Figure 8-3 left image. The test sample deign will also need to suit this type of work see Figure 8-3 right image with a shorter gauge length for high strain rates. Another feature for the test sample that it needs a longer grip surface on one side, this is to allow the fast jaw ramp up to right velocity before gripping the sample. Therefore further work should consider high rate tensile and 3-point bending to suit a realistic conditions for impact event.

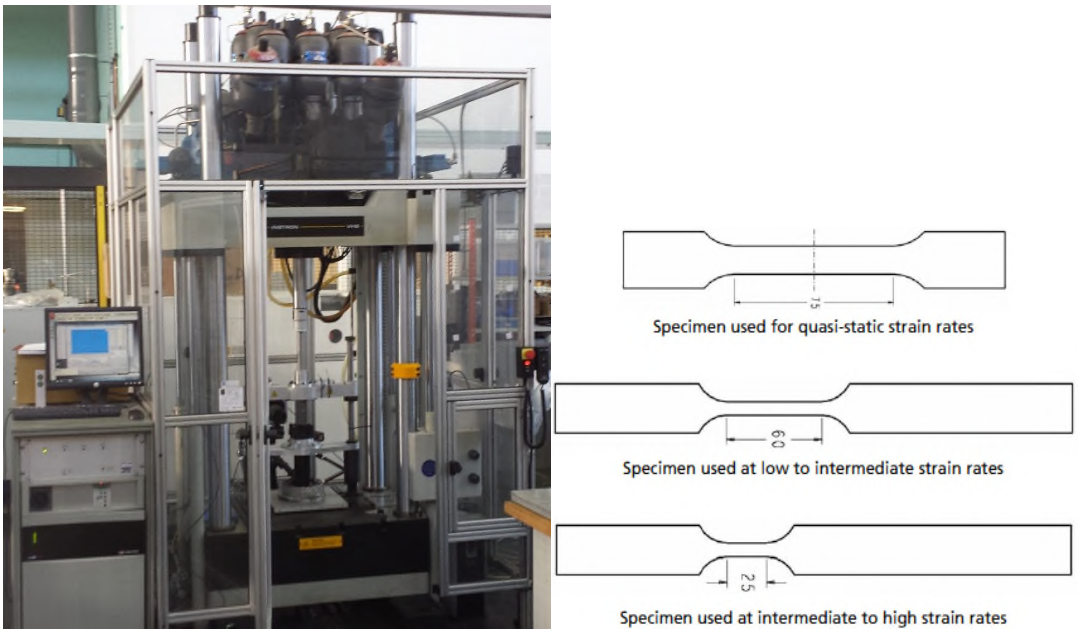

Figure 8-3: Left; Instron VHS 8800 test frame, Right; Drawing illustrating how test samples for high speed testing will need shorter gauge lengths [172]

References

[1] A. I. Taub, P. E. Krajewski, A. A. Luo, and J. N. Owens, ‘Yesterday, today and tomorrow: The evolution of technology for materials processing over the last 50 years: The automotive example’, *JOM*, vol. 59, no. 2, pp. 48–57, 2007.

[2] ‘Road Vehicles - Transport - Air - Environment - European Commission’. [Online]. Available: http://ec.europa.eu/environment/air/transport/road.htm. [Accessed: 22-Aug-2016].

[3] A. Elalem and M. S. EL-Bourawi, ‘Reduction of automobile carbon dioxide emissions’, *Int. J. Mater. Form.*, vol. 3, no. SUPPL. 1, pp. 663–666, 2010.

[4] ‘Vehicle tax rate tables - GOV.UK’. [Online]. Available: https://www.gov.uk/vehicle-tax-rate-tables. [Accessed: 22-Aug-2016].

[5] ‘Annual January prices of road fuels and petroleum products - Statistical data sets - GOV.UK’. [Online]. Available: https://www.gov.uk/government/statistical-data-sets/oil-and-petroleum-products-annual-statistics. [Accessed: 21-Feb-2014].

[6] Z. Mouti, K. Westwood, D. Long, and J. A. K. Njuguna, ‘Finite element analysis of localised impact loading on short glass fibrereinforced polyamide engine oil pan subjected to low velocity impact from flying projectiles’, 24-May-2011. [Online]. Available: https://dspace.lib.cranfield.ac.uk/handle/1826/7257?mode=simple. [Accessed: 02-Nov-2012].

[7] Z. Mouti, K. Westwood, D. Long, and J. Njuguna, ‘Finite element analysis of glass fiber-reinforced polyamide engine oil pan subjected to localized low velocity impact from flying projectiles’, *Steel Res. Int.*, vol. 83, no. 10, pp. 957–963, 2012.

[8] Z. Mouti, K. Westwood, K. Kayvantash, and J. Njuguna, ‘Low Velocity Impact Behavior of Glass Filled Fiber-Reinforced Thermoplastic Engine Components’, *Materials*, vol. 3, no. 4, pp. 2463–2473, Mar. 2010.

[9] J. Hilton, ‘Dana, BASF, ford recognized for all-new thermoplastic oil pan’, *Automot. Ind. AI*, vol. 189, no. 11, 2009.

[10] F. Krause, ‘Truck oil pan made from polyamide’, *Kunststoffe Int.*, vol. 101, no. 11, pp. 28–30, 2011.

[11] R. Leaversuch, ‘Nylon Oil Sump Gets Its Start in Trucks’, *Plast. Technol.*, vol. 50, no. 7, pp. 47–48, 2004.

[12] Z. Mouti, K. Westwood, D. Long, and J. Njuguna, ‘An experimental investigation into localised low-velocity impact loading on glass fibre-reinforced polyamide automotive product’, *Compos. Struct.*

[13] Z. Mouti, ‘Localised Low Velocity Impact Performance of Short Glass Fibre Reinforced Polyamide 66 Oil Pans’, PhD Thesis, Cranfield, Cranfield, 2012.

[14] A. Van Geenen, K. Titzschkau, and J. Bongers, ‘New methods to produce reinforced polyamide-6 for improved material properties in engineering plastic applications’, presented at the SPE Automotive and Composites Division - 8th Annual Automotive Composites Conference and Exhibition, ACCE 2008 - The Road to Lightweight Performance, 2008, vol. 1, pp. 310–314.

[15] C. Kalogeridis, ‘Plastic proves advantageous in seat pan design’, *Automot. Ind. AI*, vol. 184, no. 9, 2004.

[16] S. Yu, W. M. Yek, S. Y. Ho, S. A. D. Rannou, and S. H. Lim, ‘Microstructure and impact strength of polyamide 6 composites’, *Mater. Today Commun.*, vol. 4, pp. 199–203, Sep. 2015.

[17] X. Xu, B. Li, H. Lu, Z. Zhang, and H. Wang, ‘The effect of the interface structure of different surface-modified nano-SiO2 on the mechanical properties of nylon 66 composites’, *J. Appl. Polym. Sci.*, vol. 107, no. 3, pp. 2007–2014, 2008.

[18] Q.-Q. Yang, Z.-X. Guo, and J. Yu, ‘Preparation and characterization of polyamide 66/montmorillonite nanocomposites with methyl methacrylate as cointercalation agent’, *J. Appl. Polym. Sci.*, vol. 108, no. 1, pp. 1–6, 2008.

[19] L. A. Utracki, *Clay-containing Polymeric Nanocomposites*. iSmithers Rapra Publishing, 2004.

[20] S. Sinha Ray and M. Okamoto, ‘Polymer/layered silicate nanocomposites: a review from preparation to processing’, *Prog. Polym. Sci.*, vol. 28, no. 11, pp. 1539–1641, Nov. 2003.

[21] Y. Kojima *et al.*, ‘Mechanical properties of nylon 6-clay hybrid’, *J. Mater. Res.*, vol. 8, no. 05, pp. 1185–1189, 1993.

[22] A. Leszczyńska, J. Njuguna, K. Pielichowski, and J. R. Banerjee, ‘Polymer/montmorillonite nanocomposites with improved thermal properties: Part I. Factors influencing thermal stability and mechanisms of thermal stability improvement’, *Thermochim. Acta*, vol. 453, no. 2, pp. 75–96, Feb. 2007.

[23] J. Xiong, Z. Zheng, H. Jiang, S. Ye, and X. Wang, ‘Reinforcement of polyurethane composites with an organically modified montmorillonite’, *Compos. Part Appl. Sci. Manuf.*, vol. 38, no. 1, pp. 132–137, Jan. 2007.

[24] Claude Duval, ‘Plastiques et automobile - D’aujourd’hui à demain’. Techniques de l’ingenieur, 10-Jul-2007.

[25] J. M. Garcés, D. J. Moll, J. Bicerano, R. Fibiger, and D. G. McLeod, ‘Polymeric Nanocomposites for Automotive Applications’, *Adv. Mater.*, vol. 12, no. 23, pp. 1835–1839, 2000.

[26] Damien M. Marquis, Eric Guillaume, and Carine Chivas-Joly, ‘Properties of Nano fillers in Polymer’, in *Nanocomposites and Polymers with Analytical Methods*, InTech, 2011, pp. 261–284.

[27] M. Rafiee, F. Yavari, J. Rafiee, and N. Koratkar, ‘Fullereneepoxy nanocomposites-enhanced mechanical properties at low nanofiller loading’, *J. Nanoparticle Res.*, vol. 13, no. 2, pp. 733–737, 2011.

[28] Anne-Lise Goffin, ‘Polymer bionanocomposites reinforced by functionalized nanoparticles: impact of nanofiller size, nature and composition’, PhD Thesis, Universite de Mons, Belgium, 2010.

[29] ‘Cummins ISF Engine | Logistics, Trucking & Transport News | Prime Mover Magazine’. [Online]. Available: http://www.primemovermag.com.au/products/item/cummins-isf-engine. [Accessed: 17-Dec-2012].

[30] A. Sethi, ‘Wet Sump Design for a FSAE Racing Car’, *Appl. Mech. Mater.*, vol. 165, pp. 175–181, Apr. 2012.

[31] A. Sethi, *Wet sump design for an FSAE racing car*, vol. 165. 2012.

[32] ‘Automotive: Functions of Oil Pan’. [Online]. Available: http://automotiveservices.blogspot.co.uk/2011/02/functions-of-oil-pan.html. [Accessed: 03-Dec-2012].

[33] ‘BASFPlasticsPortalAsia - Case studies - Automotive powertrain’. [Online]. Available: http://www.plasticsportalasia.net/wa/plasticsAP~en_GB/portal/show/content/markets/case_studies/automotive/powertrain. [Accessed: 03-Dec-2012].

[34] ‘BS EN ISO 291:2008 - Plastics. Standard atmospheres for conditioning and testing’. BSI, 30-Jun-2008.

[35] ‘J300_200405: Engine Oil Viscosity Classification Standard’. SAE International, 10-May-2005.

[36] ‘Tangram Technology Ltd. - Polymer Data File - PA’. [Online]. Available: http://www.tangram.co.uk/TI-Polymer-PA.html#OI. [Accessed: 20-Dec-2012].

[37] W. J. Cantwell and J. Morton, ‘The impact resistance of composite materials — a review’, *Composites*, vol. 22, no. 5, pp. 347–362, Sep. 1991.

[38] ‘Global Scenario of Polyamide, Nylon Automotive Under Hood Application - Market Report’. [Online]. Available:

http://www.plastemart.com/upload/Literature/marketscenarioofpolyamide.asp. [Accessed: 18-Dec-2012].

[39] ‘Search Engineering Material by Property Value’. [Online]. Available: http://www.matweb.com/search/PropertySearch.aspx. [Accessed: 21-Jan-2013].

[40] ‘CAMPUSplastics | Grade Names’, *CAMPUS - a material information system for the plastics industry*. [Online]. Available: http://www.campusplastics.com/campus/list/. [Accessed: 15-Mar-2013].

[41] B. Mouhmid, A. Imad, N. Benseddiq, S. Benmedakhène, and A. Maazouz, ‘A study of the mechanical behaviour of a glass fibre reinforced polyamide 6,6: Experimental investigation’, *Polym. Test.*, vol. 25, no. 4, pp. 544–552, Jun. 2006.

[42] M. Gomina, L. Pinot, R. Moreau, and E. Nakache, ‘Fracture behaviour of short glass fibre-reinforced rubber-toughened nylon composites’, in *European Structural Integrity Society*, vol. Volume 32, A. P. and J. G. W. B.R.K. Blackman, Ed. Elsevier, 2003, pp. 399–418.

[43] BASF, ‘Ultramid Product Brochure’. BASF, 2007.

[44] E. Carlson and K. Nelson, ‘Nylon under the hood: A history of innovation’, *Automot. Eng. Int.*, vol. 104, no. 12, pp. 84–89, 1996.

[45] P. Malnati, ‘Under the hood: Thermoplastics tackle tough jobs’, *Composites Technology*, vol. 9, no. 4, p. 2, Apr-2011.

[46] T. Hohenstein, U. Gleiter, S. Glaser, and T. Fritz, ‘First volume application of impact-resistant plastic oil pans’, *MTZ Worldw.*, vol. 71, no. 1, pp. 28–34.

[47] Ribeiro, C.J, Viana, and J.C, *Optimization of Injection Moulded Polymer Automotive Components*. 2011.

[48] A. Launay, M. H. Maitournam, Y. Marco, I. Raoult, and F. Szmytka, ‘Cyclic behaviour of short glass fibre reinforced polyamide: Experimental study and constitutive equations’, *Int. J. Plast.*, vol. 27, no. 8, pp. 1267–1293, Aug. 2011.

[49] P.-A. Eriksson, A.-C. Albertsson, P. Boydell, G. Prautzsch, and J. -a. E. Månson, ‘Prediction of mechanical properties of recycled fiberglass reinforced polyamide 66’, *Polym. Compos.*, vol. 17, no. 6, pp. 830–839, 1996.

[50] ‘Polyamide Resin Technologies for High Temperature and Automotive Chemical Exposure Environments’. [Online]. Available: http://papers.sae.org/2009-01-1297/. [Accessed: 09-Sep-2016].

[51] P. Cazuc, ‘Driving new lightweight and high strength solutions for the automotive industry’, *Reinf. Plast.*

[52] ‘Autocomposites Update: Engine oil pans : CompositesWorld’. [Online]. Available: http://www.compositesworld.com/articles/autocomposites-update-engine-oil-pans. [Accessed: 04-Oct-2016].

[53] N. Drake, *Thermoplastics and Thermoplastic Composities in the Automotive Industry 1997-2000*. iSmithers Rapra Publishing, 1998.

[54] J. L. Thomason, ‘The influence of fibre length, diameter and concentration on the strength and strain to failure of glass fibre-reinforced polyamide 6,6’, *Compos. Part Appl. Sci. Manuf.*, vol. 39, no. 10, pp. 1618–1624, 2008.

[55] J. L. Thomason, ‘The influence of fibre length, diameter and concentration on the impact performance of long glass-fibre reinforced polyamide 6,6’, *Compos. Part Appl. Sci. Manuf.*, vol. 40, no. 2, pp. 114–124, 2009.

[56] J. L. Thomason, ‘Structure-property relationships in glass reinforced polyamide, part 2: The effects of average fiber diameter and diameter distribution’, *Polym. Compos.*, vol. 28, no. 3, pp. 331–343, 2007.

[57] F. Ramsteiner and R. Theysohn, ‘The influence of fibre diameter on the tensile behaviour of short-glass-fibre reinforced polymers’, *Compos. Sci. Technol.*, vol. 24, no. 3, pp. 231–240, 1985.

[58] B. Yang, J. Leng, B. He, H. Liu, Y. Zhang, and Z. Duan, ‘Influence of fiber length and compatibilizer on mechanical properties of long glass fiber reinforced polyamide 6,6’, *J. Reinf. Plast. Compos.*, vol. 31, no. 16, pp. 1103–1112, Aug. 2012.

[59] J. L. Thomason, ‘The influence of fibre length, diameter and concentration on the modulus of glass fibre reinforced polyamide 6,6’, *Compos. Part Appl. Sci. Manuf.*, vol. 39, no. 11, pp. 1732–1738, 2008.

[60] A. Hassan, R. Yahya, A. H. Yahaya, A. R. M. Tahir, and P. R. Hornsby, ‘Tensile, impact and fiber length properties of injection-molded short and long glass fiber-reinforced polyamide 6,6 composites’, *J. Reinf. Plast. Compos.*, vol. 23, no. 9, pp. 969–986, 2004.

[61] V. Srinivasan, R. Karthikeyan, G. Ganesan, and B. Asaithambi, ‘Comparative study on the wear behavior of long and short glass fiber reinforced plastics’, *Met. Mater. Int.*, vol. 16, no. 2, pp. 205–212, 2010.

[62] J. Karger-Kocsis, ‘Swirl mat- and long discontinuous fiber mat-reinforced polypropylene composites - status and future trends’, *Polym. Compos.*, vol. 21, no. 4, pp. 514–522, 2000.

[63] *Wiley: Fundamentals of Materials Science and Engineering, 4th Edition SI Version - William D. Callister, David G. Rethwisch*. .

[64] R. A, *Wiley: Polymer Science and Technology for Engineers and Scientists- R. A. Pethrick*. Caithness: Wiley.

[65] E. M. Silverman, 'EFFECT OF GLASS FIBER LENGTH ON THE CREEP AND IMPACT RESISTANCE OF REINFORCED THERMOPLASTICS.', *Polym. Compos.*, vol. 8, no. 1, pp. 8–15, 1987.

[66] Q. T. H. Shubhra, A. K. M. M. Alam, and M. A. Quaiyyum, 'Mechanical properties of polypropylene composites: A review', *J. Thermoplast. Compos. Mater.*, vol. 26, no. 3, pp. 362–391, 2013.

[67] H. Ku, H. Wang, N. Pattarachaiyakoop, and M. Trada, 'A review on the tensile properties of natural fiber reinforced polymer composites', *Compos. Part B Eng.*, vol. 42, no. 4, pp. 856–873, 2011.

[68] B. Madsen, A. Thygesen, and H. Lilholt, 'Plant fibre composites - porosity and stiffness', *Compos. Sci. Technol.*, vol. 69, no. 7–8, pp. 1057–1069, 2009.

[69] B.-H. Lee, H.-J. Kim, and W.-R. Yu, 'Fabrication of long and discontinuous natural fiber reinforced polypropylene biocomposites and their mechanical properties', *Fibers Polym.*, vol. 10, no. 1, pp. 83–90, 2009.

[70] G. I. Williams and R. P. Wool, 'Composites from natural fibers and soy oil resins', *Appl. Compos. Mater.*, vol. 7, no. 5–6, pp. 421–432, 2000.

[71] L. Uma Devi, S. S. Bhagawan, and S. Thomas, 'Mechanical properties of pineapple leaf fiber-reinforced polyester composites', *J. Appl. Polym. Sci.*, vol. 64, no. 9, pp. 1739–1748, 1997.

[72] A. Güllü, A. Özdemir, and E. Özdemir, 'Experimental investigation of the effect of glass fibres on the mechanical properties of polypropylene (PP) and polyamide 6 (PA6) plastics', *Mater. Des.*, vol. 27, no. 4, pp. 316–323, 2006.

[73] S. K. Samal, S. Mohanty, and S. K. Nayak, 'Polypropyleneĝ€"bamboo/glass fiber hybrid composites: Fabrication and analysis of mechanical, morphological, thermal, and dynamic mechanical behavior', *J. Reinf. Plast. Compos.*, vol. 28, no. 22, pp. 2729–2747, 2009.

[74] M. M. Hassan, M. H. Wagner, H. U. Zaman, and M. A. Khan, 'Physico-mechanical performance of hybrid betel nut (Areca catechu) short fiber/seaweed polypropylene composite', *J. Nat. Fibers*, vol. 7, no. 3, pp. 165–177, 2010.

[75] N.-J. Lee and J. Jang, 'Effect of fibre content on the mechanical properties of glass fibre mat/polypropylene composites', *Compos. Part Appl. Sci. Manuf.*, vol. 30, no. 6, pp. 815–822, 1999.

[76] J. L. Thomason, ‘The influence of fibre length and concentration on the properties of glass fibre reinforced polypropylene. 6. the properties of injection moulded long fibre PP at high fibre content’, *Compos. Part Appl. Sci. Manuf.*, vol. 36, no. 7, pp. 995–1003, 2005.

[77] D. Notta-Cuvier, F. Lauro, B. Bennani, and R. Balieu, ‘Damage of short-fibre reinforced materials with anisotropy induced by complex fibres orientations’, *Mech. Mater.*, vol. 68, pp. 193–206, 2014.

[78] Y. J. Phua, Z. A. M. Ishak, and R. Senawi, ‘Injection Molded Short Glass and Carbon Fibers Reinforced Polycarbonate Hybrid Composites: Effects of Fiber Loading’, *J. Reinf. Plast. Compos.*, vol. 29, no. 17, pp. 2592–2603, Jan. 2010.

[79] J. Summerscales and D. Short, ‘Carbon fibre and glass fibre hybrid reinforced plastics’, *Composites*, vol. 9, no. 3, pp. 157–166, Jul. 1978.

[80] H. Anuar, S. H. Ahmad, R. Rasid, A. Ahmad, and W. N. W. Busu, ‘Mechanical properties and dynamic mechanical analysis of thermoplastic-natural-rubber-reinforced short carbon fiber and kenaf fiber hybrid composites’, *J. Appl. Polym. Sci.*, vol. 107, no. 6, pp. 4043–4052, Mar. 2008.

[81] K. Jarukumjorn and N. Suppakarn, ‘Effect of glass fiber hybridization on properties of sisal fiber–polypropylene composites’, *Compos. Part B Eng.*, vol. 40, no. 7, pp. 623–627, Oct. 2009.

[82] G. P. Karayannidis, D. N. Bikiaris, G. Z. Papageorgiou, and V. Bakirtzis, ‘Rubber toughening of glass fiber reinforced nylon-6,6 with functionalized block copolymer SEBS-g-MA’, *Adv. Polym. Technol.*, vol. 21, no. 3, pp. 153–163, 2002.

[83] H. Keskkula, *Rubber-Modified Thermoplastics*. iSmithers Rapra Publishing, 2000.

[84] R. J. M. Borggreve, R. J. Gaymans, and J. Schuijer, ‘Impact behaviour of nylon-rubber blends: 5. Influence of the mechanical properties of the elastomer’, *Polymer*, vol. 30, no. 1, pp. 71–77, Jan. 1989.

[85] V. Tanrattanakul, N. Sungthong, and P. Raksa, ‘Rubber toughening of nylon 6 with epoxidized natural rubber’, *Polym. Test.*, vol. 27, no. 7, pp. 794–800, Oct. 2008.

[86] L.-F. Ma *et al.*, ‘Toughening of polyamide 6 with β-nucleated thermoplastic vulcanizates based on polypropylene/ethylene–propylene–diene rubber grafted with maleic anhydride blends’, *Mater. Des.*, vol. 33, pp. 104–110, Jan. 2012.

[87] M. Kroll, B. Langer, and W. Grellmann, ‘Toughness optimization of elastomer-modified glass-fiber reinforced PA6 materials’, *J. Appl. Polym. Sci.*, vol. 127, no. 1, pp. 57–66, 2013.

[88] F. D. Alsewailem and R. K. Gupta, ‘Effect of impact modifier types on mechanical properties of rubber-toughened glass-fibre-reinforced nylon 66’, *Can. J. Chem. Eng.*, vol. 84, no. 6, pp. 693–703, 2006.

[89] J. Ma, Y. . Feng, J. Xu, M. . Xiong, Y. . Zhu, and L. . Zhang, ‘Effects of compatibilizing agent and in situ fibril on the morphology, interface and mechanical properties of EPDM/nylon copolymer blends’, *Polymer*, vol. 43, no. 3, pp. 937–945, Feb. 2002.

[90] H. Huang, T. Ikehara, and T. Nishi, ‘Observation of morphology in EPDM/nylon copolymer thermoplastic vulcanizates by atomic force microscopy’, *J. Appl. Polym. Sci.*, vol. 90, no. 5, pp. 1242–1248, 2003.

[91] E. Laredo, M. Grimau, F. Sánchez, and A. Bello, ‘Water Absorption Effect on the Dynamic Properties of Nylon-6 by Dielectric Spectroscopy’, *Macromolecules*, vol. 36, no. 26, pp. 9840–9850, Dec. 2003.

[92] C.-C. Pai, R.-J. Jeng, S. J. Grossman, and J.-C. Huang, ‘Effects of moisture on thermal and mechanical properties of nylon-6,6’, *Adv. Polym. Technol.*, vol. 9, no. 2, pp. 157–163, 1989.

[93] L. Liu *et al.*, ‘Influence of moisture regain of aramid fibers on effects of atmospheric pressure plasma treatment on improving adhesion with epoxy’, *J. Appl. Polym. Sci.*, vol. 102, no. 1, pp. 242–247, 2006.

[94] W. Gacitua, A. Ballerini, and J. Zhang, ‘Polymer nanocpmposites: sysnthetic and natral fillers’, *Maderas Cienc. Tecnol.*, vol. 7, no. 3, pp. 159–178, 2005.

[95] P. M. Ajayan, L. S. Schadler, and P. V. Braun, *Nanocomposite science and technology*. Wiley, 2003.

[96] M. J. Pitkethly, ‘Nanomaterials – the driving force’, *Mater. Today*, vol. 7, no. 12, Supplement, pp. 20–29, Dec. 2004.

[97] H. Gu, Y. Guo, S. Y. Wong, C. He, X. Li, and V. P. W. Shim, ‘Effect of interphase and strain-rate on the tensile properties of polyamide 6 reinforced with functionalized silica nanoparticles’, *Compos. Sci. Technol.*, vol. 75, pp. 62–69, Feb. 2013.

[98] D. P. N. Vlasveld, P. P. Parlevliet, H. E. N. Bersee, and S. J. Picken, ‘Fibre–matrix adhesion in glass-fibre reinforced polyamide-6 silicate nanocomposites’, *Compos. Part Appl. Sci. Manuf.*, vol. 36, no. 1, pp. 1–11, Jan. 2005.

[99] M. Kawasumi, ‘The discovery of polymer-clay hybrids’, *J. Polym. Sci. Part Polym. Chem.*, vol. 42, no. 4, pp. 819–824, 2004.

[100] Y. Chunze, S. Yusheng, Y. Jinsong, and L. Jinhui, ‘A Nanosilica/Nylon-12 Composite Powder for Selective Laser Sintering’, *J. Reinf. Plast. Compos.*, vol. 28, no. 23, pp. 2889–2902, Jan. 2009.

[101] S. Zhu, M. Okazaki, A. Usuki, and M. Kato, ‘Tensile and fatigue behavior in clay reinforced nylon 6 nanocomposites’, *Zair. Soc. Mater. Sci. Jpn.*, vol. 58, no. 12, pp. 969–974, 2009.

[102] J.-H. Lin, C.-W. Lin, C.-H. Huang, C.-L. Huang, and C.-W. Lou, ‘Manufacturing technique and mechanical properties of plastic nanocomposite’, *Compos. Part B Eng.*, vol. 44, no. 1, pp. 34–39, 2013.

[103] J. Jordan, K. I. Jacob, R. Tannenbaum, M. A. Sharaf, and I. Jasiuk, ‘Experimental trends in polymer nanocomposites - A review’, *Mater. Sci. Eng. A*, vol. 393, no. 1–2, pp. 1–11, 2005.

[104] A. Okada and A. Usuki, ‘Twenty years of polymer-clay nanocomposites’, *Macromol. Mater. Eng.*, vol. 291, no. 12, pp. 1449–1476, 2006.

[105] Y.-C. Chung, T. K. Cho, and B. C. Chun, ‘Dependence of montmorillonite dispersion in nanocomposites on polymer matrix and compatibilizer content, and the impact on mechanical properties’, *Fibers Polym.*, vol. 9, no. 1, pp. 7–14, 2008.

[106] L. Mészáros, T. Deák, G. Balogh, T. Czvikovszky, and T. Czigány, ‘Preparation and mechanical properties of injection moulded polyamide 6 matrix hybrid nanocomposite’, *Compos. Sci. Technol.*, vol. 75, pp. 22–27, 2013.

[107] S.-P. Liu, S.-S. Hwang, J.-M. Yeh, and C.-C. Hung, ‘Mechanical properties of polyamide-6/montmorillonite nanocomposites — Prepared by the twin-screw extruder mixed technique’, *Int. Commun. Heat Mass Transf.*, vol. 38, no. 1, pp. 37–43, Jan. 2011.

[108] H. Lu, X. Xu, X. Li, and Z. Zhang, ‘Morphology, crystallization and dynamic mechanical properties of PA66/nano-SiO2 composites’, *Bull. Mater. Sci.*, vol. 29, no. 5, pp. 485–490, 2006.

[109] X. Xu, B. Li, H. Lu, Z. Zhang, and H. Wang, ‘The interface structure of nano-SiO2/PA66 composites and its influence on material’s mechanical and thermal properties’, *Appl. Surf. Sci.*, vol. 254, no. 5, pp. 1456–1462, 2007.

[110] B. Zhang, J. S.-P. Wong, D. Shi, R. C.-M. Yam, and R. K.-Y. Li, ‘Investigation on the mechanical performances of ternary nylon 6/SEBS elastomer/nano-SiO2 hybrid composites with controlled morphology’, *J. Appl. Polym. Sci.*, vol. 115, no. 1, pp. 469–479, 2010.

[111] H. Mahfuz *et al.*, ‘Reinforcement of nylon 6 with functionalized silica nanoparticles for enhanced tensile strength and modulus’, *Nanotechnology*, vol. 19, no. 44, p. 445702, Nov. 2008.

[112] L. Gendre, J. Njuguna, H. Abhyankar, and V. Ermini, ‘MECHANICAL PROPERTIES OF THREE-PHASE POLYAMIDE 6 NANOCOMPOSITES’, Cranfield University, 2013.

[113] G. A. Schoeppner and S. Abrate, ‘Delamination threshold loads for low velocity impact on composite laminates’, *Compos. Part Appl. Sci. Manuf.*, vol. 31, no. 9, pp. 903–915, Sep. 2000.

[114] B. Weidenfeller, M. Höfer, and F. R. Schilling, ‘Thermal conductivity, thermal diffusivity, and specific heat capacity of particle filled polypropylene’, *Compos. Part Appl. Sci. Manuf.*, vol. 35, no. 4, pp. 423–429, Apr. 2004.

[115] V. Patel and Y. Mahajan, ‘Polymer nanocomposites drive opportunities in the automotive sector’, *Nanowerk Spotlight*, Oct-2011.

[116] B.-R. Höhn and K. Michaelis, ‘Influence of oil temperature on gear failures’, *Tribol. Int.*, vol. 37, no. 2, pp. 103–109, Feb. 2004.

[117] B. H. Stuart, *Polymer Analysis*. John Wiley & Sons, 2002.

[118] ‘Radilon® A USX200 100 NAT data sheet’. Radici Partecipazioni SpA, 2013.

[119] ‘Radilon® A CF300K 333 NER data sheet’. Radici Partecipazioni SpA, 2013.

[120] Y. Kodama, S. J. Zhu, Y. Nakahara, A. Usuki, and M. Kato, ‘Fatigue Fracture of Clay Reinforced Nylon Nanocomposites’, *Mater. Sci. Forum*, vol. 750, pp. 11–14, Mar. 2013.

[121] Y. Nakahara, Y. Kodama, S. J. Zhu, A. Usuki, and M. Kato, ‘Effect of Thermal Exposure on Tensile and Fatigue Properties of Clay Reinforced Nylon Nanocomposites’, *Mater. Sci. Forum*, vol. 833, pp. 52–55, Nov. 2015.

[122] J. Jin, R. Rafiq, Y. Q. Gill, and M. Song, ‘Preparation and characterization of high performance of graphene/nylon nanocomposites’, *Eur. Polym. J.*, vol. 49, no. 9, pp. 2617–2626, Sep. 2013.

[123] H. Salehi-Mobarakeh, A. Yadegari, F. Khakzad-Esfahlan, and A. Mahdavian, ‘Modifying montmorillonite clay via silane grafting and interfacial polycondensation for melt compounding of nylon-66 nanocomposite’, *J. Appl. Polym. Sci.*, vol. 124, no. 2, pp. 1501–1510, Apr. 2012.

[124] S. R. Chowdhury, S. Francis, and K. S. Sarma, ‘Electron beam modified nylon 6-clay nanocomposites: morphology and water absorption behavior’, *J. Polym. Eng.*, vol. 34, no. 8, pp. 715–726, 2014.

[125] K. Saeed and I. Khan, ‘Preparation and characterization of single-walled carbon nanotube/nylon 6, 6 nanocomposites’, *Instrum. Sci. Technol.*, vol. 0, no. 0, pp. 1–10, Dec. 2015.

[126] F. Fasahat, R. Dastjerdi, and M. R. M. Dastjerdi, ‘Abrasion Resistance of Ag/SiO2/PA6 Nanocomposite Fabrics’, 2013.

[127] Z. Mouti, K. Westwood, D. Long, and J. Njuguna, ‘An experimental investigation into localised low-velocity impact loading on glass fibre-

reinforced polyamide automotive product', *Compos. Struct.*, vol. 104, pp. 43–53, 2013.

[128] Z. Mouti, 'Localised low velocity impact performance of short glass fibre reinforced polyamide 66 oil pans', Mar-2012. [Online]. Available: https://dspace.lib.cranfield.ac.uk/handle/1826/7843. [Accessed: 17-Dec-2014].

[129] 'BS EN ISO 527-1:1996, BS 2782-3:Method 321:1994,ISO 527-1:1993 - Plastics. Determination of tensile properties. General principles – BSI British Standards'. BSI, 15-Jan-1994.

[130] 'BS EN ISO 178:2010 - Plastics. Determination of flexural properties – BSI British Standards'. BSI, 31-Jan-2011.

[131] 'BS EN ISO 6603-1:2000 - Plastics. Determination of multi-axial impact behaviour of rigid plastics. Falling dart method'. BSI, 31-Jan-2011.

[132] 'BS EN ISO 527-2:1996, BS 2782-3:Method 322:1994 - Plastics. Determination of tensile properties. Test conditions for moulding and extrusion plastics – BSI British Standards'. BSI, 15-Jan-1994.

[133] M. Watanabe and H. Yamaguchi, 'The friction and wear properties of nylon', *Wear*, vol. 110, no. 3–4, pp. 379–388, Aug. 1986.

[134] S. D. Bartus and U. K. Vaidya, 'Performance of long fiber reinforced thermoplastics subjected to transverse intermediate velocity blunt object impact', *Compos. Struct.*, vol. 67, no. 3, pp. 263–277, Mar. 2005.

[135] V. Pettarin, G. E. Eliçabe, P. M. Frontini, K. Leskovics, G. B. Lenkey, and T. Czigany, 'Analysis of low temperature impact fracture data of thermoplastic polymers making use of an inverse methodology', *Eng. Fract. Mech.*, vol. 73, no. 6, pp. 738–749, Apr. 2006.

[136] S. D. Gehman, P. J. Jones, C. S. Wilkinson, and D. E. Woodford, 'Low Temperature Stiffening of Elastomers.', *Ind. Eng. Chem.*, vol. 42, no. 3, pp. 475–482, Mar. 1950.

[137] M. Mehrabzadeh and R. P. Burford, 'Studies of mechanical properties, thermal behaviour and morphology of polyamide 11 and nitrile rubber blends: effect of rubber and acrylonitrile content', *Iran. J. Polym. Sci. Technol.*, vol. 4, no. 3, pp. 156–168, 1995.

[138] R. J. M. Borggreve, R. J. Gaymans, J. Schuijer, and J. F. I. Housz, 'Brittle-tough transition in nylon-rubber blends: effect of rubber concentration and particle size', *Polymer*, vol. 28, no. 9, pp. 1489–1496, Aug. 1987.

[139] A. Rozanski and A. Galeski, 'Plastic yielding of semicrystalline polymers affected by amorphous phase', *Int. J. Plast.*

[140] Y. Kojima *et al.*, ‘Mechanical properties of nylon 6-clay hybrid’, *J. Mater. Res.*, vol. 8, no. 05, pp. 1185–1189, 1993.

[141] D. P. N. Vlasveld, H. E. N. Bersee, and S. J. Picken, ‘Nanocomposite matrix for increased fibre composite strength’, *Polymer*, vol. 46, no. 23, pp. 10269–10278, 2005.

[142] H. R. Dennis *et al.*, ‘Effect of melt processing conditions on the extent of exfoliation in organoclay-based nanocomposites’, *Polymer*, vol. 42, no. 23, pp. 9513–9522, Nov. 2001.

[143] D. Homminga, B. Goderis, S. Hoffman, H. Reynaers, and G. Groeninckx, ‘Influence of shear flow on the preparation of polymer layered silicate nanocomposites’, *Polymer*, vol. 46, no. 23, pp. 9941–9954, Nov. 2005.

[144] S. Pavlidou and C. D. Papaspyrides, ‘A review on polymer–layered silicate nanocomposites’, *Prog. Polym. Sci.*, vol. 33, no. 12, pp. 1119–1198, Dec. 2008.

[145] T. McNally, W. Raymond Murphy, C. Y. Lew, R. J. Turner, and G. P. Brennan, ‘Polyamide-12 layered silicate nanocomposites by melt blending’, *Polymer*, vol. 44, no. 9, pp. 2761–2772, Apr. 2003.

[146] J. W. Cho and D. R. Paul, ‘Nylon 6 nanocomposites by melt compounding’, *Polymer*, vol. 42, no. 3, pp. 1083–1094, 2001.

[147] L. Chen, I. Y. Phang, S.-C. Wong, P.-F. Lv, and T. Liu, ‘Embrittlement mechanisms of nylon 66/organoclay nanocomposites prepared by melt-compounding process’, *Mater. Manuf. Process.*, vol. 21, no. 2, pp. 153–158, 2006.

[148] K. Stade, ‘Techniques for compounding glass fiber-reinforced thermoplastics’, *Polym. Eng. Sci.*, vol. 17, no. 1, pp. 50–57, Jan. 1977.

[149] B. Lin, A. Thümen, H.-P. Heim, G. Scheel, and U. Sundararaj, ‘Nylon 66/clay nanocomposite structure development in a twin screw extruder’, *Polym. Eng. Sci.*, vol. 49, no. 4, pp. 824–834, Apr. 2009.

[150] A. Benedito, I. Buezas, E. Giménez, B. Galindo, and A. Ortega, ‘Dispersion and characterization of thermoplastic polyurethane/multiwalled carbon nanotubes by melt mixing’, *J. Appl. Polym. Sci.*, vol. 122, no. 6, pp. 3745–3751, 2011.

[151] A. K. Barick and D. K. Tripathy, ‘Effect of organoclay on the morphology, mechanical, thermal, and rheological properties of organophilic montmorillonite nanoclay based thermoplastic polyurethane nanocomposites prepared by melt blending’, *Polym. Eng. Sci.*, vol. 50, no. 3, pp. 484–498, Mar. 2010.

[152] C. Hou *et al.*, ‘Ag-nanoparticle-decorated Au-fractal patterns on bowl-like-dimple arrays on Al foil as an effective SERS substrate for the rapid

detection of PCBs', *Chem. Commun.*, vol. 50, no. 5, pp. 569–571, Dec. 2013.

[153] C. Meola, G. M. Carlomagno, and L. Giorleo, 'The use of infrared thermography for materials characterization', *J. Mater. Process. Technol.*, vol. 155–156, pp. 1132–1137, Nov. 2004.

[154] 'An intro to infrared thermography for mechanical applications'. [Online]. Available: http://www.reliableplant.com/Read/20181/infrared-thermography-mechanical. [Accessed: 29-Jan-2013].

[155] J. L. Thomason, 'The influence of fibre length, diameter and concentration on the strength and strain to failure of glass fibre-reinforced polyamide 6,6', *Compos. Part Appl. Sci. Manuf.*, vol. 39, no. 10, pp. 1618–1624, 2008.

[156] I. Butterworth, J. Njuguna, R. Abhyankar, J. Brighton, K. Westwood, and Z. Mouti, 'The effect of temperature changes on to quasi-static tensile and flexural performance of glass fibre reinforced pa66 composites', in *11th International Conference on Manufacturing Research*, Cranfield University, 2013, pp. 381–386.

[157] L. Liu, Z. Qi, and X. Zhu, 'Studies on nylon 6/clay nanocomposites by melt-intercalation process', *J. Appl. Polym. Sci.*, vol. 71, no. 7, pp. 1133–1138, Feb. 1999.

[158] Y. Li, J. Yu, and Z.-X. Guo, 'The influence of interphase on nylon-6/nano-SiO2 composite materials obtained from in situ polymerization', *Polym. Int.*, vol. 52, no. 6, pp. 981–986, Jun. 2003.

[159] H. Mahfuz, M. M. Hasan, V. K. Rangari, and S. Jeelani, 'Reinforcement of Nylon-6 Filaments with SiO2 Nanoparticles and Comparison of Young's Modulus with Theoretical Bounds', *Macromol. Mater. Eng.*, vol. 292, no. 4, pp. 437–444, Apr. 2007.

[160] F. Yang, Y. Ou, and Z. Yu, 'Polyamide 6/silica nanocomposites prepared by in situ polymerization', *J. Appl. Polym. Sci.*, vol. 69, no. 2, pp. 355–361, Jul. 1998.

[161] B. Han, G. Ji, S. Wu, and J. Shen, 'Preparation and characterization of nylon 66/montmorillonite nanocomposites with co-treated montmorillonites', *Eur. Polym. J.*, vol. 39, no. 8, pp. 1641–1646, Aug. 2003.

[162] R. Jarrar, M. A. Mohsin, and Y. Haik, 'Alteration of the mechanical and thermal properties of nylon 6/nylon 6,6 blends by nanoclay', *J. Appl. Polym. Sci.*, vol. 124, no. 3, pp. 1880–1890, 2012.

[163] A. Dasari, Z.-Z. Yu, Y.-W. Mai, G.-H. Hu, and J. Varlet, 'Clay exfoliation and organic modification on wear of nylon 6 nanocomposites processed by different routes', *Compos. Sci. Technol.*, vol. 65, no. 15–16, pp. 2314–2328, Dec. 2005.

[164] P.-A. Eriksson, P. Boydell, K. Eriksson, J. -a. E. Månson, and A.-C. Albertsson, ‘Effect of thermal-oxidative aging on mechanical, chemical, and thermal properties of recycled polyamide 66’, *J. Appl. Polym. Sci.*, vol. 65, no. 8, pp. 1619–1630, Aug. 1997.

[165] P. Kiliaris, C. D. Papaspyrides, and R. Pfaendner, ‘Influence of accelerated aging on clay-reinforced polyamide 6’, *Polym. Degrad. Stab.*, vol. 94, no. 3, pp. 389–396, Mar. 2009.

[166] N. Jia and V. A. Kagan, ‘Effects of time and temperature on the tension-tension fatigue behavior of short fiber reinforced polyamides’, *Polym. Compos.*, vol. 19, no. 4, pp. 408–414, Aug. 1998.

[167] S. H. BOTROS, A. F. YOUNAN, and M. M. ESSA, ‘Effect of Fiber Reinforcement on Thermal Stability and Swelling Behavior of Cr/Nbr Blends’, *Polym.-Plast. Technol. Eng.*, vol. 39, no. 2, pp. 393–414, May 2000.

[168] ‘Ricardo to display revolutionary ultra-lightweight rear drive unit at LCV 2015 - Ricardo’. [Online]. Available: http://www.ricardo.com/ru-RU/News--Media/Press-releases/News-releases1/2015/Ricardo-to-display-revolutionary-ultra-lightweight-rear-drive-unit-at-LCV-2015/. [Accessed: 25-Aug-2016].

[169] E. C. Lee, D. F. Mielewski, and R. J. Baird, ‘Exfoliation and dispersion enhancement in polypropylene nanocomposites by in-situ melt phase ultrasonication’, *Polym. Eng. Sci.*, vol. 44, no. 9, pp. 1773–1782, 2004.

[170] J. G. Ryu, H. Kim, and J. W. Lee, ‘Characteristics of polystyrene/polyethylene/clay nanocomposites prepared by ultrasound-assisted mixing process’, *Polym. Eng. Sci.*, vol. 44, no. 7, pp. 1198–1204, Jul. 2004.

[171] K. Y. Kim, D. U. Ju, G. J. Nam, and J. W. Lee, ‘Ultrasonic Effects on PP/PS/Clay Nanocomposites during Continuous Melt Compounding Process’, *Macromol. Symp.*, vol. 249–250, no. 1, pp. 283–288, Apr. 2007.

[172] ‘Strain Rate Testing of Metallic Materials and Their Modelling for Use in CAE Based Automotive Crash Simulation Tools - Recommendations and Procedures - Knovel’. [Online]. Available: https://app.knovel.com/web/toc.v/cid:kpSRTMMTM1/viewerType:toc/root_slug:strain-rate-testing-metallic/url_slug:strain-rate-testing-metallic/. [Accessed: 25-Aug-2016].

Appendices

Appendix A

E-mail Correspondence

Butterworth, Ian

From: Heather Dyson <heather.dyson@quorumtech.com>
Sent: 13 April 2015 17:54
To: Butterworth, Ian
Subject: RE: my phone call about coating Nylon66

Dear Ian,

Thank you for sending the micrograph, yes this is definitely a coating artefact, it is as I explained on the telephone, due to thickness, deposition rate, sputter current, argon bleed vacuum etc.

Please see below.

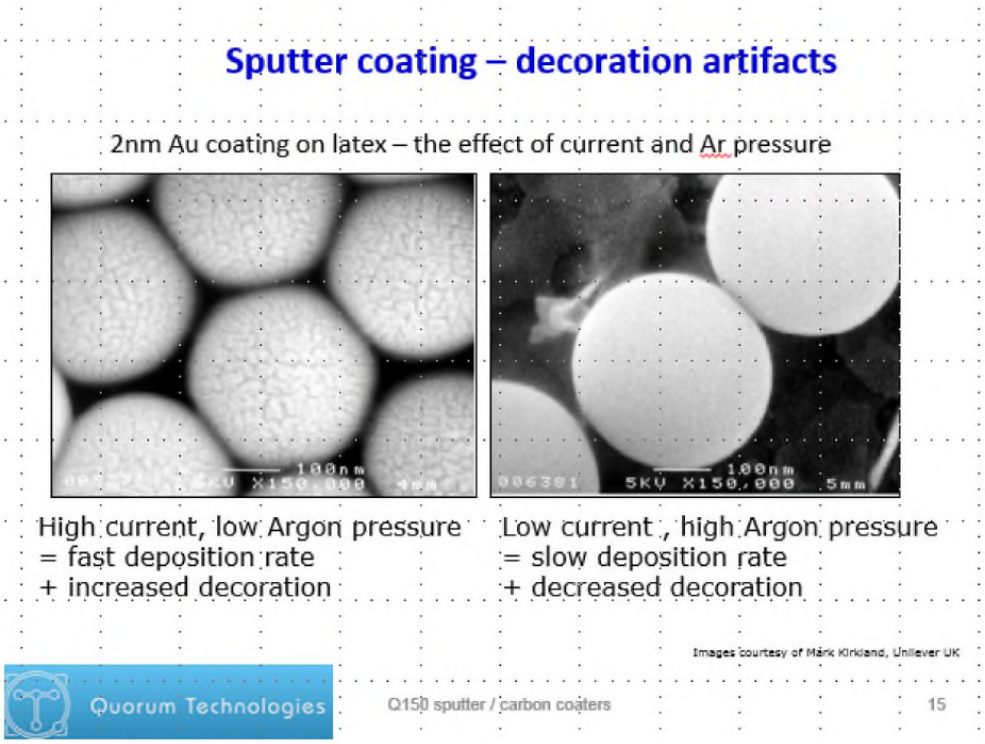

What I suggest is that you try and slow down the deposition rate by lowering the sputter current and not coating for such a long time.

Au:Pd should look like the images below, you should just start seeing the grainat 100,000 x mag.

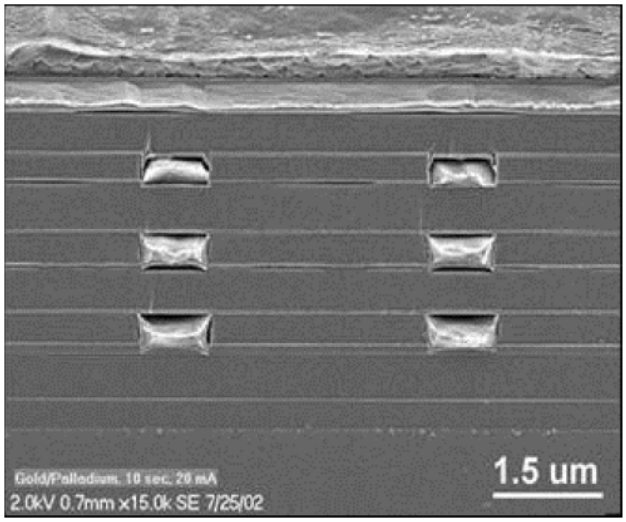

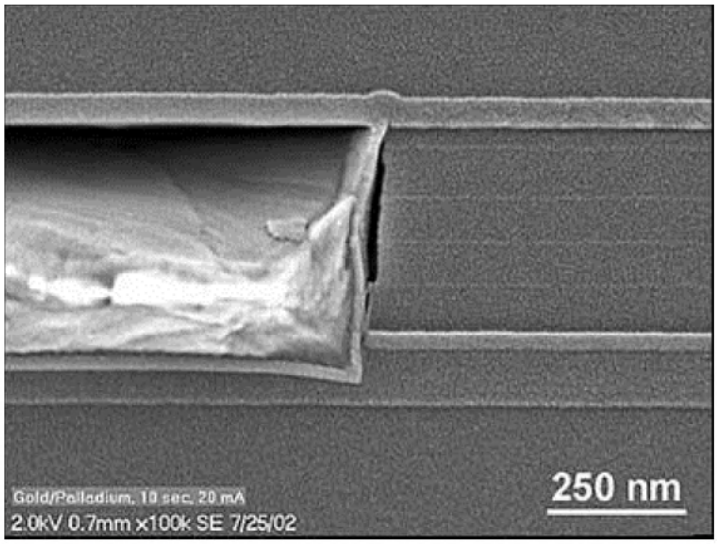

50,000 x mag 100,000 x mag

Best wishes,

Heather

Dr Heather Dyson

Technical Sales Manager

Mobile: +44(0) 7540 201193

heather.dyson@quorumtech.com | www.quorumtech.com

Quorum Technologies is a Judges Scientific company

Quorum Technologies

Judges House, Lewes Road, Laughton, East Sussex, England, BN8 6BN

T: +44 (0)1323 810981 F: +44 (0)1323 811999 E: sales@quorumtech.com

Cryo-SEM Preparation

SEM/TEM Coaters

For more information on our products visit: www.quorumtech.com

---

From: Butterworth, Ian [mailto:i.butterworth@cranfield.ac.uk]
Sent: 13 April 2015 13:25
To: Heather Dyson
Subject: Re: my phone call about coating Nylon66

Hi Heather,

Re: my phone call about coating Nylon66.
Thank you for the information over the phone.

Equipment: SEM coating unit E5100 using a gold-palladium target.

The matrix material is Nylon66

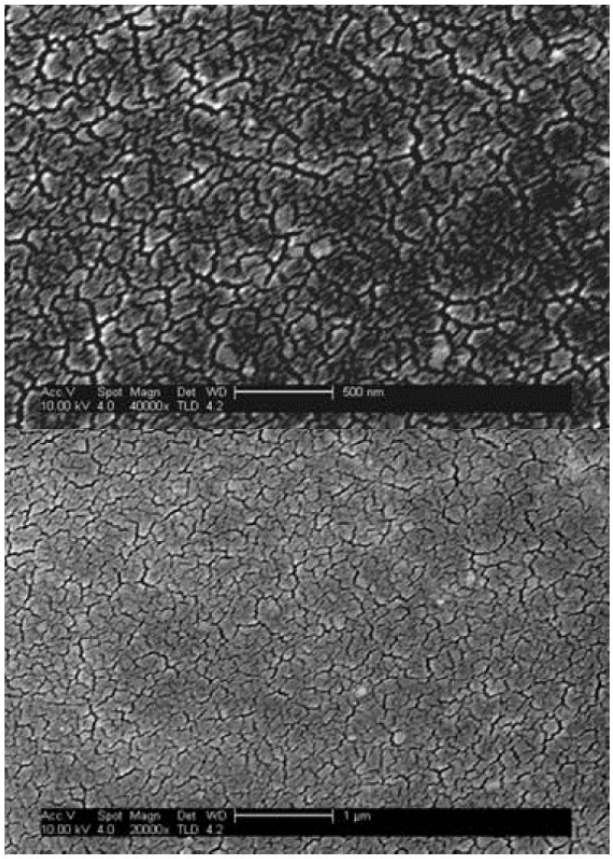

I would appreciate any further information.

Kind Regards,
Ian Butterworth
PhD Student Researcher, Centre for Automotive Technology
School of Aerospace, Transport and Manufacturing
BLD 56b 1st Floor, Cranfield University, Cranfield, Bedfordshire MK43 0AL
W: www.cranfield.ac.uk E: i.butterworth@cranfield.ac.uk
T: 01234 750111 ext 2816